A General Method for the Resummation of Jet Observables in e^+e^- Annihilation

or On The Weirdness of Tiny Things

Heather Turmeau McAslan

A thesis presented for the degree of
Doctor of Philosophy

Department of Physics and Astronomy
University of Sussex
United Kingdom
February 2017

Declaration

The content of Chapters 3 and 4 are based upon work which resulted in the publication of ref. [1]. The content of Chapter 5 is based upon work resulting in the publication of ref. [2].

I hereby declare that this thesis has not been and will not be, submitted in whole or in part to another University for the award of any other degree.

Signature: .....

Heather Turmeau McAslan

UNIVERSITY OF SUSSEX

HEATHER TURMEAU MCASLAN, DOCTOR OF PHILOSOPHY

A GENERAL METHOD FOR THE RESUMMATION OF JET OBSERVABLES IN e^+e^- ANNIHILATION

SUMMARY

This thesis introduces a novel technique for resummation of a wide class of observables to next-to-next-to-leading-logarithmic accuracy in e^+e^- annihilation, and potentially beyond. The method is applicable to observables that exhibit recursive infrared and collinear (rIRC) safety and continuous globalness. A systematic analysis of logarithmic counting in emission phase space reveals the contributions necessary to achieve NNLL-accurate results. A detailed description of the derivation and subsequent calculation of these effects is given. A framework of computer code (called `ARES`) has been developed to carry out automated numerical implementation of each of the NNLL contributions. `ARES` (Automated Resummer of Event Shapes) provides the user with an efficient determination of the resummed result for a desired observable. New results for several observables are presented, including the first NNLL resummation of the two-jet rate in the Durham and Cambridge algorithms which is crucial for determination of the strong coupling of Quantum Chromodynamics (QCD). This work as a whole presents an important addition to phenomenological precision calculations. Validation of the obtained predictions is performed, using both matching to NNLO fixed order calculations and comparison to data from the Large Electron-Positron collider at CERN.

Contents

Chapter 1

Introduction

in which I outline the context and scope of my research.

Particle physics collider phenomenology has been extraordinarily successful since its inception in the 1960s. It has allowed us insight into principles and elements of the physical world previously hidden by the limitations in our empirical capabilities. In order to obtain physical predictions within reasonable times successive approximations are made, yielding calculations which are accurate in appropriate energy regimes and particle kinematics. These 'fixed-order' determinations admit remarkably successful predictions of particle interactions. This approach is, however, not complete. There are problematic effects arising from particle dynamics occuring on multiple scales. When high energy particles emit radiation that is relatively much lower in energy or smaller in angle the fixed-order results are unreliable. For a fully comprehensive description of small distance dynamics it is essential to enhance the standard fixed-order calculations with resummation methods. Maximising the precision of available resummed results is vital to achieve optimum insight from current and past collider experiments.

This thesis will present a method, devised over the last three years, for the soft gluon resummation of a class of hadronic observables in e^+e^- annihilation, accurate to next-to-next-to-leading logarithmic (NNLL) order. Studying various kinematic scenarios for a catch-all observable elucidates the origins of effects that are relevant for NNLL accuracy. Particular attention is paid to deriving kinematics that are exactly NNLL order, i.e. without contamination from previously determined or subleading pieces.

In contrast with the majority of resummed calculations our method is not exclusive to a specific observable. Instead it is applicable to any observable satisfying the properties of continuous globalness and recursive infrared and collinear safety. Starting with the principles outlined in the `CAESAR` methodology [3] we use a generic observable that is sensitive to all emissions above a given softness and collinearity and within the resummed regime. The generic observable parametrisation covers the majority of Quantum Chromodynamics (QCD) observables used in phenomenological collider studies.

The resummation methodology is automated by construction of a framework of computer code; thus the numerical Monte Carlo package Automated Resummer of Event Shapes (`ARES`) enables a user to resum an observable of their choice, providing it lives within the

domain of the generic observable parametrisation.
Explicit application of the ARES technique will be carried out for seven event shapes and the two-jet rate. The results shown herein for event shapes were first published in the Journal of High Energy Physics in May 2015 [1], and for the two-jet rate in Physical Review Letters in October 2016 [2].
The structure of this thesis is as follows. Chapter 2 will give a brief introduction to the theory of QCD, and will go on to discuss the considerations of calculating QCD observables at particle colliders. An outline of the CAESAR resummation philosophy by which our technique is inspired is given in Chapter 3. The various contributions needed to capture all effects relevant to NNLL accuracy are studied and then derived in detail for event shapes in Chapter 4. Chapter 5 will introduce jet objects and jet algorithms, before evaluating the contributions required for NNLL resummation of the two-jet rate. Finally in Chapter 6 the resummed results will be matched to fixed-order calculations and compared to data from the Large Electron Positron Collider (LEP). In Chapter 7 an overview of the achievements and impact of these observable resummations will be presented, with some thought to future extensions.

Chapter 2

Background Theory

This chapter will summarise the theory of Quantum Chromodynamics (QCD) and its application to the physics of particle colliders (phenomenology). In particular we will discuss the challenge of translating the abstract degrees of freedom of QCD into observable quantities and the approximations that are placed on theoretical calculations in order to describe the interactions taking place at collider detectors.
For a more in-depth excursion see for example [4–6].

2.1 QCD: The Theory of Quarks and Gluons

in which I give an overview of the theory of QCD and highlight some of its theoretical and experimental properties.

2.1.1 Quark and Gluon Dynamics

QCD is the theory of strong interactions and the particles that are charged under the strong force, quarks and gluons. QCD is a non-Abelian gauge theory with the gauge group SU(3). Quarks are Dirac spinors charged under the fundamental representation of SU(3), thus carrying three colour charges that are normally typified as red, green and blue. Bound states of quarks are invariant under SU(3) transformations and as such are colourless, the most common configurations being mesons ($q\bar{q}$) and baryons (qqq). Quarks exist in six flavours: up, charm, top which carry electric charge $= \frac{2}{3}e$ and down, strange, bottom which carry electric charge $= -\frac{1}{3}e$. The mediators of the strong force are the gluons: spin-1 vector gauge bosons that also carry colour charge. Collectively, quarks and gluons are called partons.
Scattering amplitudes in QCD involve quark-gluon and gluon-gluon interaction vertices. Allowed vertices and their corresponding Feynman colour rules are shown in Fig. 2.1 (we show only those relevant to the calculations in this thesis). In order to compute cross-sections the amplitudes of Fig 2.1 must be squared and integrated over phase space, with the resulting terms generically involving sums of traces of the eight SU(3) generators: the

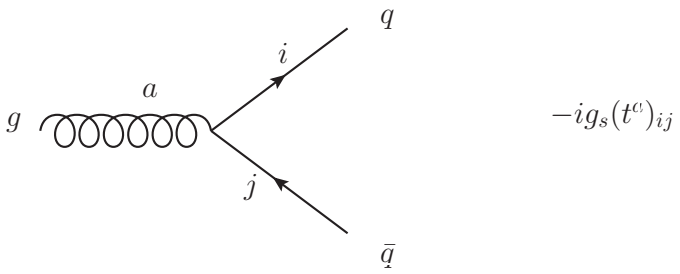

(a) $gq\bar{q}$ vertex

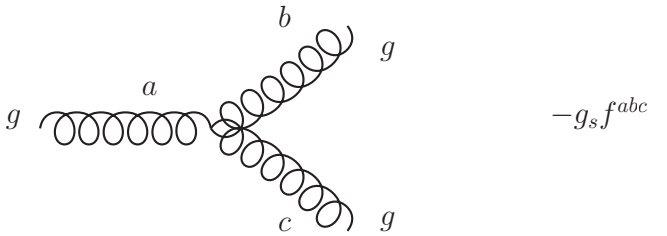

(b) ggg vertex

Figure 2.1: QCD vertices and their associated Feynman colour rules. a) shows a gluon-quark-antiquark vertex with the colour charges of the quarks denoted by i, j and the colour charge of the gluon by a. b) shows a triple-gluon vertex, with the colour charges a, b, c.

colour matrices t^a. The commutator of two colour matrices is,

$$[t^a, t^b] = if^{abc}t^c\,, \tag{2.1}$$

where the f^{abc} are the totally antisymmetric structure constants. The colour factors of cross-sections are most simply expressed by the group invariant Casimir operators. For a squared $gq\bar{q}$ vertex the colour factor is,

$$(t^a t^a)_{ij} = \frac{1}{2}\left(\delta_{ij}N_C - \frac{\delta_{ij}}{N_C}\right) = \delta_{ij}\frac{N_C^2 - 1}{2N_C} \equiv \delta_{ij}C_F; \quad C_F = \frac{4}{3}\,, \tag{2.2}$$

And for a ggg vertex,

$$f^{acd}f^{bcd} = \delta_{ab}N_C \equiv \delta_{ab}C_A; \quad C_A = 3\,, \tag{2.3}$$

where δ_{ab} is the usual Kronecker delta and N_C is the number of colours. The factor of g_s in the vertices of Fig. 2.1 is the strong coupling constant, governing each QCD interaction. When we square the vertex contributions and integrate over phase space to obtain cross-sections this becomes,

$$\alpha_s = \frac{g_s^2}{4\pi}\,, \tag{2.4}$$

which from now on we will call the strong coupling of QCD.

2.1.2 Perturbative QCD

The QCD coupling α_s runs with energy scale ($\alpha_s = \alpha_s(Q)$), being large at low energy (large distances) and small at high energy (small distances). At short distances QCD is

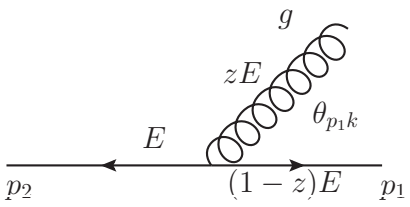

Figure 2.2: The emission of a gluon from the quark in a quark-antiquark event. z is the energy fraction carried away from the emitter p_1 by the gluon emission k. θ_{p_1k} is the angle between the gluon emission and the final-state emitter.

an asymptotically free theory, with quarks and gluons behaving as free particles. At long distances, quarks and gluons experience confinement. This accounts for the fact that free quarks have not been observed experimentally. We take advantage of asymptotic freedom and perform a series expansion around the QCD coupling; when the coupling is small the first few terms in the expansion should give a good approximation to the full result. Each QCD emission carries one power of α_s, as we have seen in Fig. 2.1, therefore we expect the cross-section with the fewest emissions to have the largest value, or equivalently, be the most likely to occur (in fact we will see in Sec. 2.2.4 that this is not always the case). A theory in which such an approximation is made is called a perturbative theory. The strong coupling is safely within the perturbative regime at 100 GeV ($\alpha_s \sim 0.1$), and can be considered a 'strong' coupling around and below 1 GeV [7]. A series expansion method ensures that we can rely on the perturbation calculations to calculate QCD observables within the energy regimes probed by current and recent particle collider experiments (The Large Electron-Positron Collider (LEP) at CERN observed high-energy collisions around 200 GeV and the Large Hadron Collider (LHC) at CERN has probed interaction energies of 7-14 TeV).

Now we consider the interactions that can occur in perturbative QCD (pQCD). As we have seen in Sec. 2.1.1 a gluon can split into a quark-antiquark pair or a pair of gluons. For instructive purposes we now consider the second-to-simplest cross-section in pQCD: $e^+e^- \to q\bar{q}g$, the production of a $q\bar{q}$ pair from a virtual photon (or Z boson) with an additional gluon radiated from one of the quarks. We will not start from first principles but instead from the squared amplitude for emission of a gluon k from, say, the q of a $q\bar{q}$ pair (see Fig. 2.2) and the corresponding phase space integration. Additionally we will assume that the energy of the gluon is small (the gluon is 'soft'): $E_k \ll E_{p_1}, E_{p_2}$, i.e. that z is small.

$$\sigma_{q\bar{q}g} = \int [d\Phi_{q\bar{q}g}]\mathcal{M}^2_{q\bar{q}g} = \int [d\Phi_{q\bar{q}}]\mathcal{M}^2_{q\bar{q}} \frac{d^3\vec{k}}{2E_k(2\pi)^3}\Theta(E_k)C_F g_s^2 \frac{2p_1p_2}{(p_1k)(p_2k)}\,, \tag{2.5}$$

where one can see that both the squared amplitude $\mathcal{M}^2_{q\bar{q}g}$ and the phase space $[d\Phi_{q\bar{q}g}]$ of the high-energy ('hard') $e^+e^- \to q\bar{q}$ cross-section factorise into a gluon piece and a $q\bar{q}$

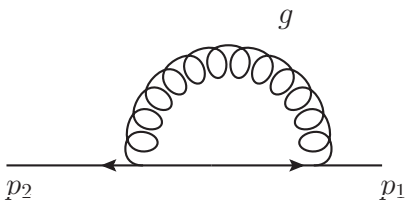

Figure 2.3: A virtual gluon loop arising in a quark-antiquark event.

piece. Considering only the gluon piece,

$$\sigma_g^R = \int \frac{d^3\vec{k}}{2E_k(2\pi)^3}\Theta(E_k)C_F g^2 \frac{2p_1p_2}{(p_1k)(p_2k)} = \int \frac{2\alpha_s C_F}{\pi}\frac{dE_k}{E_k}\frac{d\theta_{p_1k}}{\sin\theta_{p_1k}}\frac{d\phi}{2\pi}\,, \tag{2.6}$$

where ϕ is the angle in the out-of-page direction. The gluon can be emitted anywhere in a 4π solid angle, with no lower energy bound. This, however, will clearly lead to issues in our calculation: the phase space integration is singular for $E_k \to 0$ and $\theta_{p_1k} \to 0, \pi$. These are the soft (or infrared) and collinear divergences. Infrared and collinear (IRC) singularities appear because of the unphysical nature of the cross-section we have just considered. In nature there is no event consisting of a single quark-antiquark pair, rather the event will always be accompanied by additional gluon emissions. IRC divergences appear for each gluon radiated, i.e. at every order in perturbation theory, since the latter argument is true for any number of emissions; one cannot choose the number of final-state particles appearing in an event.

The gluon emission shown in Fig. 2.2 is a real gluon, but of course in perturbative QCD we must include all diagrams kinematically allowed at a given order. So we must also include a virtual gluon loop (as shown in Fig. 2.3) when computing amplitudes for the cross-section of $e^+e^- \to q\bar{q}g$ to first order in α_s. The squared amplitudes of real and virtual contributions to the $q\bar{q}$ event combine to give a finite result. This real-virtual cancellation occurs for any event and at every order in perturbation theory, and should not be too suprising since when the gluon becomes infinitely soft or collinear the final state is indistinguishable from that of a quark-antiquark pair with a virtual gluon and so the two must cancel. These singularities are not physical, rather they are manifestations of the approximations that we perform in our theory.

2.2 Collider Phenomenology

in which I talk about particle physics collider experiments and how we can try to predict what they will tell us.

2.2.1 High-Energy Colliders

The calculations presented in Sec. 2.1 are purely theoretical. In order to accurately describe the physics of high-energy quarks and gluons we must engage with the quarks and gluons of the real world, via particle-colliding experiments. Multi-purpose detectors such as those

at the LHC and previously LEP at CERN cover nearly[1] a whole solid angle around the beam-line. However the majority of final state particles lie in the forward region and so we want to have maximum sensitivity here. We use a parameter proportional to the logarithm of the angle away from the beam, pseudorapidity $\eta = -\ln(\tan\left(\frac{\theta}{2}\right))$. For hadron colliders the natural axis from which to measure angles is the beam axis, i.e. two back-to-back hadronic events at high-energy. For lepton colliders such as LEP we use an axis which roughly aligns with the outgoing hadrons. The azimuth ϕ is measured with respect to an axis perpendicular to the longitudinal plane.
When studying collider phenomenology it is crucial to keep in mind that detectors are physical objects with finite pixel-size, blind regions and variable sensitivity across different regions of phase-space. As such, a detector does not 'see' a particle, it registers an energy deposit in a collection of pixels that passes a series of kinematic triggers. The partons of experiment and theory are separated by a fine grid, and phenomenology must take both sides into account.

2.2.2 Factorisation

We wish to test quantum field theory predictions at colliders. The obvious starting point would seem to be to look at the particle objects produced by collider interactions. In QCD this immediately poses a problem: the fundamental degrees of freedom of QCD (quarks and gluons) are *not* final-state objects. The partons involved in energetic energy transfers of order the center-of-mass energy evolve down to lower energy scales by emission of increasingly low-energy radiation and finally by hadronisation. The final-state particles are hadrons and hadron decay products, often grouped into objects called jets. There is an in-depth discussion on the construction and properties of experimental and theoretical jets later in this thesis, in Sec. 5.1. Schematically the evolution of a QCD state from the high-energy (or 'hard') interaction down to the final-state jets is well represented by the ubiquitous diagram shown in Fig. 2.4 [8]. The various processes taking place in Fig. 2.4 occur over very different time scales and hence the mechanisms occuring in the different regimes cannot communicate with one another. We treat these various processes using different techniques. In this thesis we only concern ourselves with the calculation of one of the evolution stages: all calculations in this thesis are mathematical expressions of the type of the red pieces of Fig. 2.4.

Recall from Sec. 2.1.2 that at high energies α_s is small and we can perform a series expansion around the coupling, keeping only the first few terms. Calculating the terms in the truncated series expansion is a so-called fixed-order calculation. Each real emission or virtual correction contributes one power of the coupling to this calculation. Taking into account events with the fewest powers of α_s is called a leading-order approximation (LO), taking also the events with the next fewest powers is a next-to-leading-order approximation (NLO), and so on. This method of expansion is only mathematically valid when α_s

[1] This adjective becomes important when considering certain types of variables which incur 'non-global' effects: see the discussions on globalness in Sec. 3.1.1

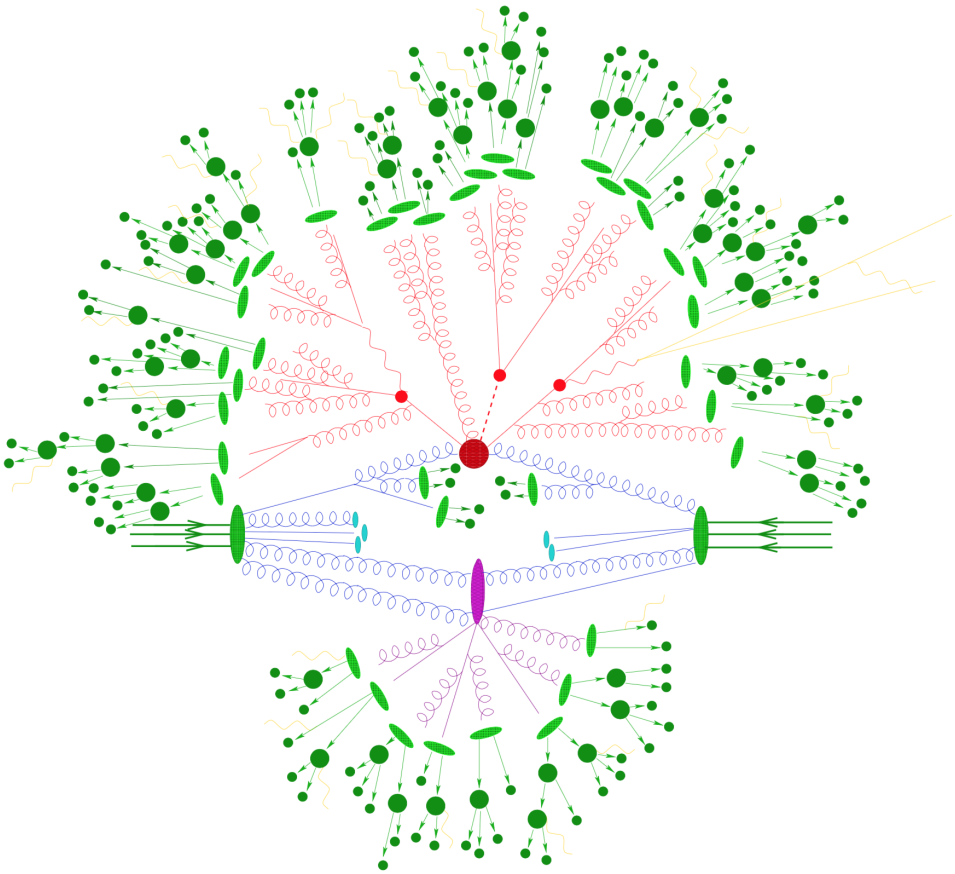

Figure 2.4: The evolution of a hard scattering. The energy scale decreases as one moves radially out from the centre of the diagram. The initial interaction, shown by the central red circle, produces high-energy, possibly heavy, particles, shown by the smaller red circles. These products will decay, or at least emit radiation, via the interactions available to its charges, depicted as the red propagators. Subsequent radiation will be emitted until the hadronisation scale is reached. Colourless hadrons, shown as light green blobs, will be produced and subsequently decay to lighter particles, shown as dark green blobs. Meanwhile any remnants from the beam that did not take part in the hard scattering can spur a secondary interaction called the underlying event, shown by the purple interactions. The underlying event will similarly emit radiation down to the hadronisation scale, produce hadrons and their decay modes which form the final-state particles. (This is a pictorial representation of a $t\bar{t}h$ event but the mechanisms occurring at different scales are present in all high-energy collisions.)

is small; in the perturbative regime.
The perturbative regime safely includes the initial hard scattering and emission of decreasing-energy partons that we wish to calculate. The hadronisation stage lies in the non-pertubative regime and is not theoretically well-understood. There exist several models which mimic the grouping of coloured partons into colourless hadrons [9–12]. The effects of hadronisation on perturbative distributions can be minimised by considering the inclusive energy flow of an event rather than stipulating the specific particle content.

One can calculate inclusive cross-sections of QCD processes, but to glean more nuanced information about the particle interactions we construct collider observables. There exist hundreds of these observables, defined to probe the energy spread, the number of particles or the angular properties in an event, to highlight a few. The perturbative integrated cross-section for a QCD observable v can be written,

$$\Sigma(v) = \frac{1}{\sigma}\int_{v_{\min}}^{v_{\max}} dv \frac{d\sigma(v)}{dv} = \Sigma_0(v) + \Sigma_1(v)\alpha_s + \Sigma_2(v)\alpha_s^2 + \cdots , \tag{2.7}$$

where v is the observable we consider and σ is the lowest order (Born) cross-section of the process in question. $\Sigma(v)$ is the full, exact result (which is practically unattainable). $\Sigma_i(v)$ is the result taking into account only interactions allowed at i^{th} order in α_s. The series is convergent to the first few orders. The current standard for calculations of collider observables is NLO or NNLO, i.e. taking the first two or three terms, depending on the observable and the process in question.

2.2.3 IRC Safety

Recall from Sec. 2.1.2 that interactions involving quarks and gluons exhibit soft and collinear singularities. For suitably inclusive measurements, such as the total cross-section, IR divergences cancel between real and virtual contributions. For observables which specify exclusive kinematic scenarios, e.g. a particular particle content, not all possible kinematics are included in the calculation and the IR divergences *do not* exactly cancel.
In order to avoid these issues from the outset we construct our observables to be infrared and collinear safe, meaning that they are insensitive to the emission of any parton that i) has vanishingly small energy (IR), or ii) is collinear to its parent. Eq. (2.8) is a necessary condition for IRC safety.

$$\begin{aligned} V(\{q\}, k_1, \cdots, k_n) = V(\{q\}, k_1, \cdots, k_{j+1}, \cdots, k_n)\,, \\ \text{when } E_{j+1} \to 0 \text{ or } \vec{k}_{j+1} \parallel \vec{q}_{\text{emit}}\,, \end{aligned} \tag{2.8}$$

where V is the observable in question, $\{q\}$ are hard partons and q_{emit} is the parent of the extra gluon k_{j+1}. While Eq. (2.8) shows a single observable becoming soft or collinear to its parent, the above property holds for any number of emissions for IRC safe observables. Hence cross-sections can be safely calculated at every order in a perturbation expansion in α_s.

In using pQCD to calculate cross-sections we are effectively neglecting the unknown hadronisation piece of the calculation and approximating the cross-section to just the high-energy part. This is known as local parton-hadron duality (LPHD). For the fully inclusive observables for which LPHD has been studied in detail [13], hadronisation corrections amount to power-suppressed terms,

$$V\left(\frac{m_i^2}{Q^2}, \alpha_s(Q^2)\right) = V\left(0, \alpha_s(Q^2)\right)\left(1 + \mathcal{O}\left(\frac{m_i^2}{Q^2}\right)^p\right), \quad p \geq 0\,, \tag{2.9}$$

where V is the observable, a function of some participating masses m_i and the hard-scale of the problem Q (typically equal to the total energy in the event). One can see that as the event energy increases the total cross-section tends to that described only by partons. Alternatively at small event energies there exists a shift $\sim \left(\frac{m_i^2}{Q^2}\right)^p$ between the hadronic and partonic cross-sections. The same power-suppressed behaviour is believed[2] to hold for the many standard observables that are used to probe QCD at current and past colliders, such as event shapes (introduced later in this chapter) and jet rates (described in Chapter 5).

2.2.4 The Need for Resummation

We now have a formalism in place with which to calculate particle interactions at particle colliders: perturbative QCD using IRC safe observables. However there remains one more glitch in this approach. When the value of the observable is small ($v \approx 0$) an implicit constraint is placed on the observable's radiation, meaning that it can only be soft and collinear as to not affect the value of the observable too far away from its Born value. We will show the exact parametrisation of this effect in Secs. 2.2.5 and 3.1. Note that a redefinition of the observable might be required to keep in line with this description, an example being the thrust observable of Eq. (2.11): the resummation is carried out for $1-T$. The constrained nature of the observable value results in remnant logarithms which come from the cancellation of the real and virtual divergences discussed in Sec. 2.1.2, which appear at every order in α_s. Each power of α_s can be accompanied by up to two kinematic logarithms: originating from either the soft or the collinear divergence.

Although infrared and collinear safety ensures that observable cross-sections are finite to every order in perturbation theory, there is an additional IR physics effect in play here: the logarithms are large ($\alpha_s L \simeq 1$) and ruin the hierarchy of the powers of α_s. The smallness of the strong coupling alone no longer ensures the validity of the cross-section's convergence in this region and the fixed order approach of Eq. (2.7) is no longer reliable. The effect of the large logarithms can be seen in Fig. 2.5 [14]. The troublesome logarithmic terms dominate in the region in which the majority of events occur.

We undertake a schematic shuffling of terms in the series in the region of small v, giving dominant logarithmic terms priority rather than those with fewest powers of α_s. The determination of terms of the now-shuffled series is called a resummation. The now-cured

[2] Not least because of the high precision to which data matches perturbative QCD calculations.

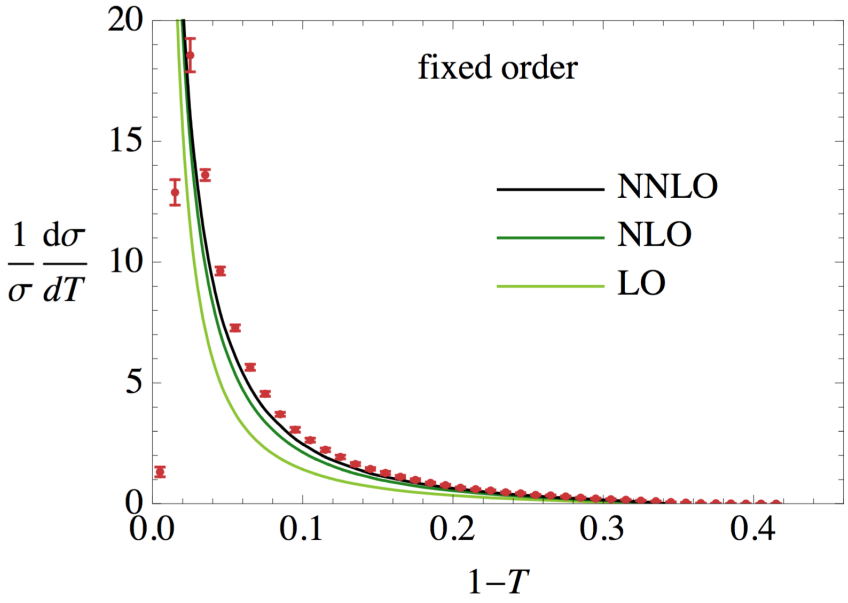

Figure 2.5: Calculation of the thrust observable's (Eq. 2.11) differential distribution using a standard fixed order expansion in α_s. The distribution starts to sharply diverge at small values of $\tau = 1 - T$. The theoretical determination of the thrust differential distribution clearly coincides with the data points shown in red (from ALEPH at LEP, at centre-of-mass energy 91.2 GeV), for large values of τ. For very small values of τ, however, the data points tend back to small values. Notice also the success of the successive orders in perturbation theory for large-τ: the leading-order approximation shows a good qualitative agreement with the data, with NLO and NNLO contributions incrementally improving the result, as expected. However adding higher order terms does not fix the poor prediction at low-τ. Resummation is required to accurately describe this region.

perturbative resummed series takes the form [15]

$$\Sigma(v) \simeq (1 + C(\alpha_s)) \exp\{L g_1(\alpha_s L) + g_2(\alpha_s L) + \alpha_s g_3(\alpha_s L) + \ldots\}, \quad L \equiv \ln\left(\frac{1}{v}\right), \quad (2.10)$$

where the exponent takes into account terms to all orders in α_s, to a given logarithmic order. $g_1(\alpha_s L)$ resums all of the leading logarithmic terms (LL); $g_2(\alpha_s L)$ the next-to-leading terms (NLL), and so on. This exponentiated form is exhibited by the majority of observables of interest to phenomenology, and expresses the fact that we take into account emissions and virtual corrections to all orders in α_s. In Eq. (2.10) equality holds up to power-suppressed corrections due to the parton-hadron shift described in the previous section, and a finite remainder from fixed-order calculations.

It is the aim of this thesis to carry out the calculation of IRC safe observables in high-energy particle interactions, in the small-observable limit using resummation techniques.

2.2.5 Event Shapes

In this section we will define the particular IRC safe observables that are used in our resummed calculations. All but one fall into the class of event shape observables. (The resummation of the two-jet rate can be handled as an extension to event shape resummation and will be discussed later in Chapter 5.) Event shapes are measures of the hadronic energy flow in an event. Event shapes were first defined for e^+e^- annihilation events [16–18] and have provided robust experimental tests of the theory of QCD. These collider observables are excellent tools allowing for extraction of the strong coupling α_s and the tuning of Monte Carlo event generators. Additionally, the range of values available to event shapes are directly related to the geometry of the energy flow in the event, giving a useful literal picture of what is occuring. In this work we have carried out the resummation of seven event shapes: thrust, heavy-jet mass, C-parameter, total and wide jet broadenings, thrust major and oblateness. In the following we give the definitions of these event shapes, for massless particles.

Thrust and Thrust-type Event Shapes

The canonical event shape, and a useful observable exemplifying the geometries of these observables, is the thrust [16]

$$T \equiv \max_{\vec{n}} \frac{\sum_i |\vec{p_i} \cdot \vec{n}|}{Q}, \qquad \tau \equiv 1 - T, \quad (2.11)$$

where $\{p_i\}$ are the momenta of each final-state particle in the event. Q is the hard scale, e.g. the sum of all momenta in the event, and the vector $\vec{n}$ that maximizes the sum defines the direction of the thrust axis, $\vec{n_T}$. The thrust axis divides each event into two hemispheres, $\mathcal{H}^{(1)}$ and $\mathcal{H}^{(2)}$ as shown in Fig. 2.6a. For an event with two back-to-back jets the thrust axis lies along either one of the quark directions (they must of course be equally energetic), and $\tau = 0$. The thrust is maximised for a spherically symmetric event

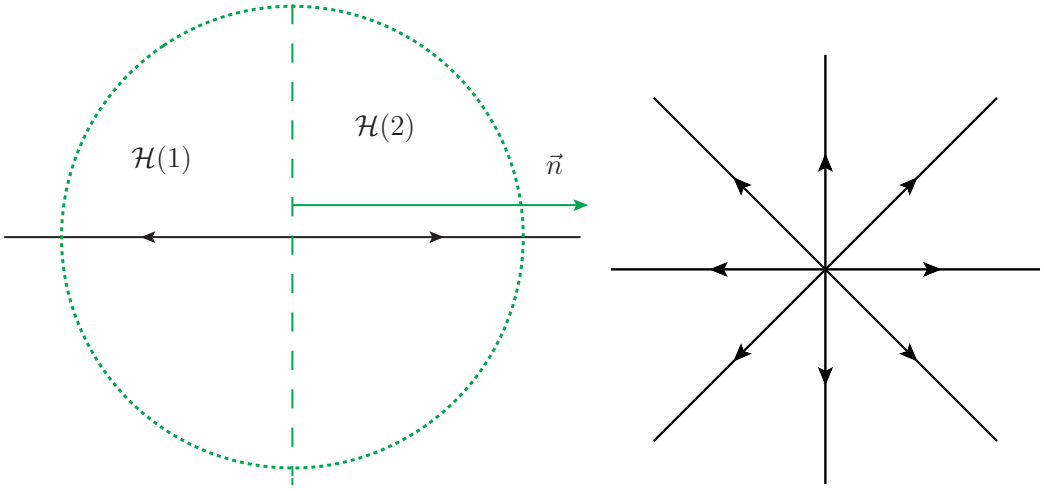

(a) Back-to-back (b) Spherical

Figure 2.6: Values for thrust in different event 'shapes'. a) shows the pencil-like geometry of an event with $\tau = 0$. The thrust axis $\vec{n}_T$ divides the system into two hemispheres, in which transverse momentum is separately conserved. Lines shown in green are not physical but display the position of the thrust axis and the two hemispheres. b) shows the spherical geometry of an event with $\tau = \frac{1}{2}$. $\vec{n}_T$ and the hemispheres are not shown, they will simply be determined by the most energetic particle.

such as the one presented in Fig. 2.6b, where $\vec{n_T}$ will lie along the direction of the most energetic particle, and $\tau = \frac{1}{2}$. A value of zero signifies Born kinematics and the maximum value the kinematics furthest deviating from Born.
The heavy-jet mass is a relative of the thrust

$$\rho_H \equiv \max_{i=1,2} \frac{M_i^2}{Q^2}\,, \qquad M_i^2 \equiv \left(\sum_{j\in\mathcal{H}^{(i)}} p_j\right)^2\,, \tag{2.12}$$

as is the C-parameter

$$C \equiv 3\left(1 - \frac{1}{2}\sum_{i,j}\frac{(p_i\cdot p_j)^2}{(p_i\cdot Q)(p_j\cdot Q)}\right)\,. \tag{2.13}$$

Thrust, heavy-jet mass and C-parameter are so-called additive observables, meaning that, for soft emissions $\{k_i\}$,

$$V(\{\tilde{p}\}, k_1, \ldots, k_n) = \sum_{i=1}^{n} V(\{\tilde{p}\}, k_i) + \mathcal{O}(V^2)\,, \tag{2.14}$$

where V represents any of the three observables, and $\{\tilde{p}\}$ denotes the hard partons in the event, recoiled by emission of the soft emissions. This property allows simplifications to be made when carrying out calculations for such observables. We will use this property in Section 4.6 to give explicit results for the resummation of thrust, heavy-jet mass and the C-parameter.

Broadening and Broadening-type Event Shapes

Using the hemispheres defined in the previous section we define total jet broadening [19]

$$B_T \equiv B_L + B_R, \tag{2.15}$$

where

$$B_L \equiv \sum_{i \in \mathcal{H}^{(1)}} \frac{|\vec{p_i} \times \vec{n_T}|}{2Q}, \quad B_R \equiv \sum_{i \in \mathcal{H}^{(2)}} \frac{|\vec{p_i} \times \vec{n_T}|}{2Q}, \tag{2.16}$$

as well as wide jet broadening,

$$B_W \equiv \max\{B_L, B_R\}. \tag{2.17}$$

Thrust-major is defined

$$T_M \equiv \max_{\vec{n} \cdot \vec{n_T} = 0} \frac{\sum_i |\vec{p_i} \cdot \vec{n}|}{Q}, \tag{2.18}$$

where the vector $\vec{n}$ for which the sum is maximised defines the thrust-major axis. Lastly we define oblateness,

$$O \equiv T_M - T_{\mathrm{m}}, \tag{2.19}$$

where

$$T_{\mathrm{m}} \equiv \frac{\sum_i |p_{i,x}|}{Q}, \tag{2.20}$$

and where x is the direction perpendicular to both the thrust and the thrust-major axes. It is simple to confirm that all of the event shapes defined here are indeed IRC safe.

Fig. 2.7 [20] shows the differential distribution of two event shape observables. Notice the qualiative difference in behaviour between the thrust plot of Fig. 2.5, using only fixed-order results, and the resummation+fixed-order results shown in Fig. 2.7. Resummation of large soft and collinear logarithms cures the divergence of the fixed-order result at low values of the observable. The qualiative agreement between theoretical calculations and data is very good across all possible event shape values. There are, however, significant errors arising from the small orders at which the resummed and fixed-order calculations have been respectively truncated.

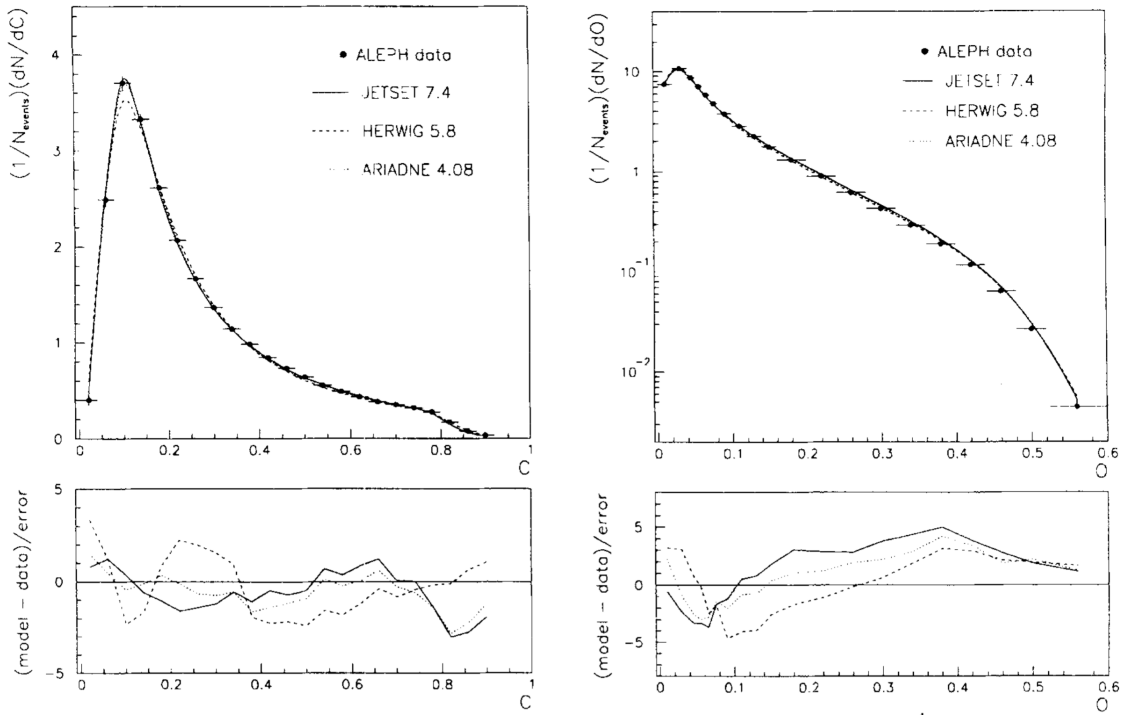

(a) C-parameter (b) Oblateness

Figure 2.7: Data from the ALEPH detector at LEP (centre-of-mass energy 91.2 GeV) compared to fixed order+resummed theoretical results given by three different Monte Carlo models: JETSET 7.4, HERWIG 5.8 and ARIADNE 4.08. The theoretical-experimental agreement is qualitatively good across the full range of C-parameter and oblateness values.

Chapter 3

State-of-the-art Resummation

in which I describe the CAESAR *methodology.*

Since the first leading logarithmic resummation was carried out for the thrust event shape [16] there has been a wealth of work in the area. There exist many resummed results at NLL accuracy for specific observables in e^+e^-, Drell-Yan and hadron-hadron collisions [15, 21–28]. The majority of these studies are observable-dependent as they depend on a factorisation formula that is specific to each observable. In [29] an approach appeared which made it possible to resum event shapes and jet rates with a single procedure. This approach completed the space of NLL soft-gluon resummations.
Consequently there has been a move towards making NNLL the state-of-the-art. Various results for single event shapes can be found in [14, 30–36]. It is often the case that theory uncertainties are larger than experimental errors, thanks to the advancement of experimental precision studies. Continued parallel advancements in theory are necessary in order to fully take advantage of the data coming from colliders.

Our goal is to build a single framework to carry out the resummation of a wide class of observables to NNLL accuracy. We will implement the method in a computer code so that one may attain an automated result, given the basic characteristics of an observable in question. We start from the CAESAR formalism for generic-observable NLL resummation [3] and systematically extend it to include all the necessary components to achieve NNLL precision. In the following section we will give a thorough introduction to the CAESAR philosophy. This will include an explanation of the event kinematics, the applicability conditions placed on the generic observable, the separation of various types of emissions and finally the derivation of the master resummation formula.

3.1 CAESAR Formalism

The Computer Automated Expert Semi-Analytical Resummer (CAESAR) [3] is a complete methodology for the resummation of collider observables at next-to-leading logarithmic accuracy, and the accompanying computer code to semi-numerically carry out such a calculation. The method has produced a vast number of results in e^+e^-, DIS and hadron-

hadron collisions. These include both new results and previously-known findings which mutually validate alternative approaches. In particular CAESAR produced the first determination of the Durham two-jet rate [37], a useful observable for the determination of α_s [38]. (See Sec. 5.1 for a definition of jets and jet rates.) The capabilities of the method are only limited by the availability of observables of interest that are continuously global and rIRC safe (these applicability conditions will be discussed in the subsequent paragraphs).
The material in this chapter is based on our recent interpretation of this formalism [1].

Consider an $(n+1)$-jet observable V that is a positive definite function of all final-state momenta in an event,

$$V(\tilde{q_1}, \ldots, \tilde{q_k}, k_1, \ldots, k_m) > 0\,, \tag{3.1}$$

where the final states are a set of Born momenta $\{\tilde{q_i}\}$, and additional emissions $\{k_i\}$. The tildes denote that the Born momenta recoil from the extra emissions. V is a measure of a given event's deviation from the Born kinematics. As such, the observable should have the behaviour that it goes smoothly to zero for the Born event,

$$V(q_1, \ldots, q_k) = 0\,, \tag{3.2}$$

as well as being IRC, *recursively* IRC safe and continuously global. Before continuing to derive the master resummation formula for the generic observable V we will detail these three characteristics that ensure the applicability of the method.

3.1.1 Formalities of Globalness, IRC Safety and rIRC Safety

An observable is global if it is sensitive to all emissions in an event. Continuous globalness stipulates that the scaling of the observable with respect to an emission's energy is the same everywhere. Observables not satifying these behaviours introduce additional sources of large logarithms that will not be addressed in our formalism.
As discussed in Section 2.2.3, IRC safety is necessary to ensure full cancellation of IR and collinear singularities at every order in perturbation theory.
Recursive infrared and collinear safety (rIRC) is an additional requirement on the observable that ensures it is insensitive to additional soft and collinear emissions on a disparate range of scales. Recursive infrared and collinear safety first appeared in [29]. Original IRC safety deals with the behaviour of observables when there are emissions occuring over two disparate scales: the hard partons and additional soft-collinear emissions. rIRC safety introduces another scale and requires that the observable be additionally insensitive to emissions in this region of phase space. Given an ensemble of soft-collinear emissions, the observable should not be changed by additional emissions living at much softer or more collinear regions of phase space. Formally,

$$V(\tilde{q_1}, \ldots, \tilde{q_k}, k_i) = \zeta_i\,, \tag{3.3}$$

where $\zeta_i \to 0$ in the soft-collinear limit. Eq. (3.3) implies $k_i = k_i(\zeta_i)$. rIRC stipulates that the limit

$$\lim_{\epsilon\to 0} \frac{1}{\epsilon} V(\tilde{q_1}, \ldots, \tilde{q_k}, k_1(\epsilon\zeta_1), \ldots, k_m(\epsilon\zeta_m))) \tag{3.4}$$

should be well-defined and non-zero, and that

$$\begin{aligned} &\lim_{\zeta_{m+1}\to 0} \lim_{\epsilon\to 0} \frac{1}{\epsilon} V(\tilde{q_1}, \ldots, \tilde{q_k}, k_1(\epsilon\zeta_1), \ldots, k_m(\epsilon\zeta_m), k_{m+1}(\epsilon\zeta_{m+1})) \\ &= \lim_{\epsilon\to 0} \frac{1}{\epsilon} V(\tilde{q_1}, \ldots, \tilde{q_k}, k_1(\epsilon\zeta_1), \ldots, k_m(\epsilon\zeta_m)) \,. \end{aligned} \tag{3.5}$$

Similar requirements can be expressed for collinear singularities (arising from the angle between a hard parton and an emission, and also from the angle between a soft-collinear emission pair).

The above requirements ensure that the observable will have the same parametric behaviour regardless of the number of soft and collinear emissions in the event, as well as being insensitive to emissions below a certain scale. In fact, recursive IRC safety allows us to place constraints on each emission individually:

$$V(\tilde{q_1}, \ldots, \tilde{q_k}, k_1, \ldots, k_m) < v \quad \Longrightarrow \quad \epsilon v \lesssim V(\tilde{q_1}, \ldots, \tilde{q_k}, k_i) \lesssim v \,, \tag{3.6}$$

where ϵ satifies

$$v \ll \epsilon \ll 1 \,. \tag{3.7}$$

The reliance of the observable on individual emission behaviour as in Eq. (3.6) implies that the leading logarithms will exponentiate, and that the region in which additional real radiation exists is next-to-leading logarithmic.

3.1.2 Event Set-up

Given the applicability conditions on the generic observable, we will now consider the phase space available to the final-state momenta and show how the master formula for the resummed cross-section of V arises. Very generally, the resummed cumulative distribution of our observable $V(\tilde{q_1}, \ldots, \tilde{q_k}, k_1, \ldots, k_m)$, normalised to the Born cross-section σ, can be written

$$\Sigma(v) = \frac{1}{\sigma} \int_0^v dv' \frac{d\sigma(v')}{dv'} \,, \tag{3.8}$$

where the upper limit on the value of the observable ensures that we are in the resummed regime of small-v. We recall the form of $\Sigma(v)$ for resummed observables (Eq. (2.10)),

$$\Sigma(v) = (1 + C(\alpha_s)) \exp\{L g_1(\alpha_s L) + g_2(\alpha_s L) + \alpha_s g_3(\alpha_s L) + \ldots\} \,, \tag{3.9}$$

where $L = \ln 1/v$. In Eq. (3.9) $C(\alpha_s)$ contains all the constant terms,

$$1 + C(\alpha_s) = 1 + C_1\alpha_s + C_2\alpha_s^2 + C_3\alpha_s^3 + \ldots \,, \tag{3.10}$$

in other words, a fixed-order series in α_s. The first term in the exponent of Eq. (3.9), $Lg_1(\alpha_s L)$, resums the dominant leading logarithms of form $\alpha_s^n L^{n+1}$, $g_2(\alpha_s L)$ resums next-to-leading logs $\alpha_s^n L^n$, and so on[1]. The conditions of recursive IRC safety ensure exponentiation of the leading logarithmic terms.

We will now concentrate solely on the resummation of observables in the process of an e^+e^- pair annihilating to two jets. Electron-positron annihilation is the simplest and cleanest environment in which to work. The absence of incoming hadrons eliminates initial state radiation (ISR) which could otherwise interact with the final state. We are also free from the effects of the underlying event (UE) - fragments of hadrons that did not collide. In terms of Fig. 2.4 we eliminate the lower part of the diagram coming from interactions shown in blue and purple, and their subsequent decay and hadronisation. Avoiding these hadron-hadron issues results in a system where we must only consider interactions that occur after the collision of an electron and a positron. Our Born event is the back-to-back dijet system shown in Fig 2.6a.
On top of the Born event we allow any number of extra emissions. To ensure that we stay within the relevant region for resummation - that of small-v - these emissions must have a small effect on the value of the observable. We restrict the additional emissions to be soft, collinear and widely separated in angle from each other. This limits the precision of the resummation to NLL. While we want to carry out a NNLL resummation it is instructive to first formulate the calculation at NLL. We will then use the NLL master formula as a basis for that of NNLL.

It is useful to write each emission in its Sudakov parametrisation:

$$k = z^{(1)} p_1 + z^{(2)} p_2 + k_t \,, \tag{3.11}$$

where p_1 and p_2 are light-like vectors which have

$$p_1 = \frac{Q}{2}(1, \vec{n}_T) = \frac{Q}{2}(1, 0, 0, 1) \,, \quad p_2 = \frac{Q}{2}(1, -\vec{n}_T) = \frac{Q}{2}(1, 0, 0, -1) \,, \tag{3.12}$$

and represent the hard quarks, before any additional emissions occur. The second equalities in Eq. (3.12) hold for p_1 and p_2 being identically the Born partons for the definition $Q^2 = 2p_1 \cdot p_2$. The thrust axis is denoted by $\vec{n}_T$, and $z^{(\ell)}$ is the energy fraction that k takes from p_ℓ. The gluon's transverse momentum k_t is a space-like vector orthogonal to p_1, p_2, with

$$k_t = (0, \vec{k_t}) \,, \quad k_t^2 = -k_t^2 \,. \tag{3.13}$$

As such k_t consists of a contribution in the $\vec{p_1}$-$\vec{p_2}$ plane and a contribution orthogonal to

[1] To achieve the maximal logarithmic dominance of two powers of L per α_s, as discussed in Sec. 2.2.4, one simply expands the exponential.

that plane:

$$k_t = k_t(\hat{n}_{\text{in}} \cos\phi + \hat{n}_{\text{out}} \sin\phi)\,, \tag{3.14}$$

where $\hat{n}_{\text{in}}$, $\hat{n}_{\text{out}}$ are spacelike unit vectors parametrising the other directions,

$$\hat{n}_{\text{in}} = (0,1,0,0)\,, \qquad \hat{n}_{\text{out}} = (0,0,1,0)\,. \tag{3.15}$$

The condition that k is massless implies

$$\frac{k_t^2}{Q^2} = z^{(1)} z^{(2)}\,, \tag{3.16}$$

and the rapidity is given by

$$\eta_i = \frac{1}{2} \ln\left(\frac{z_i^{(1)}}{z_i^{(2)}}\right)\,, \tag{3.17}$$

where rapidity is positive (negative) for an emission with p_1 (p_2) as its parent.

For an event consisting of the Born event $e^+e^- \to q\bar{q}$ plus a single extra soft and collinear emission k we consider observables that can be parametrised thus

$$V(\{\tilde{p}\}, k) = d_\ell \left(\frac{k_t^{(\ell)}}{Q}\right)^a e^{-b_\ell \eta^{(\ell)}} g_\ell(\phi^{(\ell)})\,. \tag{3.18}$$

$\{\tilde{p}\} = \tilde{p_1}, \tilde{p_2}$ represent the quark-antiquark pair, with the tilde signifying that their momenta are recoiled against the extra emission k.[2] The index ℓ runs over the number of hard partons, or 'legs'; here $\ell = 1, 2$. The parameters $a, b_\ell, d_\ell, g_\ell$ are constants which encode specific observable definitions within the generic expression. a does not have a leg index since, by the property of continuous globalness (Sec. 3.1.1), the observable must have the same scaling to an emission's energy everywhere. Therefore $a_1 = a_2 \equiv a$. The variables $k_t^{(\ell)}, \eta^{(\ell)}, \phi^{(\ell)}$ are respectively the emission's transverse momentum, rapidity and azimuthal angle measured with respect to its emitter $\tilde{p}_\ell$. It is easy to see that as the emission k becomes either soft or collinear to its emitter the value of the observable goes to its Born value of zero, i.e. the generic observable of Eq. (3.18) is IRC safe.

All of the observables defined in Section 2.2.5 are expressed by the parametrisation in Eq. (3.18) in the soft-collinear limit. The thrust-type event shapes can be recovered by setting $a = b_\ell = 1$ and the broadening-type by setting $a = 1, b_\ell = 0$. Outwith events which exist in the soft-collinear limit this parametrisation will in general no longer hold. The implications of this situation will be discussed in Chapter 4.

At NLL and small-v the relevant events consist of a hard diquark pair and an ensemble of soft-collinear emissions each defined in terms of its Sudakov parametrisation (Eq. (3.11)). Of course we must also consider emissions that are unresolved, as well as

[2] In practice the recoil effect will be tiny due to the huge separation in scale between the hard partons and the soft-collinear emission. See Sections 4.3.1 and 5.5.2 for discussions on recoil effects.

virtual corrections. The difference between resolved and unresolved emissions is arbitrary, depending on the value of our cutoff or, experimentally, the detector resolution. By definition unresolved emissions will not contribute to the value of the observable, but we cannot ignore them when calculating its cross-section. The line separating resolved and unresolved radiation is not a physical one, and so any cutoff cannot appear in our final result. We choose the cutoff ϵv, as introduced in Sec. 3.1.1. To ensure unitary we must allow radiation to occur across the whole of soft-collinear phase space. We collect unresolved real emissions together with virtual corrections since neither contribution has an effect on the value of the observable. In fact, the vanishingly low-enery and collinear emissions that have no contribution to the observable are exactly the source of IRC divergences. Since we know that real and virtual IRC singularities cancel at every order in perturbation theory, the combination of real unresolved emissions and virtual corrections is finite, despite being separately divergent. Generically we can write

$$\Sigma(v) = [\text{virt.} + \text{unres.}] \times \sum_{n=0}^{\infty} \frac{1}{n!} \int_{\epsilon v} \prod_{i=1}^{n} [dk_i] \mathcal{M}^2(k_i) \Theta(v - V(\{\tilde{p}\}, \{k_i\})) \,, \tag{3.19}$$

simply a phase-space integral over a product of matrix elements for the soft-collinear ensemble $\{k_i\}$, constrained by the value of the observable, multiplied by radiation not contributing to the value of the observable. $1/n!$ is a combinatorial factor encoding the various permutations of the emissions of identical particles. The one-gluon emission probability is:

$$\begin{aligned}[dk]\mathcal{M}^2(k) = dz^{(1)} dz^{(2)} \frac{d\phi}{2\pi} \frac{dk_t^2}{k_t^2} \delta\left(z^{(1)} z^{(2)} - \frac{k_t^2}{Q^2}\right) \times \\ \times \frac{\alpha_s^{\text{CMW}}(k_t) C_F}{4\pi} \frac{z^{(1)} p_{gq}(z^{(1)})}{C_F} \frac{z^{(2)} p_{gq}(z^{(2)})}{C_F} \,,\end{aligned} \tag{3.20}$$

with

$$p_{gq}(z) = C_F \frac{1 + (1-z)^2}{z} \tag{3.21}$$

the splitting-function for a gluon from a quark [39]. This encodes the likelihood that a gluon with energy fraction z will be emitted from a quark. C_F is the colour factor associated with quark-gluon vertices. α_s^{CMW} is the strong coupling plus subsequent soft branching of gluons [40], related to the more widely used $\alpha_s^{\overline{\text{MS}}}$ by

$$\alpha_s^{\text{CMW}}(k_t) = \alpha_s^{\overline{\text{MS}}}(k_t) \left(1 + \frac{\alpha_s^{\overline{\text{MS}}}(k_t)}{2\pi} K\right) + \mathcal{O}\left(\left(\alpha_s^{\overline{\text{MS}}}(k_t)\right)^3\right), \quad K = \left(\frac{67}{18} - \frac{\pi^2}{6}\right) C_A - \frac{5}{9} n_f \,. \tag{3.22}$$

K contains the remnants of the cancellation between virtual corrections and unresolved

emssions. Taking the soft-collinear limit of Eq. (3.20),

$$\begin{aligned}[dk]\mathcal{M}^2_{\text{sc}}(k) &= \lim_{\substack{z^{(1)}\to 0,\\ z^{(2)}\to 0}} [dk]\mathcal{M}^2(k) \\ &= \sum_{\ell=1,2} 2C_\ell \frac{\alpha_s^{\text{CMW}}(k_t)}{\pi}\frac{dk_t}{k_t} d\eta^{(\ell)}\,\Theta\left(\ln\left(\frac{Q}{k_t}\right) - \eta^{(\ell)}\right)\Theta(\eta^{(\ell)})\frac{d\phi}{2\pi}\,.\end{aligned} \tag{3.23}$$

3.1.3 The Sudakov Form Factor

The virtual corrections and unresolved real emssions can be captured in a so-called Sudakov factor which represents the no-emission probability. It is perhaps easier to think of a no-emission probability in terms of the textbook example of radioactive decay. The probability that no decay will occur must go to zero as time goes to infinity, whilst the probability that no decay will occur must be one at time zero. At all times the no-decay and decay probabilities must sum to one. The well-known expression for the change in population N over a given time interval is

$$dN = -\lambda N dt\,, \tag{3.24}$$

where λ is the decay constant. The survival probability at time t is

$$e^{-\lambda t}\,. \tag{3.25}$$

The analogy to time in our case is energy scale (specifically $t = \ln 1/v$), and the change in population corresponds to the gluon emission probability

$$\lambda N dt = \int [dk]\, M^2(k)\,\Theta\left(\epsilon v - V(\{\tilde{p}\}, k)\right)\,. \tag{3.26}$$

The no-emission expression now becomes a no-resolved-emission probability, but the form is the same. The probability of not emitting a gluon between two scales is equal to the initial no-emission probability multiplied by the negative change in emission probability. The probability of emitting no gluons above ϵv is

$$[\text{virt.} + \text{unres.}] = e^{-\int [dk]\, M^2(k)\,\Theta(V(\{\tilde{p}\},k)-\epsilon v)}\,, \tag{3.27}$$

the exponential of the single-gluon emission probability of Eq. (3.20). As discussed above the exact placement of this cut is arbitrary, the only requirements on ϵ being determined by rIRC safety, and having been already given in Eq. (3.7).

3.1.4 NLL Approximations

Having visited the various pieces of Eq. (3.19) we can return to the full expression, replacing the placeholder for virtual and unresolved real radiation in Eq. (3.19) with the Sudakov

form factor,

$$\Sigma(v) = e^{-\int [dk]\, M^2(k)\, \Theta(V(\{\tilde{p}\},k)-\epsilon v)} \sum_{n=0}^{\infty} \frac{1}{n!} \int \prod_{i=1}^{n} [dk_i] \mathcal{M}^2(k_i) \Theta\left(v - V(\{\tilde{p}\}, k_1, \ldots, k_n)\right) \times \\ \times \Theta\left(V(\{\tilde{p}\}, k_i) - \epsilon v\right) . \tag{3.28}$$

We note that the expressions for $\Sigma(v)$ given up to this point are in fact more general than is needed for NLL accuracy. We wish to neglect subleading terms (terms of form $\alpha_s^n L^{n-i}$ where $i > 0$), to attain a result that contains only LL and NLL terms. In the following paragraphs we will manipulate the expression in Eq. (3.28) to obtain one that is precisely NLL-accurate and can be easily implemented in computer code, or in some cases, by an analytical calculation. In order to do this we explicitly separate each piece of the expression in Eq. (3.28) into a soft-collinear, NLL-accurate part and a subleading part. In Chapter 4 we will 'undo' some of these approximations to obtain a NNLL-accurate expression.

The generic observable expression in Eq. (3.18) holds exactly to NLL accuracy, i.e. in the presence of soft-collinear emissions only. In subsequent chapters we will discuss how the expression must be modified to deal with emissions that are soft but wide-angle, or collinear but hard. To make this explicit, and to allow for ease of modification later, we write

$$\begin{aligned} \Theta\left(v - V(\{\tilde{p}\}, k_i)\right) =& \Theta\left(v - V_{\mathrm{sc}}(\{\tilde{p}\}, k_i)\right) + \\ &+ \left[\Theta\left(v - V(\{\tilde{p}\}, k_i)\right) - \Theta\left(v - V_{\mathrm{sc}}(\{\tilde{p}\}, k_i)\right)\right] , \end{aligned} \tag{3.29}$$

where now $V_{\mathrm{sc}}(\{\tilde{p}\}, k_i)$ refers to the parametrisation of Eq. (3.18) and to the observable V when all k_i are soft and collinear. At NLL we can separate the observable's dependence on the parameters (a, b_ℓ) and (d_ℓ, g_ℓ).

$$\begin{aligned} \Theta\left(V_{\mathrm{sc}}(\{\tilde{p}\}, k) - v\right) \simeq\ & \Theta\left(\ln\left(\frac{k_t}{Q}\right)^a e^{-b_\ell \eta^{(\ell)}} - \ln v\right) \\ & + \delta\left(\ln\left(\frac{k_t}{Q}\right)^a e^{-b_\ell \eta^{(\ell)}} - \ln v\right) \ln d_\ell\, g_\ell(\phi) . \end{aligned} \tag{3.30}$$

Similarly we separate the matrix element into its soft-collinear approximation and the remaining pieces

$$[dk] M^2(k) = [dk] M^2_{\mathrm{sc}}(k) + \sum_{\ell=1,2} \frac{dk_t^2}{k_t^2} \frac{dz^{(\ell)}}{z^{(\ell)}} \left(z^{(\ell)} p_\ell(z^{(\ell)}) - 2C_\ell\right) \frac{\alpha_s(k_t^2)}{2\pi} . \tag{3.31}$$

Now we introduce the 'radiator' which lives in the exponent,

$$R(\epsilon v) \equiv \int [dk]\, M^2(k)\, \Theta\left(V(\{\tilde{p}\}, k) - \epsilon v\right) = R(v) + \int_{\epsilon v}^{v} [dk] M^2(k) , \tag{3.32}$$

where the limits on the integration are taken to be limits on the observable value $V(\{\tilde{p}\}, k)$. One might be worried that separating the origins of IR divergences will introduce problems. However we do not explicitly carry out the cancellation in our calculation, but take the radiator, with only finite pieces left, from the literature. The reason we split the contributions is to cancel the dependence on the cutoff ϵ between the resolved and unresolved real emissions. Notice that $R(v)$ is a function of one emission only: all possible virtual effects are summed via the exponentiation. Substituting the observable definition and matrix element for their NLL-accurate expressions as given in Eqs. (3.30) and (3.31) into $R(v)$ gives the next-to-leading logarithmic radiator:

$$\begin{aligned} R_{\mathrm{NLL}}(v) \equiv & \int [dk] M^2_{\mathrm{sc}}(k) \sum_{\ell=1,2} \Theta\left(\ln\left(\frac{k_t}{Q}\right)^a e^{-b_\ell \eta^{(\ell)}} - \ln v\right) \Theta(\eta^{(\ell)}) \\ & + \int [dk] M^2_{\mathrm{sc}}(k) \sum_{\ell=1,2} \ln \bar{d}_\ell \, \delta\left(\ln\left(\frac{k_t}{Q}\right)^a e^{-b_\ell \eta^{(\ell)}} - \ln v\right) \Theta(\eta^{(\ell)}) \\ & + \sum_{\ell=1,2} C_\ell B_\ell \int \frac{dk_t^2}{k_t^2} \frac{\alpha_s(k_t^2)}{2\pi} \Theta\left(\ln\left(\frac{k_t}{Q}\right)^{a+b_\ell} - \ln v\right), \end{aligned} \tag{3.33}$$

where

$$C_\ell B_\ell = \int_0^1 \frac{dz}{z} \left(z p_{gq}(z) - 2C_\ell\right) = -\frac{3}{2} C_F \,, \qquad \ln \bar{d}_\ell = \int_0^{2\pi} \frac{d\phi}{2\pi} \ln d_\ell g_\ell(\phi) \,, \tag{3.34}$$

and we have used $e^{-\eta^{(\ell)}} = \frac{k_t}{Q} \frac{1}{z^{(\ell)}}$ to write

$$\Theta\left(\frac{d_\ell \, g_\ell(\phi)}{z^{b_\ell}} \left(\frac{k_t}{Q}\right)^{a+b_\ell} - v\right) \simeq \Theta\left(\ln\left(\frac{k_t}{Q}\right)^{a+b_\ell} - \ln v\right). \tag{3.35}$$

The radiator taking into account all virtual corrections to the resummation of an observable at next-to-leading logarithmic accuracy is

$$R_{\mathrm{NLL}}(v) = -L g_1(\lambda) - g_2(\lambda) \,, \tag{3.36}$$

where $\lambda = \alpha_s(Q)\beta_0 L$, $L = \ln(1/v)$ and $\beta_0 = (11N_c - 4n_f T_F)/(12\pi)$. All the information concerning the resummation of an observable is encoded within the generic parametrisation, and the kinematic particulars of every emission are integrated over phase space. Thus the functions g_1 and g_2 can be written solely in terms of the constants a, b_ℓ, d_ℓ, $g_\ell(\phi)$ as well as the QCD colour factors associated with the emission vertices. The full expressions for the $g_i(\lambda)$ functions are given in Appendix A.

We now deal with the remaining pieces of Eq. (3.28): the unresolved and the resolved

real emissions. We introduce the 'multiple emissions function':

$$\begin{aligned}\mathcal{F}(v) =& e^{-\int_{\epsilon v}^{v}[dk]\mathcal{M}^2(k)}\sum_{n=0}^{\infty}\frac{1}{n!}\int\left(\prod_i[dk_i]\mathcal{M}^2(k_i)\,\Theta\left(V(\{\tilde{p}\},k_i)-\epsilon v\right)\right)\times \\ &\times\Theta\left(v-V(\{\tilde{p}\},k_1,\ldots,k_n)\right)\,.\end{aligned} \tag{3.37}$$

Notice that the real-emission integrals in Eq. (3.37) are restricted by an upper boundary of v and a lower boundary of ϵv. This corresponds to the physical statements that the emissions must live in the logarithmically enhanced region of phase space relevant for resummation, and that they are characterised by a resolution cutoff. These two boundaries imply that the region of phase space accessible to real emissions is of size $\approx \ln\frac{1}{v}$, i.e. it is at most single logarithmic. Ignoring subleading terms in the matrix element and observable parametrisation (the second terms in Eq. (3.31), and Eqs. (3.29) and (3.30), respectively), the NLL-accurate multiple emissions function is:

$$\mathcal{F}_{\mathrm{NLL}}(v) = e^{-\int_{\epsilon v}^{v}[dk]M^2_{\mathrm{sc}}(k)}\sum_{n=0}^{\infty}\frac{1}{n!}\int_{\epsilon v}^{v}\prod_i[dk_i]\mathcal{M}^2_{\mathrm{sc}}(k_i)\,, \tag{3.38}$$

where we have used the shorthand of using integration limits as limits on the value of $V_{\mathrm{sc}}(\{\tilde{p}\},\{k_i\})$ and $V_{\mathrm{sc}}(\{\tilde{p}\},k)$ in the resolved and unresolved contributions, respectively. As expected the final result has no dependence on the resolution cutoff ϵ since the cutoff in the unresolved exponentiated expression cancels with that in the real expression.

3.1.5 Reparametrisation of the Multiple Emissions Function

Now that we have all the pieces of the resummed cross-section at our disposal we will expend some effort carrying out kinematic manipulations on the multiple emissions function. These adjustments better lend the expression to evaluation using Monte Carlo integration. There are also further assumptions that we can make on the kinematics of events valid for NLL resummation only. Explicitly showing these assumptions now will make it clear how they should be relaxed at subsequently higher levels of precision.

Firstly we introduce a variable signifying the value of the generic observable in the presence of a single soft-collinear emission k_i:

$$v_i = V_{\mathrm{sc}}(\{\tilde{p}\},k_i)\,. \tag{3.39}$$

This will allow us to rank the emissions in terms of their individual contributions. Secondly, we give each emission its rapidity fraction:

$$\xi_i^{(\ell)} = \frac{\eta_i^{(\ell)}}{\eta_{\mathrm{max}}^{(\ell)}}\,,\quad \eta_{\mathrm{max}}^{(\ell)} = \frac{1}{a+b_\ell}\ln\frac{g_\ell(\phi_i)d_\ell}{v_i}\,, \tag{3.40}$$

where η_{max} is determined by rearranging for $\eta^{(\ell)}$ in Eq. (3.18) and imposing that $z_i^{(\ell)}<1$. We employ a trick that allows us to more easily parametrise the multiple emissions func-

tion. Definining

$$R'_\ell\left(\frac{v}{d_\ell g_\ell(\bar{\phi})}\right) = \int [dk] M^2_{\rm sc}(k)\,(2\pi)\delta(\phi-\bar{\phi})\,v\delta\left(v - V_{\rm sc}(\{\tilde{p}\},k)\right)\theta(\eta^{(\ell)})\,, \tag{3.41}$$

where $\eta^{(\ell)} = +\eta$ when it is emitted by p_1 and $\eta^{(\ell)} = -\eta$ when it is emitted by p_2, with the total $R'(v,\phi)$ being the sum of each leg contribution. The soft-collinear matrix element for a single gluon becomes:

$$\begin{aligned}[dk_i]M^2_{\rm sc}(k_i) &= \frac{dv_i}{v_i}\frac{d\phi_i}{2\pi}\sum_{\ell_i=1,2} d\xi_i^{(\ell_i)}\Theta(1-\xi_i^{(\ell_i)})\Theta(\xi_i^{(\ell_i)})R'_{\ell_i}\left(\frac{v_i}{d_{\ell_i}g_{\ell_i}(\phi_i)}\right)\\ &= \frac{d\zeta_i}{\zeta_i}\frac{d\phi_i}{2\pi}\sum_{\ell_i=1,2} d\xi_i^{(\ell_i)}\Theta(1-\xi_i^{(\ell_i)})\Theta(\xi_i^{(\ell_i)})R'_{\ell_i}\left(\frac{\zeta_i v}{d_{\ell_i}g_{\ell_i}(\phi_i)}\right)\,,\end{aligned} \tag{3.42}$$

where $\zeta_i = v_i/v$. We have rephrased the phase space in terms of (ζ_i,ϕ_i,ξ_i). We can reduce the phase space further by employing the fact that event shapes have no sensitivity to the rapidity of individual emissions. We can keep v_i, ϕ_i and ℓ_i fixed, and integrate out the $\{\xi_i^{\ell_i}\}$. Integrating out the rapidity fractions gives:

$$\begin{aligned}\mathcal{F}(v) = e^{-\int \frac{d\zeta_i}{\zeta_i}\frac{d\phi_i}{2\pi}\sum_{\ell_i} R'_{\ell_i}\left(\frac{\zeta_i v}{d_{\ell_i}g_{\ell_i}(\phi_i)}\right)}\sum_{n=0}^{\infty}\frac{1}{n!}\prod_{i=1}^{n}\int_\epsilon^\infty\frac{d\zeta_i}{\zeta_i}\int_0^{2\pi}\frac{d\phi_i}{2\pi}\times\\ \times\sum_{\ell_i=1,2}R'_{\ell_i}\left(\frac{\zeta_i v}{d_{\ell_i}g_{\ell_i}(\phi_i)}\right)\Theta\left(v - V_{\rm sc}(\{\tilde{p}\},k_1,\ldots,k_n)\right)\,.\end{aligned} \tag{3.43}$$

All of the $\{k_i\}$ now possess an arbitrary rapidity fraction. We will now make one final adjustment to the multiple emissions function. The function $R'(v)$ encodes the physical rapidity bounds for each emission, but including this bound leads to a term of order NNLL, i.e. it is subleading. We can eliminate this term and produce a purely NLL-accurate result by using a 'fake' rapidity boundary:

$$|\eta_i| < \frac{1}{a+b}\ln\frac{1}{v}\,, \tag{3.44}$$

or, equivalently, by expanding $R'(v)$:

$$R'_\ell\left(\frac{\zeta v}{d_\ell g_\ell(\phi)}\right) = R'_\ell(v) + \mathcal{O}(R''_\ell) \qquad R''_\ell = -v\frac{dR'_\ell(v)}{dv}\,, \tag{3.45}$$

and further expanding $R'_\ell(v)$:

$$R'_\ell(v) = R'_{{\rm NLL},\ell}(v) + \delta R'_{{\rm NNLL},\ell}(v)\,, \tag{3.46}$$

where R''_ℓ and $\delta R'_{{\rm NNLL},\ell}(v)$ are not relevant for our calculation since they induce terms of order NNLL and beyond. The effect of including these terms is dealt with in Sec. 4.2.

With these terms removed the multiple emissions function becomes:

$$\mathcal{F}_{\rm NLL}(\lambda) = \epsilon^{R'_{\rm NLL}} \sum_{n=0}^{\infty} \frac{1}{n!} \prod_{i=1}^{n} \int_{\epsilon}^{\infty} \frac{d\zeta_i}{\zeta_i} \int_0^{2\pi} \frac{d\phi_i}{2\pi} \sum_{\ell_i=1,2} R'_{{\rm NLL},\ell_i} \Theta\left(1 - \lim_{v\to 0} \frac{V_{\rm sc}(\{\tilde{p}\}, k_1, \ldots, k_n)}{v}\right), \tag{3.47}$$

where $R'_{\rm NLL} = R'_{{\rm NLL},1} + R'_{{\rm NLL},2}$.

We take the limit $v \to 0$ in the Θ-function to remove power corrections of the form discussed above Eq. (2.9). Thus $\mathcal{F}_{\rm NLL}$ is no longer a function of v and we characterise it using the ubiquitous $\lambda = \alpha_s(Q)\beta_0 \ln(1/v)$. For future notation contraction we use Eq. (3.47) to introduce the average of a function $G(\{\tilde{p}\}, \{k_i\})$ over the measure $d\mathcal{Z}$:

$$\begin{aligned}\int d\mathcal{Z}[\{R'_{{\rm NLL},\ell_i}, k_i\}] G(\{\tilde{p}\}, \{k_i\}) = \epsilon^{R'_{\rm NLL}} \sum_{n=0}^{\infty} \frac{1}{n!} \prod_{i=1}^{n} \int_{\epsilon}^{\infty} \frac{d\zeta_i}{\zeta_i} \int_0^{2\pi} \frac{d\phi_i}{2\pi} \times \\ \times \sum_{\ell_i=1,2} R'_{{\rm NLL},\ell_i} G(\{\tilde{p}\}, k_1, \ldots, k_n)\,.\end{aligned} \tag{3.48}$$

3.1.6 The Master Formula at NLL

Finally we arrive at the master resummation formula. We have determined the form of the integrated distribution for the generic rIRC safe observable $V_{\rm sc}(\{\tilde{p}\}, \{k_i\})$, a function of all final-state momenta in an event, in the region $V_{\rm sc}(\{\tilde{p}\}, \{k_i\}) < v$. It is composed of two parts:

$$\Sigma_{\rm NLL}(v) = \frac{1}{\sigma} \int_0^v dv' \frac{d\sigma(v')}{dv'} = e^{-R_{\rm NLL}(v)} \mathcal{F}_{\rm NLL}(\lambda)\,. \tag{3.49}$$

The first term is the radiator, containing all the virtual corrections,

$$e^{-R_{\rm NLL}(v)} = e^{Lg_1(\lambda) + g_2(\lambda)}\,, \tag{3.50}$$

where the full expressions for $g_1(\lambda)$ and $g_2(\lambda)$ are given in Appendix A. The second term is the multiple emissions function, containing single logarithmic terms coming from soft-collinear real emissions that are widely separated in rapidity and independent from one another:

$$\mathcal{F}_{\rm NLL}(\lambda) = \int d\mathcal{Z}[\{R'_{{\rm NLL},\ell_i}, k_i\}] \Theta\left(1 - \lim_{v\to 0} \frac{V_{\rm sc}(\{\tilde{p}\}, k_1, \ldots, k_n)}{v}\right). \tag{3.51}$$

The phase space covered by these functions can be viewed geometrically via the Lund diagram shown in Fig. 3.1. The transverse momenta of emissions increases towards the top of the plot, with the additional kinematic z bounds restricting the hardness of an emission with a given rapidity. The absolute value of rapidity increases in both horizontal directions outwards and the central line singifies an η of zero. Given this master formula, we can semi-numerically carry out the resummation of any well-behaved observable once we have determined the coefficients $(a, b_\ell, d_\ell, g_\ell(\phi))$.

We have undertaken the derivation of the master formula using NLL-accurate assump-

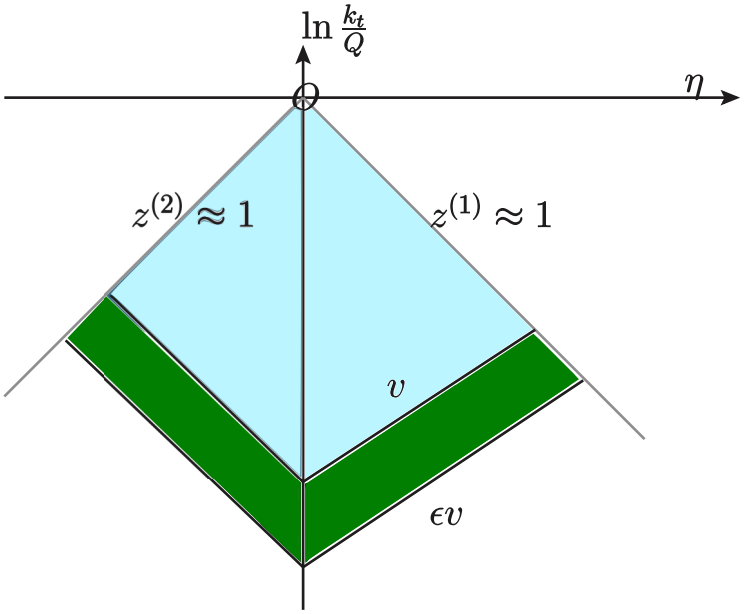

Figure 3.1: Diagram depicting the phase space in $\ln \frac{k_t}{Q}$-η captured by the Sudakov factor and the multiple emissions function. The vertical line separates the right hemisphere, inhabited by emissions emitted from p_1, from the left hemisphere in which live the emissions of p_2. The diagonal bounding lines represent the collinear limits on either leg, $z^{(\ell)} \approx 1$. The real resolved emissions live in the band bounded by v and ϵv, shaded green, whereas the unresolved real emissions and virtual corrections live in the upper region shaded blue. The lower region's size is of size $\approx \ln 1/v$, resulting in a suppression of the logarithmic accuracy of the multiple emissions function; real resolved emissions contribute with one logarithm fewer than unresolved emissions and virtual corrections.

tions, but the two-function structure of the resummation holds to all logarithmic orders. As such Eqs. (3.50) and (3.51) constitute our starting point in tackling next-to-next-to-leading logarithmic resummation. In the next chapters we will show how each term can be systematically extended to the next order of precision.

Chapter 4

Resummation of Event Shape Observables at NNLL

in which I present the ARES *method of NNLL resummation.*

The master formula derived in Sec. 3.1.6 provides us with all the ingredients necessary for NLL resummation of the generic observable parametrisation given in Eq. (3.18). In this chapter we show how the kinematics of a NLL event can be systematically extended to apply to next-to-next-to-leading logarithmic accuracy. To this end one must consider both corrections to the Sudakov form factor, and to the multiple emissions function.
The material in this chapter is based on recent collaborative work of which the resulting publication can be found in [1].

4.1 Considerations for Resummation at NNLL

4.1.1 Logarithmic Counting for the Resolved Real Emissions

In this section we will investigate the logarithmic structure of the multiple emissions function for any number of real resolved emissions. In doing so it will become clear the collections of emission properties that are relevant to consider at each order.
Consider an ensemble of soft emissions. The squared matrix element can be expressed iteratively as a sum of products of single-emission matrix elements plus a remainder $\tilde{M}^2$ describing the piece owing to the entanglement of emissions. The first few steps of this iterative definition read

$$\begin{aligned} M^2(k_1) &= \tilde{M}^2(k_1)\,, \\ M^2(k_1,k_2) &= M^2(k_1)M^2(k_2) + \tilde{M}^2(k_1,k_2)\,, \\ M^2(k_1,k_2,k_3) &= M^2(k_1)M^2(k_2)M^2(k_3) + (\tilde{M}^2(k_1,k_2)M^2(k_3) + \text{perm.}) + \\ &\quad + \tilde{M}^2(k_1,k_2,k_3)\,. \end{aligned} \tag{4.1}$$

The product of single-emission matrix elements defines the abelian contribution, while non-abelian colour factors are associated with the $\tilde{M}^2(k_1,...,k_m)$ squared amplitudes.

The $\tilde{M}^2(k_1, ..., k_m)$ matrix elements for more than one emission describe the probability of emitting m colour-connected soft partons, and they are suppressed if the involved emissions are very far in rapidity from each other. We will refer to $\tilde{M}^2(k_1, k_2)$ as the double-correlated contribution to the squared amplitude for multiple emissions.

We now study the logarithmic structure of each of the terms in Eq. (4.1). Each resolved real emission is produced by requiring that $V_{\rm sc}(\{\tilde{p}\}, k_i) > \epsilon v$, where ϵ is independent of v thanks to rIRC safety. This condition places a lower bound on the resolved emission's phase space which can potentially only give rise to a single logarithm of v (see the paragraph above Eq. (3.38)). When several emissions are considered, the same argument applies, so that each emission can at most contribute with a single logarithm. This is ensured by rIRC safety since it ensures that the observable will have the same scaling independently of the number of emissions, and therefore the condition $V_{\rm sc}(\{\tilde{p}\}, k_i) > \epsilon v$ will still impose a lower cutoff for all of the resolved emissions.
The unresolved emissions below this limit (i.e. $V_{\rm sc}(\{\tilde{p}\}, k_i) < \epsilon v$) do not contribute to the observable but serve to cancel the virtual IRC singularities. Hence a product of n independent emission matrix elements in Eq. (4.1) gives rise at most to a $\alpha_s^n L^n$ (NLL) contribution, where $L = \ln 1/v$.
$\tilde{M}^2(k_1, k_2)$ captures the colour-connected emissions effects, i.e. a soft-gluon splitting into either a $q\bar{q}$ or gg pair. The parent soft gluon carries a factor of $\alpha_s L$ and one would expect the secondary emission to have up to two extra logarithms leading to a dominant $\alpha_s^2 L^3$ term. However, rIRC safety prohibits this. Observables with this property cannot be parametrically affected by the emission of an extra soft or collinear particle. The gluon-splitting can at most lead to corrections of relative order α_s; no extra logarithms are allowed. Hence the $q\bar{q}$ or gg pair carries a term $\alpha_s^2 L$. This argument can be applied to all of the $\tilde{M}^2$ contributions, with n-particle correlations contributing at most to $\mathrm{N}^n\mathrm{LL}$ order. Additionally, multiple soft gluon splittings will lead to terms of the form $\alpha_s^n L$, which is subleading.

The argument detailed above for soft emissions equally applies to the case of one or more emissions emitted collinearly to the Born leg with high momentum. To achieve NNLL accuracy we must consider the contribution of a single splitting of a soft or collinear gluon. The contribution from a gluon parent which is soft *and* collinear and so carries a factor of $\alpha_s^2 L^2$ is encapsulated by the enhanced coupling $\alpha_s^{\rm CMW}$, given in Eq. (3.22) and explained by its preceding paragraph.

To determine the logarithmic counting of scenarios other than this we consider the regions available to ensembles of emissions. Soft, collinear and independent emissions live anywhere in a region of phase space which is of size $\ln(1/v)$ and so contribute with one logarithm fewer than unresolved emissions. Hence a NLL calculation need only take into account the contribution of ensembles of this kind. Emissions which are hard-collinear exist at the edge of phase space, in the region of $z^{(\ell)} \approx 1$. As such they live in a line of phase

space that contributes one logarithm fewer than the soft-collinear ensemble. The same is true for soft-wide angle emissions, which exist at the edge of phase space where $\eta \approx 0$. Fig. 4.1 shows the different phase space regions available to soft-collinear, soft-wide angle and hard-collinear emissions. For simplicity we have only included one hemisphere but to obtain the full picture of particles emitted from both legs one can simply imagine a mirror rotation through the vertical axis. In fact, one can also think about the correlated-matrix

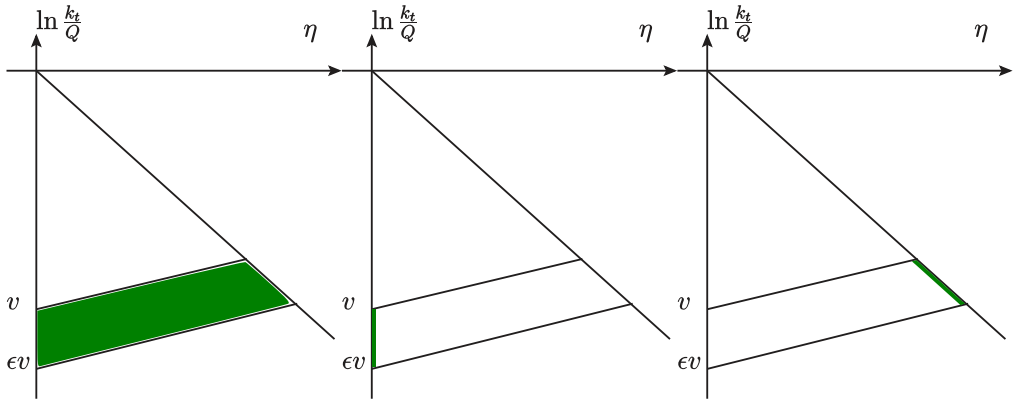

(a) Soft-collinear (b) Soft-wide angle (c) Hard-collinear

Figure 4.1: Phase spaces available to various emissions shown in one hemisphere of the Lund diagram of Fig. 3.1.

elements $\tilde{M}^2$ using the diagram of Fig. 4.1. The first soft gluon is free to choose any position within the bounds of Fig. 4.1a). As it is soft it will not recoil considerably after the secondary splitting, and its emission will live close by in k_t and η (and ϕ). As such the daughter emission cannot live anywhere in the region of soft-collinear phase space, but must end up close to its parent. This reduction in allowed phase space accounts for the prohibition of further logarithms.

Using this picture it is easy to infer the allowed scenarios for real resolved emissions at NNLL. We may have as many soft-collinear emissions as we wish, the collection contributing $\alpha_s^n L^n$, as well as the addition of *one* hard-collinear *or* soft-wide angle emission *or* extra splitting, each contributing α_s, so that the total logarithmic count is $\alpha_s^{n+1} L^n$. If we wish to limit ourselves to NLL, we simply allow an ensemble of soft-collinear emissions, as demonstrated by $F_{\text{NLL}}(\lambda)$ (Eq. (3.51)) derived in Chapter 3.
The treatments detailed above can easily be applied to any logarithmic accuracy: one simply determines the combinatorics that lead to the desired order. For instance, to N^{3}LL precision one can have an ensemble of soft-collinear emissions ($\alpha_s^n L^n$), and any *two* of the NNLL-accurate emissions: hard-collinear, soft-wide angle, gluon-splitting ($\times \alpha_s^2 = \alpha_s^{n+2} L^n$).

Additional approximations can be made that limit a resummation to a specific accuracy. For instance, in Eqs. (3.45) and (3.46) we reduced the kinematically-allowed phase space in η to neglect subleading effects. This class of approximations is not strictly neces-

sary for the resummation and their only purpose is to ensure that the multiple emissions function is free of any higher-order contamination.
Using the rIRC safety property of the generic observable and phase space considerations we have defined a logarithmic hierarchy in the multiple emissions function and systematically determined the relevant configurations that contribute to any given logarithmic order.

4.1.2 The Multiple Emissions Function at NNLL

Using the logarithmic counting arguments outlined in the previous section, we will use subsequent sections to derive the general form of $\mathcal{F}_{\rm NNLL}(v)$. We start with the NLL result and one by one include the various kinematic extensions from Sec. 4.1.1 to produce distinct NNLL kinematic functions.

The basic assumptions used to obtain $\mathcal{F}_{\rm NLL}(\lambda)$ in Eq. (3.51) were

1. each real emission k_i is soft, collinear, independent from the others, and such that $\epsilon v < V_{\rm sc}(\{\tilde{p}\}, k_i) < v$;
2. gluon splitting is treated inclusively in $R(v)$;
3. the rapidity bound of all emissions is the same.

We approximated the matrix element and the phase space in all emissions appearing in the multiple emissions function of Eq. (3.37), neglecting subleading corrections due to the exact rapidity bound for each resolved soft and collinear emission (see Eq. (3.45) and Eq. (3.46)), and the correct description of the hard-collinear region (neglecting the second piece of Eq. (3.31)). At NLL it is sufficient to treat the observable in its soft-collinear parametrisation $V_{\rm sc}$, so we neglected the second line of Eq. (3.29) to ignore any deviations to this expression.

All of the above approximations have to be relaxed for a single emission at a time, since relaxing each approximation gives rise to a correction of relative order α_s. This implies that configurations in which we correct more than one emission lead to contributions beyond NNLL which can be accordingly neglected. There are two types of correction, arising from the two classes of approximations we have made: to the matrix element and to the observable parametrisation.

We will first consider the matrix element corrections. The full expression of the multiple emissions function of Eq. (3.37)

$$\begin{aligned}\mathcal{F}(v) =& e^{-\int_{\epsilon v}^{v}[dk]\mathcal{M}^2(k)} \sum_{n=0}^{\infty} \frac{1}{n!} \int \left(\prod_i [dk_i] \mathcal{M}^2(k_i)\, \Theta\left(V(\{\tilde{p}\}, k_i) - \epsilon v\right) \right) \times \\ & \times \Theta\left(v - V(\{\tilde{p}\}, k_1, \ldots, k_n)\right)\end{aligned} \tag{4.2}$$

contains $\mathcal{F}_{\rm NLL}(\lambda)$ as well as corrections due to both the hard-collinear term of the matrix element (given by the second term of Eq. (3.31)), and to the correct rapidity bounds, which at NLL are the same for all emissions (see Eq. (3.45)). Such corrections result in the two NNLL contributions $\delta\mathcal{F}_{\rm hc}$ (computed in Sec. 4.3.2) and $\delta\mathcal{F}_{\rm sc}$ (computed in Sec. 4.2), respectively.

Eq. (4.2) also contains corrections due to any deviation from the soft-collinear observable parametrisation of Eq. (3.18). Deviations will occur when an arbitrary emission becomes hard-collinear or is emitted at a small rapidity (large angle). As was demonstrated in the logarithmic counting of Sec. 4.1.1, it is enough to consider an ensemble of soft and collinear emissions, plus a single extra emission which is free to probe the hard-collinear or the soft-wide-angle region of the phase space. We can then substitute Eq. (3.29) in the step functions in Eq. (4.2) with V, the correct parametrisation of the observable for a single emission in these limits, writing $V_{\rm hc}, V_{\rm wa}$. The corresponding NNLL corrections are: a recoil correction $\delta\mathcal{F}_{\rm rec}$ (computed in Sec. 4.3.1) which is due to the exact kinematics of a hard-collinear emission which recoils against the soft-collinear ensemble; a soft-wide-angle correction $\delta\mathcal{F}_{\rm wa}$ (computed in Sec. 4.4) which is due to a soft emission emitted near $\eta = 0$; a correlated, non-inclusive correction $\delta\mathcal{F}_{\rm correl}$ (computed in Sec. 4.5) to the inclusive treatment of the soft gluon decay in the matrix element. An important point to stress is that the soft-collinear approximation $V_{\rm sc}(\{\tilde{p}\}, k_1, \ldots, k_n)$ guarantees that all NNLL corrections arising from Eq. (4.2) are well defined and finite when the corrected emission becomes unresolved. The function

$$\delta\mathcal{F}_{\rm NNLL} = \delta\mathcal{F}_{\rm sc} + \delta\mathcal{F}_{\rm hc} + \delta\mathcal{F}_{\rm rec} + \delta\mathcal{F}_{\rm wa} + \delta\mathcal{F}_{\rm correl} \tag{4.3}$$

represents NNLL corrections due to real radiation. Sections 4.2 to 4.5 will deal with the derivation of each of these corrections in turn. We will take one emission from the soft-collinear ensemble and allow it to roam to take on the new kinematics. This emission will be called simply k, and we will pull it out of the soft-collinear measure in the formulae so as to be absolutely clear about all its properties for each correction.

4.1.3 The Sudakov Factor at NNLL

We now consider the remaining piece necessary to render $\Sigma(v)$ accurate to NNLL: the Sudakov factor. At NLL the radiator encodes the contribution of unresolved real emissions k_i with $V_{\rm sc}(\{\tilde{p}\}, k_i) < \epsilon v$ and corresponding virtual corrections. Each of these emissions is considered to be inclusive in its two-parton branchings, an effect which is encapsulated in the definition of the running coupling (Eq. (3.22)). Analogously, the NNLL Sudakov radiator has to include the effect of the inclusive soft three-parton correlation, which can be similarly dealt with by a redefinition of the coupling, together with the correct matrix element for an inclusive double collinear emission. Furthermore, it contains $\mathcal{O}(\alpha_s)$ corrections surviving the poles cancellation between real and virtual corrections (remember terms of $\Sigma(v)$ of form $C_1\alpha_s$ are NNLL).

The essential structure of the resummation is the same at NLL and NNLL so the virtual corrections and unresolved real emissions live in the exponent:

$$e^{-R_{\rm NNLL}(v)-\int_{\epsilon v}^{v}[dk]M^2(k)}, \tag{4.4}$$

where

$$\begin{aligned} R_{\rm NNLL}(v) = &\int [dk] M^2_{\rm sc}(k)\Theta\left(V_{\rm sc}(\{\tilde{p}\},k)-v\right) \\ &+\sum_{\ell=1,2}\int\frac{dk_t^2}{k_t^2}\int_0^1\frac{dz}{z}\left(zp_\ell(z)-2C_\ell\right)\frac{\alpha_s(k_t^2)}{2\pi}\Theta\left(\frac{d_\ell\, g_\ell(\phi)}{z^{b_\ell}}\left(\frac{k_t}{Q}\right)^{a+b_\ell}-v\right)+ \\ &+\frac{\alpha_s(Q)}{\pi}h(\lambda)\,, \end{aligned} \tag{4.5}$$

and where we have already placed the second term of Eq. (4.4) into the multiple emissions function of Eq. (4.2). The function $\alpha_s(Q)h(\lambda)/\pi$ contains the contribution of the triple-correlated splitting, the double hard-collinear correction and additional $\mathcal{O}(\alpha_s)$ constant terms arising from real-virtual cancellations, and corresponding running coupling effects. Eq. (4.5) contains some power-suppressed terms due to the integration limits of the non-singular phase space variables, i.e. ϕ in the soft limit and ϕ, z in the hard-collinear limit. In order to neglect these terms we have relaxed the lower bound in the z integration relative to the hard-collinear limit, and set it to zero (the physical bound being $z > k_t/Q$). In Eqs. (3.30) and (3.35) we ignored terms of the radiator in order to neglect subleading contributions. At NNLL we do the same, keeping an extra term in each expansion this time.

$$\begin{aligned} \Theta\left(d_\ell\, g_\ell(\phi)\left(\frac{k_t}{Q}\right)^a e^{-b_\ell\eta^{(\ell)}}-v\right) \simeq\ &\Theta\left(\ln\left(\frac{k_t}{Q}\right)^a e^{-b_\ell\eta^{(\ell)}}-\ln v\right) \\ &+\delta\left(\ln\left(\frac{k_t}{Q}\right)^a e^{-b_\ell\eta^{(\ell)}}-\ln v\right)\ln d_\ell\, g_\ell(\phi) \\ &+\frac{1}{2}\delta'\left(\ln\left(\frac{k_t}{Q}\right)^a e^{-b_\ell\eta^{(\ell)}}-\ln v\right)\ln^2 d_\ell\, g_\ell(\phi)\,, \end{aligned} \tag{4.6}$$

$$\begin{aligned} \Theta\left(\frac{d_\ell\, g_\ell(\phi)}{z^{b_\ell}}\left(\frac{k_t}{Q}\right)^{a+b_\ell}-v\right) \simeq\ &\Theta\left(\ln\left(\frac{k_t}{Q}\right)^{a+b_\ell}-\ln v\right)+ \\ &+\delta\left(\ln\left(\frac{k_t}{Q}\right)^{a+b_\ell}-\ln v\right)\ln\frac{d_\ell\, g_\ell(\phi)}{z^{b_\ell}}\,. \end{aligned} \tag{4.7}$$

We observe that the dependence on the normalisation $d_\ell g_\ell(\phi)$ is a local rescaling of the observable. This induces a local shift of the logarithm $\ln 1/v$ and gives rise to subleading contributions at each logarithmic order. This implies that, at NNLL accuracy, the dependence on $d_\ell g_\ell(\phi)$ in the Sudakov radiator is completely encoded in the first two integrals of Eq. (4.5), and it corresponds to a shift in the logarithms of the NLL radiator. An important consequence of this is that the function $h(\lambda)$ depends exclusively on the scaling

in η and k_t through the a and b_ℓ coefficients. One can conclude that the resummations of all observables which have the same soft-collinear scaling in k_t and η (i.e. the same a and b_ℓ coefficients) will have the same $h(\lambda)$ function. For example, the function $h(\lambda)$ will be the same for thrust $1-T$, C-parameter, and heavy jet mass ρ_H, and it can be taken from [14, 30]. The jet broadenings B_T and B_W, thrust major T_M and oblateness O are relatives of the k_t resummation, from which we take $h(\lambda)$ [34] (after replacing the constant one loop virtual corrections with the corresponding ones in $e^+e^- \to$ hadrons). We parametrise the final NNLL Sudakov radiator as

$$R_{\rm NNLL}(v) = -Lg_1(\lambda) - g_2(\lambda) - \frac{\alpha_s(Q)}{\pi} g_3(\lambda)\,. \tag{4.8}$$

The full expressions for the g_1, g_2, and g_3 functions in terms of as and b_ℓ are reported in Appendix A.

4.1.4 ϵ-independence of the Resummation

Before explicitly deriving the relevant real resolved NNLL corrections to $\Sigma(v)$ it is worth making an important remark. Our particular resummation procedure depends on a specific choice of the variable on which the cutoff ϵ is applied. This choice is reflected in the exponentiated part of the resummed cross section. Our default choice is to define unresolved emissions as those for which $V_{\rm sc}(\{\tilde{p}\}, k) < \epsilon v$, where $V_{\rm sc}$ is defined by Eq. (3.18). Different choices for ϵ will simply lead to different terms in the Sudakov exponent and in the real corrections described by the multiple emissions function. We have chosen to work in the soft-collinear prescription in which the cutoff ϵ is applied on the soft-collinear approximation of the observable for a generic emission k_i. This prescription has two advantages. It allows one to expand the multiple emissions function around the NLL result, which is simply determined by the soft-collinear approximation (meaning that the $V_{\rm sc}$ approximation of Eq. (3.18) is enough to account for all NLL contributions). It also ensures that all NNLL corrections to the multiple emissions function are finite since the singularities of any unresolved emission are encoded in the soft-collinear approximation of which the NNLL approximation is an extension. It also allows us to define the NNLL function $h(\lambda)$ in such a way that it is independent of the observable's normalisation $d_\ell g_\ell(\phi)$ and it only depends on the a and b_ℓ coefficients. As stated in the previous section, this implies that the function $h(\lambda)$ is universal for all observables which have the same a and b_ℓ scaling in the soft-collinear region.

...

To sum up, in this chapter so far we have shown that extending the NLL master formula of Eq. (3.49) involves corrections to both the Sudakov factor and the multiple emissions function. The general form of the NNLL expression for $\Sigma(v)$ is therefore

$$\Sigma(v) = e^{Lg_1(\lambda)+g_2(\lambda)+\frac{\alpha_s(Q)}{\pi}g_3(\lambda)} \left[\mathcal{F}_{\rm NLL}(\lambda) + \frac{\alpha_s(Q)}{\pi}\delta\mathcal{F}_{\rm NNLL}(\lambda)\right]. \tag{4.9}$$

As discussed, for the scope of this work we will simply take advantage of the fact the Su-

dakov factor depends only on the soft-collinear scaling of an observable. As such we will make use of previously determined NNLL pieces for the observables considered here. On the other hand the multiple emissions function at NNLL has not previously been derived, let alone calculated. Our goal in the remainder of this chapter is to compute the real emission contribution to $\Sigma(v)$ for a generic observable via the various pieces of $\delta\mathcal{F}_{\rm NNLL}(\lambda)$. In the final part of this chapter we will use a property of certain event shapes to give explicit analytic results for a subclass of observables.

4.2 Soft-collinear Correction

The first NNLL correction we consider arises when we take into account the exact rapidity bounds for a single emission in the generated soft-collinear ensemble. At NLL, the correct rapidity limit for the emission k_i,

$$\eta_i^{(\ell_i)} < \frac{1}{a+b_{\ell_i}} \ln \frac{g_\ell(\phi_i) d_\ell}{\zeta_i v}\,, \tag{4.10}$$

was replaced by $1/(a+b_{\ell_i})\ln(1/v)$ through the expansion of a single gluon contribution (Eqs. (3.45) and (3.46)) into pieces of varying logarithmic dominance. The NNLL-accurate rapidity kinematics are captured by the next term in the expansion of R'_ℓ, both in real and in virtual corrections, as follows

$$R'_\ell\left(\frac{\zeta v}{d_\ell g_\ell(\phi)}\right) \simeq R'_{{\rm NLL},\ell}(v) + \delta R'_{{\rm NNLL},\ell}(v) + R''_\ell(v) \ln \frac{d_\ell g_\ell(\phi)}{\zeta}\,. \tag{4.11}$$

Substituting the NNLL pieces of R'_ℓ into the expression for the NLL multiple emissions function of Eq. (3.51) gives

$$\begin{aligned}
\mathcal{F}(v) \simeq \epsilon^{R'_{\rm NLL}} &\left(1 - \sum_\ell \left(\delta R'_{{\rm NNLL},\ell} + R''_\ell \int \frac{d\phi}{2\pi} \ln(d_\ell g_\ell(\phi))\right) \ln\frac{1}{\epsilon} - \frac{1}{2}\sum_\ell R''_\ell \ln^2\frac{1}{\epsilon}\right) \times \\
&\times \sum_{n=0}^{\infty} \frac{1}{n!} \prod_{i=1}^{n} \int_\epsilon^\infty \frac{d\zeta_i}{\zeta_i} \int_0^{2\pi} \frac{d\phi_i}{2\pi} \sum_{\ell_i=1,2} \left(R'_{{\rm NLL},\ell_i} + \delta R'_{{\rm NNLL},\ell_i} + R''_{\ell_i} \ln \frac{d_{\ell_i} g_{\ell_i}(\phi_i)}{\zeta_i}\right) \times \\
&\times \Theta\left(1 - \lim_{v\to 0} \frac{V_{\rm sc}(\{\tilde{p}\}, k_1, \ldots, k_n)}{v}\right) \simeq \mathcal{F}_{\rm NLL}(\lambda) + \frac{\alpha_s(Q)}{\pi} \delta\mathcal{F}_{\rm sc}(\lambda)\,.
\end{aligned} \tag{4.12}$$

As demonstrated in Sec. 4.1.1, to achieve NNLL accuracy we must only correct one emission at a time. Hence in Eq. (4.12) we keep terms in the sum which are linear in $R'_{{\rm NNLL},\ell}$ or R''_{ℓ_i}. For convenience we express the virtual correction in Eq. (4.12) as the integral over an extra dummy emission as follows,

$$\ln\frac{1}{\epsilon} = \int_\epsilon^1 \frac{d\zeta}{\zeta}\,, \qquad \frac{1}{2}\ln^2\frac{1}{\epsilon} = \int_\epsilon^1 \frac{d\zeta}{\zeta} \ln\frac{1}{\zeta}\,. \tag{4.13}$$

The final form of the soft-collinear correction then reads

$$\delta\mathcal{F}_{\rm sc}(\lambda) = \frac{\pi}{\alpha_s(Q)}\int_0^\infty \frac{d\zeta}{\zeta}\int_0^{2\pi}\frac{d\phi}{2\pi}\sum_{\ell=1,2}\left(\delta R'_{\mathrm{NNLL},\ell} + R''_{\ell_i}\ln\frac{d_\ell g_\ell(\phi)}{\zeta}\right)\int d\mathcal{Z}[\{R'_{\mathrm{NLL},\ell_i}, k_i\}]\times \\ \times\left[\Theta\left(1-\lim_{v\to0}\frac{V_{\rm sc}(\{\tilde p\},k,\{k_i\})}{v}\right) - \Theta(1-\zeta)\Theta\left(1-\lim_{v\to0}\frac{V_{\rm sc}(\{\tilde p\},\{k_i\})}{v}\right)\right], \tag{4.14}$$

representing a single NNLL-accurate emission with the correct rapidity bound and an ensemble of soft-collinear emissions with the NLL-approximate rapidity bound. In the first Θ-function of Eq. (4.14), $k = k(\zeta,\phi,\ell)$ represents the additional real emission, and the second corresponds to the virtual correction, in which the special emission does not contribute to the observable. One can see that if the special emission becomes unresolved, the two Θ-functions will force the cancellation of that emission with its virtual counterpart, hence we can safely set the ζ lower integration limit to zero.

4.3 Hard-collinear Corrections

Another source of NNLL contributions arises when one of the emissions is collinear to one of the legs but hard, i.e. it carries a sizeable fraction of its emitter's energy. The probability $M^2_\ell(k)$ for the emission of a gluon k collinear to leg ℓ is given by

$$[dk]M^2_\ell(k) = \frac{C_F\alpha_s^{\rm CMW}(\tilde k_t^{(\ell)})}{4\pi}\frac{d\phi}{2\pi}\frac{d\tilde k_t^{(\ell)2}}{\tilde k_t^{(\ell)2}}dz^{(\ell)}p_{gq}(z^{(\ell)})\,, \tag{4.15}$$

where $\tilde k_t^{(\ell)}$ is the relative transverse momentum between the emitted gluon and the final state parton $\tilde p_\ell$. In Eq. (4.15), we identified the energy fraction taken by the emission with the Sudakov variable $z^{(\ell)}$ defined in Eq. (3.11). This was justified by the fact that all emissions were soft and hence do not change the energy fraction in an appreciable way. Therefore the recoiled hard legs coincide with their initial positions, $\tilde p_\ell \approx p_\ell$.
However, this is no longer true for a hard emission. Likewise the generated transverse momentum of the gluon $\tilde k_t^{(\ell)}$ relative to its emitter is different from its Sudakov transverse momentum k_t of Eq. (3.11), which is relative to the constant thrust axis. In order to reliably compute $V(\{\tilde p\},k,k_1,\ldots,k_n)$ we need to determine the emission's physical transverse momentum, i.e. that with respect to its emitter. In short we need to relate $\tilde k_t^{(\ell)}$ and k_t.
For simplicity we consider the case $\ell = 1$ and rename $\tilde k_t^{(1)} \to \tilde k_t$. We start from the Sudakov parametrisation of k with respect to the initial leg p_1 and the recoiled leg $\tilde p_1$, respectively

$$k = z^{(1)}p_1 + z^{(2)}p_2 + \kappa_t = \tilde z^{(1)}\tilde p_1 + \tilde z^{(2)}p_2 + \tilde\kappa_t\,, \tag{4.16}$$

where κ_t and $\tilde\kappa_t$ are spacelike vectors with $\kappa_t^2 = -k_t^2$ and $\tilde\kappa_t^2 = -\tilde k_t^2$. They can be related by plugging in the parametrisation of the recoiled momentum $\tilde p_1$ in terms of the Born

momenta p_1 and p_2

$$\tilde{p}_1 = z_p^{(1)} p_1 + z_p^{(2)} p_2 + p_{t,1}\,, \qquad z_p^{(2)} = \frac{p_{t,1}^2}{z_p^{(1)} Q^2}\,, \tag{4.17}$$

and requiring the equality of Eq. (4.16) to hold, obtaining

$$\vec{\tilde{k}}_t = \vec{k}_t - z^{(1)} \frac{\vec{p}_{t,1}}{z_p^{(1)}}\,. \tag{4.18}$$

From energy-momentum conservation and the fundamental property of the thrust axis, i.e. that transverse momentum is separately conserved in each hemisphere, one has

$$z_p^{(1)} = 1 - \sum_{i \in \mathcal{H}^{(1)}} z_i^{(1)} - z^{(1)} \simeq 1 - z^{(1)}\,, \qquad \vec{p}_{t,1} = -\sum_{i \in \mathcal{H}^{(1)}} \vec{k}_{t,i} - \vec{k}_t\,. \tag{4.19}$$

The above equations express the fact that the transverse momentum of emitter p_1 is exactly equal to (minus) the transverse momentum given away to its gluon emissions, and that the energy of p_1 is equal to one minus the energy given to its emissions. Substituting the expressions of $z_p^{(1)}$ and $\vec{p}_{t,1}$ in Eq. (4.18) we obtain

$$\vec{\tilde{k}}_t \simeq \vec{k}_t - z^{(1)} \frac{\vec{p}_{t,1}}{1 - z^{(1)}} = \vec{k}_t + \frac{z^{(1)}}{1 - z^{(1)}} \left(\sum_{i \in \mathcal{H}^{(1)}} \vec{k}_{t,i} + \vec{k}_t \right) = \frac{\vec{k}_t - z^{(1)} \vec{p}^{\,\prime}_{t,1}}{1 - z^{(1)}}\,. \tag{4.20}$$

Defining $\vec{k}_t^{\,\prime} \equiv \vec{k}_t - z^{(1)} \vec{p}^{\,\prime}_{t,1}$ we arrive at

$$\vec{\tilde{k}}_t = \vec{k}_t^{\,\prime} / (1 - z^{(1)})\,. \tag{4.21}$$

Since $\vec{\tilde{k}}_t$ and $\vec{k}_t^{\,\prime}$ are related by a simple rescaling, in the collinear matrix element squared of Eq. (4.15) we can replace $d\tilde{k}_t^2/\tilde{k}_t^2$ with $dk_t'^2/k_t'^2$. We then obtain the relation between the transverse momentum with respect to the thrust axis $\vec{k}_t$ and the transverse momentum $\vec{k}_t^{\,\prime}$ which enters the collinear emission phase space,

$$\vec{k}_t = \vec{k}_t^{\,\prime} + z^{(1)} \vec{p}^{\,\prime}_{t,1}\,. \tag{4.22}$$

This implies that the hard gluon momentum k becomes a function of $\vec{k}_t^{\,\prime}, \vec{p}^{\,\prime}_{t,1}, z^{(1)}$. For the sake of simplicity, we drop the vector superscript from now on.

4.3.1 Observable-Definition Correction: Recoil

We have two NNLL contributions coming from the hard-collinear kinematics of Sec. 4.3. The first comes from replacing the soft-collinear observable parametrisation of Eq. (3.18) with the exact expression of the observable when a single emission is hard and collinear. We take the difference between the multiple emissions function with $V = V_{\mathrm{hc}}$ and that

with $V = V_{\rm sc}$,

$$\mathcal{F}_{\rm rec}(v) = e^{-\int_{\epsilon v}^{v}[dk]M^2_{\rm sc}(k)} \sum_{n=0}^{\infty} \frac{1}{n!} \int_{\epsilon v} \prod_{i=1}^{n} [dk_i] M^2_{\rm sc}(k_i) \sum_{\ell=1,2} \int_0^1 dz\, p_\ell(z) \int_0^{2\pi} \frac{d\phi}{2\pi} \int \frac{dk_t'^2}{k_t'^2} \frac{\alpha_s(k_t')}{2\pi} \times$$
$$\times \left[\Theta\left(v - V^{(k)}_{\rm hc}(\{\tilde{p}\}, k[k_t', p'_{t,\ell}, z], k_1, \ldots, k_n)\right) - \Theta\left(v - V_{\rm sc}(\{\tilde{p}\}, k[k_t', p'_{t,\ell}, 0], k_1, \ldots, k_n)\right)\right] . \tag{4.23}$$

$V^{(k)}_{\rm hc}(\{\tilde{p}\}, k[k_t', p'_{t,\ell}, z], k_1, \ldots, k_n)$ denotes the expression of the observable V where all emissions but k are treated in the soft-collinear approximation. The original $V_{\rm sc}(\{\tilde{p}\}, k, k_1, \ldots, k_n)$ treats emission k as if it were soft and collinear, so that its transverse momentum with respect to the emitting leg k_t' is equal to k_t. Notice that in Eq. (4.23) we can replace k_t' with k_t in the integration since this variable is integrated over.

To NNLL accuracy it is possible to further simplify the phase-space for k. Introducing the rescaled contribution of a single emission as we did in Eq. (3.42) of Sec. 3.1.5,

$$\zeta = \frac{1}{v} \frac{d_\ell\, g_\ell(\phi)}{z^{b_\ell}} \left(\frac{k_t}{Q}\right)^{a+b_\ell} , \tag{4.24}$$

we have, at NNLL accuracy,

$$\frac{dk_t^2}{k_t^2} \frac{\alpha_s(k_t)}{2\pi} = \frac{\alpha_s((z^{b_\ell}\zeta v/(d_\ell\, g_\ell(\phi)))^{1/(a+b_\ell)}Q)}{\pi(a+b_\ell)} \frac{d\zeta}{\zeta} \simeq \frac{\alpha_s(v^{1/(a+b_\ell)}Q)}{\pi(a+b_\ell)} \frac{d\zeta}{\zeta} . \tag{4.25}$$

rIRC safety constrains all emissions to have similarly sized contributions to the observable, so that $\zeta \sim 1$ and further terms arising from the expansion of the QCD coupling around $v^{1/(a+b_\ell)}Q$ are of relative subleading order α_s^2.

The final form of the recoil correction is

$$\delta\mathcal{F}_{\rm rec}(\lambda) = \sum_{\ell=1,2} \frac{\alpha_s(v^{1/(a+b_\ell)}Q)}{\alpha_s(Q)(a+b_\ell)} \int_0^\infty \frac{d\zeta}{\zeta} \int_0^{2\pi} \frac{d\phi}{2\pi} \int d\mathcal{Z}[\{R'_{{\rm NLL},\ell_i}, k_i\}] \times$$
$$\times \int_0^1 dz\, p_\ell(z) \left[\Theta\left(1 - \lim_{v\to 0} \frac{V^{(k')}_{\rm hc}(\{\tilde{p}\}, k', \{k_i\})}{v}\right) - \Theta\left(1 - \lim_{v\to 0} \frac{V_{\rm sc}(\{\tilde{p}\}, k, \{k_i\})}{v}\right)\right] , \tag{4.26}$$

where we have replaced, for conciseness,

$$k' = k[k_t, p'_{t,1}, z] , \qquad k = k[k_t, p'_{t,1}, 0] . \tag{4.27}$$

4.3.2 Matrix Element Correction

The second NNLL contribution coming from hard-collinear radiation arises from taking the exact hard-collinear matrix element for a single emission,

$$\begin{aligned}\mathcal{F}_{\text{collinear}}(v) =& e^{-\int_{\epsilon v}^{v}[dk]M^2_{\text{sc}}(k)}\sum_{n=0}^{\infty}\frac{1}{n!}\int_{\epsilon v}\prod_{i=1}^{n}[dk_i]M^2_{\text{sc}}(k_i)\times\\ &\times\sum_{\ell=1,2}\int_0^1 dz\, p_\ell(z)\int_0^{2\pi}\frac{d\phi}{2\pi}\int\frac{dk_t^2}{k_t^2}\frac{\alpha_s(k_t)}{2\pi}\times\\ &\times\left[\Theta\left(v-V_{\text{sc}}(\{\tilde{p}\},k,k_1,\ldots,k_n)\right)-\Theta\left(v-V_{\text{sc}}(\{\tilde{p}\},k_1,\ldots,k_n)\right)\Theta\left(v-V_{\text{sc}}(\{\tilde{p}\},k)\right)\right],\end{aligned} \tag{4.28}$$

where the second line contains the contribution from the hard-collinear gluon k. The second term in the square brackets represents virtual corrections. In the limit where k is soft, i.e. $z\to 0$, Eq. (4.28) contains configurations that have been already taken into account in the function $\mathcal{F}_{\text{NLL}}(\lambda)$ of Eq. (3.51). To eliminate this overlap we will subtract the NLL contribution

$$\begin{aligned}\mathcal{F}^{\text{NLL}}_{\text{collinear}}(v) =& e^{-\int_{\epsilon v}^{v}[dk]M^2_{\text{sc}}(k)}\sum_{n=0}^{\infty}\frac{1}{n!}\int_{\epsilon v}\prod_{i=1}^{n}[dk_i]M^2_{\text{sc}}(k_i)\int_0^{2\pi}\frac{d\phi}{2\pi}\int\frac{dk_t^2}{k_t^2}\frac{\alpha_s(k_t)}{2\pi}\sum_{\ell=1,2}2C_\ell\int_0^1\frac{dz}{z}\\ &\times\left[\Theta\left(v-V_{\text{sc}}(\{\tilde{p}\},k,k_1,\ldots,k_n)\right)-\Theta\left(v-V_{\text{sc}}(\{\tilde{p}\},k_1,\ldots,k_n)\right)\Theta\left(v-V_{\text{sc}}(\{\tilde{p}\},k)\right)\right].\end{aligned} \tag{4.29}$$

Rephrasing in terms of the individual emission contribution ζ and subsequently adjusting the phase space, as we did for $\delta\mathcal{F}_{\text{rec}}$, we arrive at

$$\begin{aligned}\delta\mathcal{F}_{\text{hc}}(\lambda) =& \sum_{\ell=1,2}\frac{\alpha_s(v^{1/(a+b_\ell)}Q)}{\alpha_s(Q)(a+b_\ell)}\int_0^\infty\frac{d\zeta}{\zeta}\int_0^{2\pi}\frac{d\phi}{2\pi}\int d\mathcal{Z}[\{R'_{\text{NLL},\ell_i},k_i\}]\times\\ &\times\int_0^1\frac{dz}{z}\left(zp_\ell(z)-2C_\ell\right)\left[\Theta\left(1-\lim_{v\to0}\frac{V_{\text{sc}}(\{\tilde{p}\},k,\{k_i\})}{v}\right)-\Theta\left(1-\lim_{v\to0}\frac{V_{\text{sc}}(\{\tilde{p}\},\{k_i\})}{v}\right)\Theta(1-\zeta)\right].\end{aligned} \tag{4.30}$$

4.4 Soft-wide angle Correction

This contribution arises when one of the soft-collinear gluons is allowed to roam to wide angles. In general the soft-collinear observable parametrisation of Eq. (3.18) will no longer hold for the special wide-angle emission. We can parametrise the observable's dependence on the angular properties of this gluon k as

$$V^{(k)}_{\text{wa}}(\{\tilde{p}\},k)=\left(\frac{k_t}{Q}\right)^a f_{\text{wa}}(\eta,\phi)\,. \tag{4.31}$$

$V^{(k)}_{\text{wa}}(\{\tilde{p}\},k,k_1,\ldots,k_n)$ denotes the observable computed by keeping the exact η,ϕ dependence of emission k, and using the soft-collinear approximation for all other emissions. For ease of comparison we recast the soft-collinear expression, valid when η is close to zero

(wide angles),

$$V_{\rm sc}(\{\tilde{p}\},k)=\left(\frac{k_t}{Q}\right)^a f_{\rm sc}(\eta,\phi)\,,\qquad f_{\rm sc}(\eta,\phi)=d_1e^{-b_1\eta}g_1(\phi)\Theta(\eta)+d_2e^{b_2\eta}g_2(\phi)\Theta(-\eta)\,. \tag{4.32}$$

This gives rise to the following correction

$$\begin{aligned}\mathcal{F}_{\rm wa}(v)=e^{-\int_{\epsilon v}^{v}[dk]M^2_{\rm sc}(k)}\sum_{n=0}^{\infty}\frac{1}{n!}\int_{\epsilon v}\prod_{i=1}^{n}[dk_i]M^2_{\rm sc}(k_i)\times\\ \times 2C_F\int_0^\infty\frac{dk_t}{k_t}\frac{\alpha_s(k_t)}{\pi}\int_{-\infty}^{\infty}d\eta\int_0^{2\pi}\frac{d\phi}{2\pi}\times\\ \times\left[\Theta\left(1-\lim_{v\to0}\frac{V^{(k)}_{\rm wa}(\{\tilde{p}\},k,k_1,\dots,k_n)}{v}\right)-\Theta\left(1-\lim_{v\to0}\frac{V_{\rm sc}(\{\tilde{p}\},k,k_1,\dots,k_n)}{v}\right)\right]\,,\end{aligned} \tag{4.33}$$

where the second line gives the contribution due to the soft-wide angle emission k. We can modify the phase space integration for the extra soft gluon in terms of its individual contribution to the observable,

$$\frac{dk_t}{k_t}\frac{\alpha_s(k_t)}{\pi}=\frac{d\zeta}{\zeta}\frac{\alpha_s((\zeta v)^{1/a}Q)}{a\pi}\simeq\frac{d\zeta}{\zeta}\frac{\alpha_s(v^{1/a}Q)}{a\pi}\,, \tag{4.34}$$

where

$$\zeta=\frac{1}{v}\left(\frac{k_t}{Q}\right)^a \tag{4.35}$$

is constrained to be of order one for rIRC safe observables. This ensures that the approximation in Eq. (4.34) is valid up to corrections beyond NNLL accuracy. The correction to the NLL multiple emissions function due to a single gluon emitted at wide angles is

$$\begin{aligned}\delta\mathcal{F}_{\rm wa}(\lambda)=\frac{2C_F}{a}\frac{\alpha_s(v^{1/a}Q)}{\alpha_s(Q)}\int_0^\infty\frac{d\zeta}{\zeta}\int_{-\infty}^{\infty}d\eta\int_0^{2\pi}\frac{d\phi}{2\pi}\int d\mathcal{Z}[\{R'_{{\rm NLL},\ell_i},k_i\}]\\ \times\left[\Theta\left(1-\lim_{v\to0}\frac{V^{(k)}_{\rm wa}(\{\tilde{p}\},k,\{k_i\})}{v}\right)-\Theta\left(1-\lim_{v\to0}\frac{V_{\rm sc}(\{\tilde{p}\},k,\{k_i\})}{v}\right)\right]\,.\end{aligned} \tag{4.36}$$

4.5 Correlated Correction

Unlike the hard-collinear and soft wide-angle emissions, an arbitrary amount of soft and collinear emissions contribute to $\Sigma(v)$. Primary gluons emitted off the hard Born legs can give rise to subsequent branchings which are taken into account at NLL accuracy as in formulated in the CAESAR methodology [3]. However, at this accuracy any rIRC observable can be treated inclusively with respect to subsequent branchings of the soft gluons. Hence the branchings are dealt with in a redefinition of the scheme for the QCD running coupling (Eq. (3.22)). This means that each soft and collinear emission contributing to NLL accuracy is fully inclusive in its branchings.

Event-shape variables are commonly non-inclusive for such splittings, however. This behaviour must be considered from NNLL accuracy [3] (and proof of this fact is included

in Sec. 4.1.1). At NNLL, the observable is sensitive to the details of the secondary soft splitting, so we need to undo a single inclusive branching in order to compute the corresponding NNLL correction. We capture these kinematics using two special emissions, k_a and k_b, which are emitted close in rapidity from parent gluon k. At NLL accuracy the observable treats the correlated emissions inclusively $V_{\rm sc}(\{\tilde{p}\}, k_a, k_b) \equiv V_{\rm sc}(\{\tilde{p}\}, k_a + k_b)$. The correlated correction computes the case in which this is no longer assumed.

$$\begin{aligned}\delta\mathcal{F}_{\rm correl}(v) = e^{-\int_{\epsilon v}^{v}[dk]M^2_{\rm sc}(k)} \sum_{n=0}^{\infty} \frac{1}{n!} \int_{\epsilon v} \prod_{i=1}^{n} [dk_i] M^2_{\rm sc}(k_i) \frac{1}{2!} \int [dk_a][dk_b] \tilde{M}^2(k_a, k_b) \times \\ \times \left[\Theta\left(v - V_{\rm sc}(\{\tilde{p}\}, k_a, k_b, k_1, \ldots, k_n)\right) - \Theta\left(v - V_{\rm sc}(\{\tilde{p}\}, k_a + k_b, k_1, \ldots, k_n)\right)\right] ,\end{aligned} \tag{4.37}$$

where $\tilde{M}^2(k_a, k_b)$ is a two-parton correlated matrix element, defined by

$$\tilde{M}^2(k_a, k_b) = M^2(k_a, k_b) - M^2(k_a) M^2(k_b) . \tag{4.38}$$

We obtain the expression for the correlated matrix element from the literature [41]. We parametrise the correlated phase space,

$$[dk_a][dk_b]\tilde{M}^2(k_a, k_b) = [dk_a][dk_b] M^2_{\rm sc}(k_a) M^2_{\rm sc}(k_b) \frac{\tilde{M}^2(k_a, k_b)}{M^2_{\rm sc}(k_a) M^2_{\rm sc}(k_b)} . \tag{4.39}$$

We rewrite the k_a integration using its contribution to the observable, v_a,

$$\begin{aligned}[dk_a] M^2_{\rm sc}(k_a) &= \frac{dv_a}{v_a} \frac{d\phi_a}{2\pi} \int [dk_a] M^2_{\rm sc}(k_a) \sum_{\ell_a} v_a \delta\left(v_a - \left(\frac{k_{ta}}{Q}\right)^a e^{-b_{\ell_a} \eta_a^{(\ell_a)}}\right) \Theta\left(\eta_a^{(\ell_a)}\right) \\ &\simeq \frac{d\zeta_a}{\zeta_a} \frac{d\phi_a}{2\pi} \int [dk_a] M^2_{\rm sc}(k_a) \sum_{\ell_a} v \delta\left(v - \left(\frac{k_{ta}}{Q}\right)^a e^{-b_{\ell_a} \eta_a^{(\ell_a)}}\right) \Theta\left(\eta_a^{(\ell_a)}\right) ,\end{aligned} \tag{4.40}$$

where, in the last line, we have defined $\zeta_a = v_a/v$, and neglected terms beyond NNLL accuracy, using the fact that rIRC safety constrains ζ_a to be of order one.

We then parametrise the phase space of the emission k_b in terms of k_a via the variables $\kappa = k_{t,b}/k_{t,a}$, $\eta = \eta_b - \eta_a$ and $\phi = \phi_b - \phi_a$,

$$[dk_b] M^2_{\rm sc}(k_b) = \left(\frac{2C_F \alpha_s(k_{t,b})}{\pi}\right) \frac{d\kappa}{\kappa} \Theta(\kappa) d\eta \frac{d\phi}{2\pi} \simeq \left(\frac{2C_F \alpha_s(k_{t,a})}{\pi}\right) \frac{d\kappa}{\kappa} \Theta(\kappa) d\eta \frac{d\phi}{2\pi} , \tag{4.41}$$

where in the last step we have set $k_{t,b} \simeq k_{t,a}$, a relation holding to NNLL accuracy by rIRC safety. Furthermore, we assume that k_b belongs to the same hemisphere as k_a, neglecting de facto the (subleading) contribution of two emissions falling into two different hemispheres.

Therefore, the phase space of the correlated emissions k_a and k_b can be rewritten as

$$[dk_a][dk_b]\tilde{M}^2(k_a,k_b) = \frac{d\zeta_a}{\zeta_a}\frac{d\phi_a}{2\pi}\sum_{\ell_a=1,2}\left(\frac{2C_{\ell_a}\lambda}{a\pi\beta_0}R''_{\ell_a}(v)\right)\frac{d\kappa}{\kappa}\Theta(\kappa)d\eta\frac{d\phi}{2\pi}C_{ab}(\kappa,\eta,\phi)\,, \quad (4.42)$$

where

$$C_{ab}(\kappa,\eta,\phi) = \frac{\tilde{M}^2(k_a,k_b)}{M^2_{\rm sc}(k_a)M^2_{\rm sc}(k_b)}\,, \quad (4.43)$$

and

$$\begin{aligned}\int[dk]M^2_{\rm sc}(k)\Theta(\eta)\left(\frac{2C_F\alpha_s(k_t)}{\pi}\right)v\delta\left(v-\left(\frac{k_t}{Q}\right)^a e^{-b_1\eta^{(1)}}\right) &= \frac{2C_F\lambda}{a\pi\beta_0}R''_1(v)\,,\\ \int[dk]M^2_{\rm sc}(k)\Theta(-\eta)\left(\frac{2C_F\alpha_s(k_t)}{\pi}\right)v\delta\left(v-\left(\frac{k_t}{Q}\right)^a e^{-b_2\eta^{(2)}}\right) &= \frac{2C_F\lambda}{a\pi\beta_0}R''_2(v)\,.\end{aligned} \quad (4.44)$$

The correction to the NLL multiple emissions function due to the non-inclusive treatment of secondary gluon branching is

$$\begin{aligned}\delta\mathcal{F}_{\rm correl}(\lambda) = \int_0^\infty\frac{d\zeta_a}{\zeta_a}\int_0^{2\pi}\frac{d\phi_a}{2\pi}\sum_{\ell_a=1,2}\left(\frac{2C_{\ell_a}\lambda}{a\beta_0}\frac{R''_{\ell_a}(v)}{\alpha_s(Q)}\right)\times\\ \times\int_0^\infty\frac{d\kappa}{\kappa}\int_{-\infty}^\infty d\eta\int_0^{2\pi}\frac{d\phi}{2\pi}\frac{1}{2!}C_{ab}(\kappa,\eta,\phi)\int d\mathcal{Z}[\{R'_{{\rm NLL},\ell_i},k_i\}]\times\\ \times\left[\Theta\left(v-V_{\rm sc}(\{\tilde{p}\},k_a,k_b,\{k_i\})\right)-\Theta\left(v-V_{\rm sc}(\{\tilde{p}\},k_a+k_b,\{k_i\})\right)\right]\,,\end{aligned} \quad (4.45)$$

where, as usual, the observable's value does not depend on emissions' rapidities, with the exception of k_b, given that it must be close in rapidity to k_a,

$$k_b = \kappa\,k_{t,a}^{(\ell_a)}(\cosh(\eta_a+\eta),\cos(\phi_a+\phi),\sin(\phi_a+\phi),\sinh(\eta_a+\eta))\,,\qquad k_{t,a}^{(\ell_a)} = Q\,v_a^{\left(\frac{1}{a}-\frac{b_{\ell_a}}{a+b_{\ell_a}}\xi_a^{(\ell_a)}\right)}\,. \quad (4.46)$$

4.6 Analytic Results for Additive Observables

Up to this point our study of NNLL corrections to the multiple emissions function of Eq. (3.51) have been relevant for all continuously global and rIRC safe observables obeying the parameterisation of Eq. (3.18) in the soft-collinear limit. We will now give specific results for a subclass of observables, namely those which are additive. Discussed in Sec. 2.2.5, the equation below holds for additive observables such as thrust, heavy-jet mass and the C-parameter.

$$V(\{\tilde{p}\},k_1,\ldots,k_n) = \sum_{i=1}^n V(\{\tilde{p}\},k_i)+\mathcal{O}(V^2)\,, \quad (4.47)$$

where $V = V_{\rm sc}(\{\tilde{p}\},k_1,\ldots,k_n)$ as long as all the emissions in the event are soft-collinear. For hard (or wide-angle) emissions we simply replace $V(\{\tilde{p}\},k)$ with $V_{\rm hc}(\{\tilde{p}\},k')$ ($V_{\rm wa}(\{\tilde{p}\},k)$), defined in Secs. 4.3.1 and 4.4, respectively.

Dealing with additive observables allows us to make further simplications to the $\delta\mathcal{F}$ functions derived in this chapter. Attaining analytic results for selected observables provides a valuable cross-check of our numerical results.

4.6.1 NLL Multiple Emissions Function

For completeness, we include the expression for the NLL multiple emissions function for an additive observable. The calculation of real resolved radiation to the NLL resummation of such an observable can be done analytically. The result, which first appeared in [15], is

$$\mathcal{F}_{\rm NLL}(\lambda) = \frac{e^{-\gamma_E R'_{\rm NLL}(v)}}{\Gamma(1+R'_{\rm NLL}(v))}\,, \tag{4.48}$$

where γ_E is the Euler constant.

4.6.2 Soft-collinear Correction

Considering the soft-collinear contribution $\delta\mathcal{F}_{\rm sc}$ of Eq. (4.14), and using the fact that for additive observables,

$$V_{\rm sc}(\{\tilde{p}\},k,\{k_i\}) = \zeta v + V_{\rm sc}(\{\tilde{p}\},\{k_i\})\,, \tag{4.49}$$

we get

$$\begin{aligned}\delta\mathcal{F}_{\rm sc}(\lambda) = \frac{\pi}{\alpha_s(Q)}\int_0^\infty \frac{d\zeta}{\zeta}\sum_{\ell=1,2}\left(\delta R'_{{\rm NNLL},\ell} + R''_{\ell_i}\ln\bar{d}_\ell + R''_{\ell_i}\ln\frac{1}{\zeta}\right)\int d\mathcal{Z}[\{R'_{{\rm NLL},\ell_i},k_i\}]\times \\ \times\left[\Theta\left(1-\zeta-\lim_{v\to0}\frac{V_{\rm sc}(\{\tilde{p}\},\{k_i\})}{v}\right)-\Theta(1-\zeta)\Theta\left(1-\lim_{v\to0}\frac{V_{\rm sc}(\{\tilde{p}\},\{k_i\})}{v}\right)\right]\,,\end{aligned} \tag{4.50}$$

where k is the special emission exhibiting its true kinematic rapidity bounds.

We can define rescaled momenta $\tilde{k}_1,\ldots,\tilde{k}_n$ in the first theta function such that $V_{\rm sc}(\{\tilde{p}\},\tilde{k}_i) = V_{\rm sc}(\{\tilde{p}\},k_i)/(1-\zeta)$. Recursive IRC safety of V guarantees that a rescaling of the emissions' contribution to the observable will not affect the value of $\delta\mathcal{F}_{\rm sc}(\lambda)$. Using the explicit expression for $d\mathcal{Z}$, and defining $\tilde{\zeta}_i = V_{\rm sc}(\{\tilde{p}\},\tilde{k}_i)/v$, one gets

$$\begin{aligned}\delta\mathcal{F}_{\rm sc}(\lambda) =& \frac{\pi}{\alpha_s(Q)}\int_0^\infty\frac{d\zeta}{\zeta}\sum_{\ell=1,2}\left(\delta R'_{{\rm NNLL},\ell}+R''_{\ell_i}\ln\bar{d}_\ell+R''_{\ell_i}\ln\frac{1}{\zeta}\right)\times \\ &\times\epsilon^{R'_{\rm NLL}}\sum_{n=0}^\infty\frac{1}{n!}\prod_{i=1}^n\sum_{\ell_i=1,2}R'_{{\rm NLL},\ell_i}\int_0^{2\pi}\frac{d\phi_i}{2\pi}\Theta(1-\zeta)\times \\ &\times\left[\int_{\frac{\epsilon}{1-\zeta}}^\infty\frac{d\tilde{\zeta}_i}{\tilde{\zeta}_i}\Theta\left(1-\lim_{v\to0}\frac{V_{\rm sc}(\{\tilde{p}\},\{\tilde{k}_i\})}{v}\right)-\int_\epsilon^\infty\frac{d\zeta_i}{\zeta_i}\Theta\left(1-\lim_{v\to0}\frac{V_{\rm sc}(\{\tilde{p}\},\{k_i\})}{v}\right)\right]\,.\end{aligned} \tag{4.51}$$

We can then rearrange the above equation to reconstruct the known function $\mathcal{F}_{\rm NLL}(\lambda)$

(Eq. (4.48)). This gives

$$\begin{aligned}\delta\mathcal{F}_{\rm sc}(\lambda) &= \mathcal{F}_{\rm NLL}(\lambda)\frac{\pi}{\alpha_s(Q)}\int_0^1\frac{d\zeta}{\zeta}\sum_{\ell=1,2}\left(\delta R'_{{\rm NNLL},\ell}+R''_{\ell_i}\ln\bar{d}_\ell+R''_{\ell_i}\ln\frac{1}{\zeta}\right)\left((1-\zeta)^{R'_{\rm NLL}}-1\right)\\ &= -\mathcal{F}_{\rm NLL}(\lambda)\frac{\pi}{\alpha_s(Q)}\sum_{\ell=1,2}\left(\left(\delta R'_{{\rm NNLL},\ell}+R''_{\ell_i}\ln\bar{d}_\ell\right)\left(\psi^{(0)}(1+R'_{\rm NLL})+\gamma_E\right)\right.\\ &\left.+\frac{R''_{\ell_i}}{2}\left(\left(\psi^{(0)}(1+R'_{\rm NLL})+\gamma_E\right)^2-\psi^{(1)}(1+R'_{\rm NLL})+\frac{\pi^2}{6}\right)\right),\end{aligned} \tag{4.52}$$

where $\psi^{(0)}(x)$ is the digamma function and $\psi^{(1)}(x)$ is the first derivative of $\psi^{(0)}(x)$.

4.6.3 Recoil Correction

Let us now consider the recoil contribution $\delta\mathcal{F}_{\rm rec}$ of Eq. (4.26). Considering a hard emission collinear to leg ℓ for an additive observable one has, in general,

$$V_{\rm hc}^{(k')}(\{\tilde{p}\},k',\{k_i\}) = \left(\frac{k'_t}{Q}\right)^{a+b_\ell} f^{(\ell)}(z^{(\ell)},\phi)+V_{\rm sc}(\{\tilde{p}\},\{k_i\}), \tag{4.53}$$

and

$$V_{\rm sc}(\{\tilde{p}\},k,\{k_i\}) = \left(\frac{k_t}{Q}\right)^{a+b_\ell} f_{\rm sc}^{(\ell)}(z^{(\ell)},\phi)+V_{\rm sc}(\{\tilde{p}\},\{k_i\}), \tag{4.54}$$

where the presence of k', rather than k, denotes that the full recoil has been taken into account in the calculation of the observable.
Substituting the above equations in the expression for the recoil correction Eq. (4.26) we get

$$\begin{aligned}\delta\mathcal{F}_{\rm rec}(\lambda) = \sum_{\ell=1,2}\frac{\alpha_s(v^{1/(a+b_\ell)}Q)}{\alpha_s(Q)(a+b_\ell)}\int_0^\infty\frac{d\zeta}{\zeta}\int_0^{2\pi}\frac{d\phi}{2\pi}\int d\mathcal{Z}[\{R'_{{\rm NLL},\ell_i},k_i\}]\int_0^1 dz\,p_\ell(z)\times\\ \times\left[\Theta\left(1-\zeta f^{(\ell)}(z,\phi)-\lim_{v\to0}\frac{V_{\rm sc}(\{\tilde{p}\},\{k_i\})}{v}\right)-\Theta\left(1-\zeta f_{\rm sc}^{(\ell)}(z,\phi)-\lim_{v\to0}\frac{V_{\rm sc}(\{\tilde{p}\},\{k_i\})}{v}\right)\right],\end{aligned} \tag{4.55}$$

where ζ is defined in Eq. (4.24). We can define rescaled momenta $\tilde{k}_1,\ldots,\tilde{k}_n$ in the second theta function such that $V_{\rm sc}(\{\tilde{p}\},\tilde{k}_i) = V_{\rm sc}(\{\tilde{p}\},k_i)/(1-\zeta f_{\rm sc}^{(\ell)}(z,\phi))$. Recursive IRC safety of V guarantees that we can safely do this for every emission and that the resulting full observable will be

$$V_{\rm sc}(\{\tilde{p}\},k_1,\ldots,k_n) = (1-\zeta f_{\rm sc}^{(\ell)}(z,\phi))V_{\rm sc}(\{\tilde{p}\},\tilde{k}_1,\ldots,\tilde{k}_n). \tag{4.56}$$

Analogously, we define soft and collinear momenta $\tilde{k}'_1,\ldots,\tilde{k}'_n$ in the theta function containing $f^{(\ell)}(z,\phi)$) such that

$$V_{\rm sc}(\{\tilde{p}\},k_1,\ldots,k_n) = (1-\zeta f^{(\ell)}(z,\phi))V_{\rm sc}(\{\tilde{p}\},\tilde{k}'_1,\ldots,\tilde{k}'_n). \tag{4.57}$$

Using the explicit expression for $d\mathcal{Z}$, one gets

$$\begin{aligned}\delta\mathcal{F}_{\rm rec}(\lambda) = &\sum_{\ell=1,2}\frac{\alpha_s(v^{1/(a+b_\ell)}Q)}{\alpha_s(Q)(a+b_\ell)}\int_0^\infty\frac{d\zeta}{\zeta}\int_0^{2\pi}\frac{d\phi}{2\pi}\int_0^1 dz\,p_\ell(z)\times\\
&\times\epsilon^{R'_{\rm NLL}}\sum_{n=0}^\infty\frac{1}{n!}\prod_{i=1}^n\sum_{\ell_i=1,2}R'_{{\rm NLL},\ell_i}\int_0^{2\pi}\frac{d\phi_i}{2\pi}\times\\
&\times\left[\Theta(1-\zeta f^{(\ell)}(z))\int_0^\infty\frac{d\tilde\zeta'_i}{\tilde\zeta'_i}\Theta\left(\tilde\zeta'_i-\frac{\epsilon}{1-\zeta f^{(\ell)}(z)}\right)\Theta\left(1-\lim_{v\to0}\frac{V_{\rm sc}(\{\tilde p\},\tilde k'_1,\dots,\tilde k'_n)}{v}\right)\right.\\
&\left.-\Theta(1-\zeta f^{(\ell)}_{\rm sc}(z))\int_0^\infty\frac{d\tilde\zeta_i}{\tilde\zeta_i}\Theta\left(\tilde\zeta_i-\frac{\epsilon}{1-\zeta f^{(\ell)}_{\rm sc}(z)}\right)\Theta\left(1-\lim_{v\to0}\frac{V_{\rm sc}(\{\tilde p\},\tilde k_1,\dots,\tilde k_n)}{v}\right)\right].\end{aligned}\tag{4.58}$$

We can then rearrange the above equation to reconstruct the function $\mathcal{F}_{\rm NLL}(\lambda)$. This gives

$$\begin{aligned}\delta\mathcal{F}_{\rm rec}(\lambda) &= \mathcal{F}_{\rm NLL}(\lambda)\sum_{\ell=1,2}\frac{\alpha_s(v^{1/(a+b_\ell)}Q)}{\alpha_s(Q)(a+b_\ell)}\int_0^{2\pi}\frac{d\phi}{2\pi}\int_0^1 dz\,p_\ell(z)\int_0^\infty\frac{d\zeta}{\zeta}\times\\
&\times\left[(1-\zeta f^{(\ell)}(z,\phi))^{R'_{\rm NLL}}\Theta(1-\zeta f^{(\ell)}(z,\phi))-(1-\zeta f^{(\ell)}_{\rm sc}(z,\phi))^{R'_{\rm NLL}}\Theta(1-\zeta f^{(\ell)}_{\rm sc}(z,\phi))\right]\\
&= \mathcal{F}_{\rm NLL}(\lambda)\sum_{\ell=1,2}\frac{\alpha_s(v^{1/(a+b_\ell)}Q)}{\alpha_s(Q)(a+b_\ell)}\int_0^{2\pi}\frac{d\phi}{2\pi}\int_0^1 dz\,p_\ell(z)\ln\frac{f^{(\ell)}_{\rm sc}(z,\phi)}{f^{(\ell)}(z,\phi)}\,.\end{aligned}\tag{4.59}$$

As an illustrative example, we consider the thrust. One can show that its expression in terms of Sudakov variables is

$$1-T=\sum_{i=1}^n\frac{k_{ti}}{Q}e^{-|\eta_i|}+\frac{1}{Q^2}\sum_{\ell=1,2}\frac{\left(\sum_{i\in\mathcal{H}^{(\ell)}}\vec k_{ti}^{(\ell)}\right)^2}{1-\sum_{i\in\mathcal{H}^{(\ell)}}z_i^{(\ell)}}\,.\tag{4.60}$$

Suppose the hard-collinear emission k is emitted by leg $\tilde p_1$. Using the Sudakov parametrisation of Eq. (4.16) we then have

$$1-T\simeq\sum_{i=1}^n\frac{k_{ti}}{Q}e^{-|\eta_i|}+\frac{k_t^2}{z^{(1)}Q^2}+\frac{k_t^2}{(1-z^{(1)})Q^2}=\sum_{i=1}^n\frac{k_{ti}}{Q}e^{-|\eta_i|}+\frac{k_t^2}{z^{(1)}(1-z^{(1)})Q^2}\,,\tag{4.61}$$

where we have used the fact that the hard-collinear k_t is larger than all soft-collinear k_{ti}, and therefore $k_t\simeq k'_t$. This can be better understood by considering the Lund diagram for the thrust, shown in Fig. 4.2. The expressions of Eqs. (4.53) and (4.54) evaluate to

$$f^{(\ell)}(z^{(\ell)},\phi)=\frac{1}{z^{(\ell)}(1-z^{(\ell)})}\,,\qquad f^{(\ell)}_{\rm sc}(z^{(\ell)},\phi)=\frac{1}{z^{(\ell)}}\,,$$

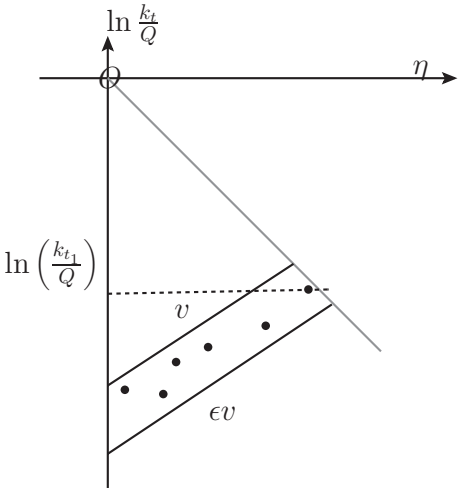

Figure 4.2: An ensemble of real resolved soft-collinear emissions, shown as black dots, populating the allowed phase space for the thrust observable. Due to the positive value of b_ℓ the boundary of the region varies in η. Since the emissions must be widely separated in rapidity the emission with the largest transverse momentum has $k_{t_1} \gg k_{t_i}$ for all i. Hence the hard-collinear emission, which by definition lives at the largest rapidity of all emissions, has the dominant contribution to the recoil of the Born system.

for the thrust. Substituting these expressions into Eq. (4.59) and evaluating the integral gives,

$$\begin{aligned}\delta\mathcal{F}_{\rm rec}(\lambda) &= \mathcal{F}_{\rm NLL}(\lambda) 2C_F \frac{\alpha_s(\sqrt{\tau}Q)}{2\alpha_s(Q)} \int_0^1 dz\, \frac{(1+(1-z)^2)}{z} \ln(1-z) \\ &= \mathcal{F}_{\rm NLL}(\lambda) \frac{C_F \alpha_s(\sqrt{\tau}Q)}{\alpha_s(Q)} \left(\frac{5}{4} - \frac{\pi^2}{3}\right) .\end{aligned} \tag{4.62}$$

This result holds also for the C-parameter and the heavy-jet mass, which behave as $1-T$ in the collinear region.

4.6.4 Hard-collinear Correction

Using the same single hard-collinear emission as in the previous section, we now compute the matrix element correction $\delta\mathcal{F}_{\rm hc}(\lambda)$ of Eq. (4.30) for additive observables. Using the soft-collinear observable of Eq. (4.49) we obtain

$$\begin{aligned}\delta\mathcal{F}_{\rm hc}(\lambda) = \sum_{\ell=1,2} \frac{\alpha_s(v^{1/(a+b_\ell)}Q)}{\alpha_s(Q)(a+b_\ell)} \int_0^\infty \frac{d\zeta}{\zeta} \int_0^\pi \frac{d\phi}{2\pi} \int_0^1 \frac{dz}{z} \left(z p_\ell(z) - 2C_\ell\right) \int d\mathcal{Z}[\{R'_{{\rm NLL},\ell_i}, k_i\}] \times \\ \times \left[\Theta\left(1-\zeta - \lim_{v\to 0} \frac{V_{\rm sc}(\{\tilde{p}\},\{k_i\})}{v}\right) - \Theta(1-\zeta)\Theta\left(1 - \lim_{v\to 0} \frac{V_{\rm sc}(\{\tilde{p}\},\{k_i\})}{v}\right)\right] .\end{aligned} \tag{4.63}$$

Rescaling the momenta in a similar way as we did in the previous section we get

$$\delta\mathcal{F}_{\rm hc}(\lambda) = \mathcal{F}_{\rm NLL}(\lambda)\sum_{\ell=1,2}\frac{\alpha_s(v^{1/(a+b_\ell)}Q)}{\alpha_s(Q)(a+b_\ell)}\int_0^\infty\frac{d\zeta}{\zeta}\int_0^{2\pi}\frac{d\phi}{2\pi}\int_0^1\frac{dz}{z}\left(zp_\ell(z)-2C_\ell\right)\times$$
$$\times\left[(1-\zeta)^{R'_{\rm NLL}}\,\Theta\left(1-\zeta\right)-\Theta(1-\zeta)\right] = \mathcal{F}_{\rm NLL}(\lambda)\sum_{\ell=1,2}\frac{\alpha_s(v^{1/(a+b_\ell)}Q)}{\alpha_s(Q)(a+b_\ell)}\times \tag{4.64}$$
$$\times\, C_\ell B_\ell\int_0^1\frac{d\zeta}{\zeta}\left[(1-\zeta)^{R'_{\rm NLL}}-1\right].$$

Considering specifically the thrust, we obtain

$$\delta\mathcal{F}_{\rm hc}(\lambda) = \frac{\alpha_s(\sqrt{\tau}Q)}{\alpha_s(Q)}C_F\frac{3}{2}\left(\psi^{(0)}(1+R'_{\rm NLL})+\gamma_E\right)\mathcal{F}_{\rm NLL}(\lambda). \tag{4.65}$$

4.6.5 Soft-wide angle Correction

We consider the case of a NNLL correction induced by a soft-wide angle emission, as given in general by Eq. (4.36). This correction is due to the inability for the soft-collinear observable parametrisation of Eq. (3.18) to accurately describe the value of an observable in the presence of a soft-wide angle emission. We express the amended additive NNLL-accurate observable and the NLL one, respectively,

$$V^{(k)}_{\rm wa}(\{\tilde{p}\},k,\{k_i\}) = \left(\frac{k_t}{Q}\right)^a f_{\rm wa}(\eta,\phi)+V_{\rm sc}(\{\tilde{p}\},\{k_i\})\,, \tag{4.66}$$

$$V_{\rm sc}(\{\tilde{p}\},k,\{k_i\}) = \left(\frac{k_t}{Q}\right)^a f_{\rm sc}(\eta,\phi)+V_{\rm sc}(\{\tilde{p}\},\{k_i\})\,, \tag{4.67}$$

where $f_{\rm sc}(\eta,\phi)$ and $f_{\rm wa}(\eta,\phi)$ are defined in Eqs. (4.31) and (4.32). Using Eq. (4.36) and performing a similar rescaling as for the additive recoil correction one finds

$$\delta\mathcal{F}_{\rm wa}(\lambda) = \mathcal{F}_{\rm NLL}(\lambda)\frac{2C_F}{a}\frac{\alpha_s(v^{\frac{1}{a}}Q)}{\alpha_s(Q)}\int_0^{2\pi}\frac{d\phi}{2\pi}\int_{-\infty}^{\infty}d\eta\ln\frac{f_{\rm sc}(\eta,\phi)}{f_{\rm wa}(\eta,\phi)}\,. \tag{4.68}$$

Now we write explicit expressions for $f_{\rm wa}$. For the thrust and the heavy-jet mass,

$$f_{\rm wa}(\eta,\phi) = f_{\rm sc}(\eta,\phi) = e^{-|\eta|}\,, \tag{4.69}$$

so that $\delta\mathcal{F}_{\rm wa}(\lambda)=0$. In the case of the C-parameter instead we have

$$f_{\rm wa}(\eta,\phi) = \frac{3}{\cosh\eta}\quad\text{and}\quad f_{\rm sc}(\eta,\phi) = 6\,e^{-|\eta|}\,. \tag{4.70}$$

This gives

$$\delta\mathcal{F}_{\rm wa}(\lambda) = \mathcal{F}_{\rm NLL}(\lambda)2C_F\frac{\alpha_s(CQ)}{\alpha_s(Q)}\int_{-\infty}^{\infty}d\eta\ \ln(2\cosh\eta e^{-|\eta|}) = \mathcal{F}_{\rm NLL}(\lambda)C_F\frac{\alpha_s(CQ)}{\alpha_s(Q)}\frac{\pi^2}{6}\,, \tag{4.71}$$

where C is the value of the C-parameter.

4.6.6 Correlated Correction

The correlated correction presented in Eq. (4.45) depends on the difference between the non-inclusive and inclusive treatments of two soft-collinear emissions that are close in angle, and is captured by the constraints,

$$\Theta\left(v - V_{\mathrm{sc}}(\{\tilde{p}\}, k_a, k_b, k_1, \ldots, k_n)\right) - \Theta\left(v - V_{\mathrm{sc}}(\{\tilde{p}\}, k_a + k_b, k_1, \ldots, k_n)\right) , \tag{4.72}$$

which is in general non-zero for additive observables. However, the above correction vanishes if the observable V_{sc} itself is inclusive, i.e. $V_{\mathrm{sc}}(k_a, k_b) = V_{\mathrm{sc}}(k_a + k_b)$. The thrust τ is inclusive only for emissions that propagate into the same hemisphere (defined by the thrust axis). In this case, the difference Eq. (4.72) is non-zero if the two correlated soft partons k_a, k_b move into opposite hemispheres. However, this configuration requires the parent gluon to be emitted at small rapidities, which gives rise to a correction which is at most $\mathrm{N^3LL}$, according to the rules laid out in Sec. 4.1.1, and can be neglected. The other additive observables treated in this thesis are also inclusive in the relevant phase space regions, so we can conclude that for T, C, and ρ_H, at NNLL

$$\delta\mathcal{F}_{\mathrm{correl}}(\lambda) = 0\,. \tag{4.73}$$

...

The NNLL corrections which have been derived in this chapter hold for any rIRC safe, continuously global observable that can be parametrised by Eq. (3.18). The sum of all of these corrections will produce a NNLL-accurate multiple emissions function for a appropriate given observable. Multiplying by the NNLL Sudakov factor of Eq. (4.8) gives a complete NNLL-accurate resummation for that observable.
In the next chapter we will extend this formalism to include the two-jet rate.

Chapter 5

Resummation of Jet Rate Observables at NNLL

in which I introduce jet objects in a theoretical and experimental context and show how the previous chapter's methodology can be applied to jet observables.

5.1 Jets and Jet Algorithms

As mentioned in Section 2.2.2, the fundamental QCD degrees of freedom - quarks and gluons - are not final-state objects. After a high-energy interaction they undergo stages of radiation and then hadronisation, leaving us with collimated streams of hadrons that are picked up by detectors as energy deposits. These usually-conical collections of hadrons are called *jets*. Jets are defined via clustering algorithms so that we may, indirectly, measure the properties of the original partons. Since jets are not fundamental there exists some choice in how to define them. In 1990 it was agreed that a good jet definition should [42,43]:

1. Be simple to implement in an experimental analysis
2. Be simple to implement in a theoretical calculation
3. Be defined at any order in perturbation theory
4. Yield finite cross sections at any order in perturbation theory
5. Yield a cross section that is insensitive to hadronisation

Jet rates, the fractions of events having a given number[1] of jets, are particularly useful observables for extracting perturbative values of α_s due to point 5 (i.e. the parton- and hadron-level results are similar). Fig. 5.1 [20] shows the comparison of differential cross-sections with and without hadronisation effects (discussed in Sec. 2.2.2) taken into account for two observables: thrust and the two-jet rate in the Durham jet clustering algorithm. These plots are obtained using the ALEPH detector at LEP with centre-of-mass energy 91.2 GeV. The resummation used is correct to NLL and is taken from [22] and [25] for

[1] This must be carefully defined using jet algorithms and jet resolution cuts, extensively discussed for e^+e^- annihilation in this chapter.

thrust and the two-jet rate, respectively. The data has been corrected for detector effects. Notice that hadronisation effects are more sizeable for the thrust distribution, skewing the result away from its partonic shape. The shoulder in Fig. 5.1 is controlled by the Sudakov factor. The downturn expresses the increasing difficulty in maintaining a three jet event as the jet resolution threshold parametrised by y_{cut} (defined in the following) becomes very small.

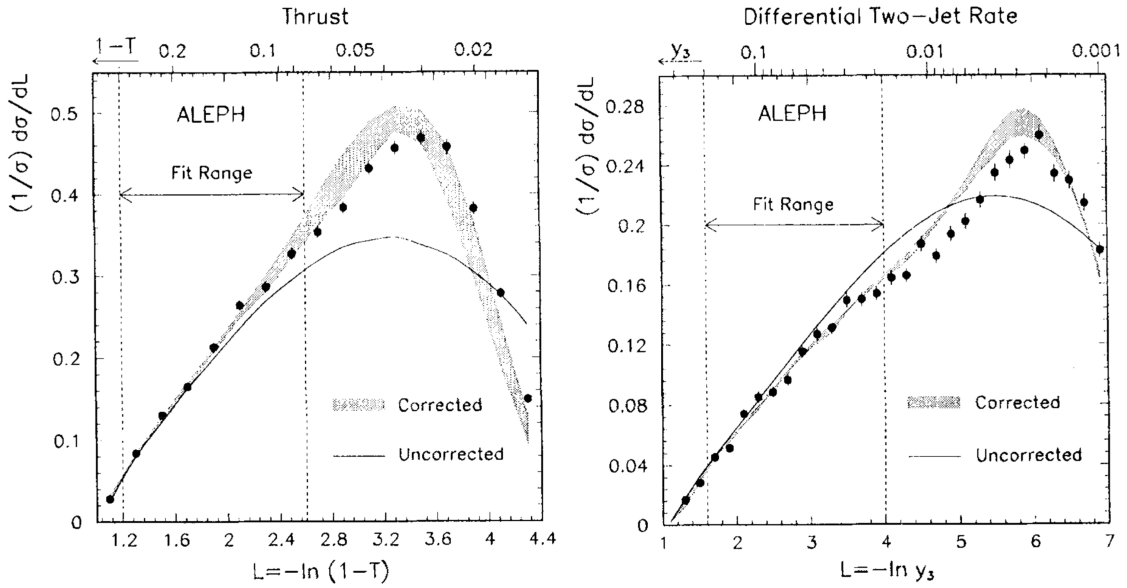

(a) Thrust (b) Two-jet rate

Figure 5.1: Comparison of NLL-resummed predictions and ALEPH data for thrust and the two-jet rate. The black dots represent the data and the black line the resummed result. The grey line shows the addition of hadronisation effects, with the band signifying the range of values predicted by three different hadronisation models in JETSET 7.2 and HERWIG 5.3.

Jets are designated by jet algorithms which group together the experimental energy deposits or theoretical final-state partons. These algorithms fall into two types: cone algorithms and sequential-recombination algorithms. Broadly speaking, a cone algorithm groups particles into a circular area in phase space by considering what fraction of the event's total energy is contained within a subgroup of particles and what size of angular space the subgroup inhabits. A sequential algorithm cycles through pairs of particles either combining them together into one jet or designating them separate jets. In this work we are interested only in sequential recombination algorithms. For a comprehensive discussion on a large number of jet algorithms see [44].
We will employ the Durham [45] and Cambridge algorithms [46, 47] for our jet definitions. These were the algorithms most commonly used at the detectors of LEP at CERN. Both of these algorithms define a distance measure y_{ij} and an ordering variable v_{ij}. For the

Cambridge algorithm,

$$y_{ij}^{(C)} = 2\frac{\min\{E_i, E_j\}^2}{Q^2}\left(1-\cos\theta_{ij}\right) , \qquad v_{ij}^{(C)} = 2\left(1-\cos\theta_{ij}\right) , \tag{5.1}$$

and for the Durham algorithm,

$$y_{ij}^{(D)} = v_{ij}^{(D)} = 2\frac{\min\{E_i, E_j\}^2}{Q^2}\left(1-\cos\theta_{ij}\right) , \tag{5.2}$$

where θ_{ij} is the angle between particles k_i and k_j, E_i is the energy of the particle k_i, and Q is the centre-of-mass energy. A sequential algorithm such as the Durham algorithm determines the pair of particles with the smallest v_{ij} and combines them into one pseudo-particle if $y_{ij} < y_{\text{cut}}$, where y_{cut} is the jet resolution parameter. The recombination scheme dictates how the pairs of particles are combined (e.g. via energy, four-momenta). The k_t recombination we will use gives a result valid for all schemes[2] (see Eq. 5.9). This process is iterated until all remaining y_{ij} are larger than the resolution cut.
Clearly the jet multiplicity of a given event will depend on the algorithm, the recombination scheme and the value of y_{cut} that one uses. The three-jet resolution parameter y_3 is defined as the value of y_{cut} lying on the boundary between a two-jet event and a three-jet event. The two-jet rate is the cumulative integral of the y_3 distribution.

We note here that both the Durham and the Cambridge distance measures tend to their Born value of zero for vanishingly soft and/or collinear emissions. Therefore these algorithms are IRC safe and as such the corresponding observable, the two-jet rate, can be reliably computed order by order in perturbation theory. In addition y_3 has the same parametric behaviour in the presence of many soft and collinear emissions, i.e. it is rIRC safe according to Eqs. (3.4) and (3.5).

The material in the remainder of this chapter is based on recent collaborative work, culminating in the publication of [2], where the first NNLL resummation of the two-jet rate was presented. The method of `ARES` is especially powerful in its resummation of y_3 since it does not require a formula to factorise the soft and collinear regions of phase space, as do most resummation technologies. For this reason the resummation of the two-jet rate was previously unattainable.

5.2 Jet Rate Resummation at NLL

Before embarking on a next-to-next-to-leading-logarithmic resummation of the two-jet rate it is worth looking in detail at how a NLL ensemble of soft-collinear emissions will cluster in the Durham and Cambridge algorithms. At NLL accuracy the procedure for clustering particles into jets can be simplified from the full definition. This will throw into relief the considerations needed to capture all NNLL kinematics. We begin by considering

[2]Since we work with soft-collinear emissions their energies are negligible and so our transverse-momenta recombination with rapidity replacement captures all of the information of the pair.

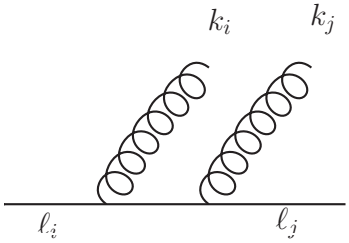

Figure 5.2: A simple event with two emissions being radiated from the $q\bar{q}$ pair. ℓ_i and ℓ_j denote the legs from which k_i and k_j, respectively, have been emitted. Note that the emission angles of k_i and k_j have been vastly exaggerated in this diagram. In reality the emissions would be unresolvable in their collinearity to their emitter(s).

the Durham algorithm.

5.2.1 The Durham Jet Algorithm at NLL

For illustrative purposes we will determine the value of y_3 for a specific event. We choose the simple diquark system with two additional soft-collinear emissions as shown in Fig. 5.2. We will calculate all the possible $y_{ij}^{(D)}$ and find the value lying on the boundary between a two-jet and a three-jet event, i.e. the smallest $y_{ij}^{(D)}$ after one clustering.
For two soft-collinear particles k_i, k_j we can use the small-angle approximation[3] to write

$$\begin{aligned} y_{ij}^{(D)} = 2\frac{\min\{E_i,E_j\}^2}{Q^2}\left(1-\cos\theta_{ij}\right) &\approx \frac{\min\{E_i,E_j\}^2}{Q^2}\left(\theta_{ij}^2\right) \\ &= \frac{\min\{E_i,E_j\}^2}{Q^2}|\vec{\theta_i}-\vec{\theta_j}|^2 \end{aligned} \tag{5.3}$$

where $\theta_{i(j)}$ denotes the angle between emission $k_i(k_j)$ and its emitter, and $\vec{\theta}_{i(j)} = \theta_{i(j)}(\cos\phi_{i(j)}, \sin\phi_{i(j)})$ includes transverse components. The pairings between an emission and its emitter must also be considered:

$$y_{ip_\ell}^{(D)} = 2\frac{\min\{E_i,E_{p_\ell}\}^2}{Q^2}\left(1-\cos\theta_i\right) \approx \frac{E_i^2}{Q^2}\theta_i^2 = \frac{k_{t_i}^2}{Q^2}\,, \tag{5.4}$$

where p_ℓ denotes one of the hard quarks, the parent of emission k_i.

To encompass all possible clusterings we keep the leg indices general; $\ell_i = 1, 2$ and $\ell_j = 1, 2$. Since we have four particles there are $\binom{4}{2} = 6$ pairings. To find the y_3 of this system we must cluster pairs of particles until we are left with three jets. At that point the value of the smallest y_{ij} defines y_3. We can immediately disregard y_{ℓ_i,ℓ_j} since the energy of the hard quarks is orders of magnitude larger than either of the soft-collinear emissions, and the two quarks are nearly back-to-back. Both of these facts separately exclude the possibility that this pair leads to the smallest distance measure. The collinearity of k_i and k_j to their emitter(s) leads to the prohibition of any clustering between two particles not in the same hemisphere (see Fig. 2.6a and the surrounding text). Therefore if $\ell_i \neq \ell_j$ the

[3]The soft-collinear ensemble are widely separated in rapidity *within* the collinear region and their shared collinearity to the emitter ensures that the angle between them can be considered a small angle.

only allowed clusterings are k_i with ℓ_i and k_j with ℓ_j; the clustering of an emission with its emitter. Any jet containing one of the original hard quarks will have energy prohibitively large to exist within the smallest distance measure. So in this case we are left to utilise only Eq. (5.4) and

$$y_3 = \frac{1}{Q^2} \max\{k_{t_i}, k_{t_j}\}^2 \,. \tag{5.5}$$

If, on the other hand, $\ell_i = \ell_j$ then the two soft-collinear emissions are also allowed to cluster together. This is the more interesting case. To analyse this further we use the fact that, by rIRC safety, all $\{k_{t_i}\}$ must be of a similar size, with corrections to this condition subleading. We can say without loss of generality that $k_{t_i} > k_{t_j}$. The pair k_i, k_j will cluster if

$$\frac{\min\{E_i, E_j\}^2}{Q^2} |\vec{\theta_i} - \vec{\theta_j}|^2 < \frac{k_{t_j}^2}{Q^2} \,. \tag{5.6}$$

The emissions are widely separated in rapidity so we end up in one of the two following cases:
1) $\theta_i \gg \theta_j$ ($\implies E_i \ll E_j$ since $k_{t_i} \sim k_{t_j}$),
for which Eq. (5.6) becomes

$$k_{t_i}^2 \left(1 - 2\frac{\theta_j}{\theta_i}\cos\phi_{ij} + \frac{\theta_j^2}{\theta_i^2}\right) < k_{t_j}^2 \,, \tag{5.7}$$

using the small-angle approximation of Eq. (5.3). However in the $\theta_i/\theta_j \to 0$ limit stipulating that the particles are widely separated (i.e. in NLL kinematics) this becomes $k_{t_i}^2 < k_{t_j}^2$, invalidating our initial assumption.
2) $\theta_i \ll \theta_j$ ($\implies E_i \gg E_j$),
in which case

$$\begin{aligned} E_j^2(\theta_j^2 - 2\theta_i\theta_j\cos\phi_{ij}) &< k_{t_j}^2 \\ (1 - 2\frac{\theta_i}{\theta_j}\cos\phi_{ij}) &< 1 \\ \cos\phi_{ij} &> 0 \,. \end{aligned} \tag{5.8}$$

If this clustering condition holds for particles k_i and k_j with $\theta_i \ll \theta_j$, we produce a pseudoparticle, or jet, that sets y_3

$$y_3 = \frac{k_{t_p}^2}{Q^2} = \frac{1}{Q^2}|\vec{k_{t_i}} + \vec{k_{t_j}}|^2 \,, \tag{5.9}$$

where k_{t_p} is the transverse momentum of the pseudoparticle.
Eqs. (5.3) and (5.4) and the above clustering procedure hold for any number of soft and collinear emissions. One could manually cycle through every y_{ij} in an event, as we have done: finding the minimum, clustering either with the emission's parent quark or with a neighbour for which $\theta_i \ll \theta_j$ and $\cos\phi_{ij} > 0$ are true. However, this procedure can be simplified even further by reflecting on the conditions that have just been derived.

We now consider an event containing two hard quarks and many soft-collinear emissions (the exact number does not matter). We again assume that $k_{t_j} < k_{t_i}$, now for all i. Firstly, by definition it is true that for arbitrary pseudoparticles k_m and k_n

$$y_{m\ell_m} > y_{mn}, \forall\ m \neq n\,, \tag{5.10}$$

for cases in which the clustering condition (Eq. (5.8)) for k_m and k_n holds. Hence the distance measures including a given pseudoparticle have an upper bound. Secondly, we have seen that for clustering of pseudoparticles k_m and k_n we require $k_{t_m} < k_{t_n}$ and $E_n \gg E_m$. Therefore m is restricted to clusterings with emissions of larger energies. This implies

$$\begin{aligned}\frac{\min\{E_m, E_n\}^2}{Q^2}|\vec{\theta_m} - \vec{\theta_n}|^2 &= \frac{E_m^2}{Q^2}(\theta_m^2 - 2\theta_m\theta_n\cos\phi_{nm}) \\ &= \frac{E_m^2}{Q^2}\theta_m^2(1 - 2\frac{\theta_n}{\theta_m}\cos\phi_{nm})\,.\end{aligned} \tag{5.11}$$

We also have that

$$(E_j\theta_j)^2 < (E_m\theta_m)^2, \forall\ m \neq j\,. \tag{5.12}$$

The clustering condition forces the ratio of angles in the second line of Eq. (5.11) to be very tiny, subsequently enforcing

$$\left(1 - 2\frac{\theta_n}{\theta_m}\cos\phi_{nm}\right) \approx 1 \tag{5.13}$$

Together Eq. (5.12) and Eq. (5.13) imply

$$\left(\frac{E_j\theta_j}{E_m\theta_m}\right)^2 < \left(1 - 2\frac{\theta_n}{\theta_m}\cos\phi_{nm}\right)\,. \tag{5.14}$$

The above relation holds for any $(j,\, m,\, n)$ such that $k_{t_j} < k_{t_m} < k_{t_n}$ and k_m, k_n-clustering is allowed. This is a powerful result stipulating that the ordering of pairings can be systematically determined. If no allowed pairing is found for a given pseudoparticle then it *must* cluster with its emitter (for which the clustering condition always holds). The definite hierarchy in y_{ij} leads to the following algorithmic sequence which we call $\overline{y}_3^{\rm sc}$:

1. Find the (pseudo)particle k_j with the smallest value of $\overline{y}_3^{\rm sc}(\{\tilde{p}\}, k_j) = (k_{t_j}/Q)^2$
2. Else, search for an emission k_i with smaller angle with respect to its emitter, in the same hemisphere as k_j, that maximises θ_i/θ_j and satisfies $\cos\phi_{ij} > 0$
3. If a successful candidate k_i is found, cluster k_i and k_j into a jet setting $\vec{k_{t_{\rm jet}}} = \vec{k_{t_i}} + \vec{k_{t_j}}$; $\theta_{\rm jet} = \theta_i$
4. If no valid k_i is found, cluster k_j with ℓ_j and remove k_j from the array of (pseudo)particles in the event
5. If there remain only three jets (each hard quark plus one pseudoparticle), $\overline{y}_3^{\rm sc}(\{\tilde{p}\}, k_1, \ldots, k_n) = (k_{t_j}/Q)^2$, otherwise go back to 1.

5.2.2 The Cambridge Jet Algorithm at NLL

Recall the Cambridge ordering variable from Eq. (5.1),

$$v_{ij}^{(C)} = 2\left(1 - \cos\theta_{ij}\right) . \tag{5.15}$$

The expression above is only dependent on the angular ordering of the emissions, which will simplify the clustering process. In fact, since at NLL the emissions are all collinear to their emitter and widely separated in angle we have

$$\theta_{ij} \gg \theta_{ip_\ell}, \quad \forall\, i\,. \tag{5.16}$$

Therefore no clustering occurs between soft-collinear emissions widely separated in rapidity in the Cambridge algorithm. The value for y_3 in any given event is simply equal to the largest $y_{ip_\ell} = k_{t_i}^2/Q^2$. The contribution of a NLL ensemble can be separated into the individual contributions of its emissions,

$$\Theta\left(1 - \lim_{y_{\rm cut}\to 0} \frac{\overline{y}_3^{\rm sc}(\{\tilde{p}\}, k_1, \ldots, k_n)}{y_{\rm cut}}\right) = \prod_{i=1}^{n} \Theta\left(1 - \lim_{y_{\rm cut}\to 0} \frac{y_3^{\rm sc}(\{\tilde{p}\}, k_i)}{y_{\rm cut}}\right) . \tag{5.17}$$

This constraint combines with the soft-collinear measure $d\mathcal{Z}[\{R'_{{\rm NLL},\ell_i}, k_i\}]$ such that, for this algorithm, $\mathcal{F}_{\rm NLL}(\lambda) = 1$. We can also use Eq. (5.17) to evaluate NNLL corrections to $\mathcal{F}_{\rm NLL}(\lambda)$ analytically, as shown explicitly in Sec. 5.9.

5.3 Considerations for Jet Rate Resummation at NNLL

This discussion of this chapter up to now has been solely concerned with observable definitions. We stress that the event set-up in $e^+e^- \to q\bar{q}$, including extra emissions' matrix elements and phase space are identical to those derived in Sec. 3.1 and subsequently extended in Secs. 4.2 to 4.5. We now focus on the ingredients of the resummation, $e^{-R_{\rm NNLL}}$ and $\delta\mathcal{F}_{\rm NNLL}$. As before we change variables and express the emissions' phase space in terms of $(\zeta_i = v_i/v, \phi_i, \xi_i^{(\ell)} = \eta_i^{(\ell)}/\eta_{\rm max}^{(\ell)})$ (see Eqs. (3.40) and (3.42)).

5.3.1 The Sudakov Factor at NNLL

The effect of virtual corrections and unresolved real emissions to the two-jet rate are taken into account by a Sudakov factor. The soft-collinear scaling of the Durham and Cambridge algorithms corresponds to parameters $a = 2, b_\ell = 0$ given in Eq. (3.18). As was discussed in Sec. 4.1.3 the NNLL Sudakov radiator is known in this case and so again we do not explicitly calculate the expression for $R_{\rm NNLL}(v) = -Lg_1(\lambda) - g_2(\lambda) - \frac{\alpha_s(Q)}{\pi} g_3(\lambda)$, but extract it from the broadening-type Sudakov factor, putting $a = 2$ (See Appendix A).

5.3.2 The Multiple Emissions Function at NNLL

We briefly discuss the applicability of the $\delta\mathcal{F}$ functions introduced in Sec. 4.1.2 and derived in Secs. 4.2 to 4.5 to jet rates. It is immediately obvious that corrections arising from the

inclusion of NNLL kinematics in the matrix element of a single emission apply to jet rates as they stand, i.e. we already possess all the tools to determine the hard-collinear correction $\delta\mathcal{F}_{\rm hc}$. Note, however, that there is an additional subtlety with the phase space integration compared to that for event shapes. Looking at Eqs. (5.1) and (5.2) one can see that the ordering of clustering, and therefore the final observable, is dependent on the angular properties of emissions. Therefore we cannot integrate over the rapidities of the gluons as we did for event shapes in Eq. (3.43). This leads to subtleties in calculating $\delta\mathcal{F}_{\rm sc}$. The soft-collinear measure present in the real emission functions (Eq. (3.48)) must therefore also include integrals over the rapidity of emissions,

$$\int d\mathcal{Z}[\{R'_{\rm NLL,\ell_i},k_i\}]G(\{\tilde{p}\},\{k_i\}) = \epsilon^{R'_{\rm NLL}}\sum_{n=0}^{\infty}\frac{1}{n!}\prod_{i=1}^{n}\int_{\epsilon}^{\infty}\frac{d\zeta_i}{\zeta_i}\int_0^{2\pi}\frac{d\phi_i}{2\pi}\sum_{\ell_i=1,2}\int_0^1 d\xi_i^{(\ell_i)}\times \\ \times R'_{\rm NLL,\ell_i}G(\{\tilde{p}\},k_1,\ldots,k_n)\,, \tag{5.18}$$

where $\zeta_i = k_{ti}^2/Q^2 y_{\rm cut}$, $\xi_i^{(\ell_i)} = |\eta_i|/\eta_{\rm max}$, and $R'_{\rm NLL,\ell}$ is defined in Appendix A. Note that $d\mathcal{Z}[\{R'_{\rm NLL,\ell_i},k_i\}]$ satisfies the normalisation condition

$$\int d\mathcal{Z}[\{R'_{\rm NLL,\ell_i},k_i\}]\prod_i\Theta\left(1-\lim_{y_{\rm cut}\to 0}\frac{\overline{y}_3^{\rm sc}(\{\tilde{p}\},k_i)}{y_{\rm cut}}\right) = 1\,. \tag{5.19}$$

The corrections owing to a change in observable definition require a modified jet algorithm. That is, $\delta\mathcal{F}_{\rm swa},\delta\mathcal{F}_{\rm rec},\delta\mathcal{F}_{\rm correl}$ will require the replacement of $\overline{y}_3^{\rm sc}$ to $y_3^{\rm wa}, y_3^{\rm hc}, y_3^{\rm sc}$, respectively. The kinematics of correlated emission begets an additional resolved real-emission correction for jet rate observables. The correlated emissions' closeness in rapidity invalidates assumptions that we made in deriving $\overline{y}_3^{\rm sc}$ in Sec. 5.2.1. At NNLL precision the two correlated emissions are allowed to cluster. To correctly determine a possible clustering between this pair the full algorithm must be used. Note that the NLL-simplified $\overline{y}_3^{\rm sc}$ algorithm is still valid for all other pairings in the event. The contribution $\delta\mathcal{F}_{\rm clust}$ captures the effect of correlated emissions clustering in the full NNLL algorithm. $\delta\mathcal{F}_{\rm correl}$ arises from treating gluon splitting non-inclusively, i.e. the correlated emissions can end up in different jets.

To summarise, the function

$$\delta\mathcal{F}_{\rm NNLL} = \delta\mathcal{F}_{\rm sc}+\delta\mathcal{F}_{\rm hc}+\delta\mathcal{F}_{\rm rec}+\delta\mathcal{F}_{\rm wa}+\delta\mathcal{F}_{\rm correl}+\delta\mathcal{F}_{\rm clust} \tag{5.20}$$

represents NNLL corrections due to real resolved radiation for jet rates. Sections 5.4 to 5.8 will deal with the derivation of each of these corrections in turn for the two-jet rate in the Durham algorithm. Once we have obtained these expressions we can apply simplifications afforded by the Cambridge algorithm to gain analytic expressions for the two-jet rate in this algorithm. In the formulation of each $\delta\mathcal{F}$ we will pick out one emission, k, from the soft-collinear ensemble that will be the 'special' emission. This emission and it alone will embody the various NNLL kinematics that lead to each correction.

...

Here it is worth commenting on the nature of observables requiring a sequential algorithm for their definition. As mentioned previously there exists no factorisation formula for y_3 in the Durham algorithm. Practically this means that we cannot determine the value of y_3 for a given event analytically. In Sec. 5.2 we determined the various allowed values for y_3 given the very simple event of Fig. 5.2. However since the clustering of emissions depends on the energy and angular properties of each emission in a non-trivial way it is not possible to determine the clustering sequence a priori, even for the simplified Durham algorithm $\bar{y}_3^{\rm sc}$. Furthermore for an event with many emissions, any intermediate clustering may disrupt the inital ordering of the $\{k_{t_i}\}$. One must simply generate emissions across the entirety of phase space and permit the algorithm to determine the final y_3 value.

5.4 Soft-collinear Correction

The soft-collinear correction takes into account the correct rapidity bound for one of the real soft-collinear emissions, as well as contributions arising from the running of the QCD coupling in the soft-collinear matrix elements. We denote by k the special emission for which we account for either effect, and rescale it such that $y_3^{\rm sc}(\{\tilde{p}\},k) = k_t^2/Q^2 = \zeta y_{\rm cut}$. There are additional subtleties in dealing with jet rate observables (on top of the event shape analysis from Sec. 4.2) since their clustering algorithms are in general angle-dependent. For event shapes, we could integrate inclusively over the rapidity fraction of each emission. As a result, the emission probability for k, collinear to the Born leg ℓ, would be proportional to the function $R'_\ell(\zeta y_{\rm cut})$ defined in Eq. (3.41). Therefore in Sec. 4.2 both NNLL effects could be accounted for by expanding $R'_\ell(\zeta y_{\rm cut})$ as follows:

$$R'_\ell(\zeta y_{\rm cut}) \simeq R'_{{\rm NLL},\ell}(y_{\rm cut}) + \delta R'_{{\rm NNLL},\ell}(y_{\rm cut}) + R''_\ell(y_{\rm cut}) \ln\frac{1}{\zeta}\,. \tag{5.21}$$

The full expressions for $\delta R'_{{\rm NNLL},\ell}(y_{\rm cut})$ and $R''_\ell(y_{\rm cut})$ are given in Appendix A. In our current case, this correction must be formulated in a slightly more general way than the corresponding one relevant for event-shape observables.

The NNLL term proportional to $\delta R'_{{\rm NNLL},\ell}(y_{\rm cut})$ in Eq. (5.21) contains the contribution from the difference in $\alpha_s^{\rm CMW}$ and $\alpha_s^{\overline{\rm MS}}$ definitions as well as from the two-loop running of the QCD coupling. In this term, the rapidity of all emissions is bounded by the NLL limit $\ln(1/\sqrt{y_{\rm cut}})$. Therefore this correction is in fact unchanged with respect to event shapes, and gives rise to

$$\begin{aligned}&\frac{\pi}{\alpha_s(\mu_R)}\int_0^\infty\frac{d\zeta}{\zeta}\int_0^{2\pi}\frac{d\phi}{2\pi}\sum_{\ell=1,2}\int_0^1 d\xi^{(\ell)}\delta R'_{{\rm NNLL},\ell}\int d\mathcal{Z}[\{R'_{{\rm NLL},\ell_i},k_i\}]\times\\ &\times\left[\Theta\left(1-\lim_{y_{\rm cut}\to0}\frac{\overline{y}_3^{\rm sc}(\{\tilde{p}\},k,\{k_i\})}{y_{\rm cut}}\right)-\Theta(1-\zeta)\Theta\left(1-\lim_{y_{\rm cut}\to0}\frac{\overline{y}_3^{\rm sc}(\{\tilde{p}\},\{k_i\})}{y_{\rm cut}}\right)\right].\end{aligned} \tag{5.22}$$

The remaining term in the right hand side of Eq. (5.21) is proportional to the function $R''_\ell(y_{\rm cut})$ given by

$$R''_\ell(y_{\rm cut}) = \frac{\alpha_s(\sqrt{y_{\rm cut}}Q)}{2\pi} C_F \left(\beta_0 \alpha_s(\sqrt{y_{\rm cut}}Q) \ln\left(\frac{1}{y_{\rm cut}}\right) + 1\right) . \tag{5.23}$$

The above function itself comprises of two distinct contributions. The term proportional to β_0 arises from expanding $\alpha_s(k_t)$ around $\alpha_s(\sqrt{y_{\rm cut}}Q)$ in the soft emission matrix element as follows

$$\alpha_s(k_t) \simeq \alpha_s(\sqrt{y_{\rm cut}}Q) + \beta_0 \alpha_s^2(\sqrt{y_{\rm cut}}Q) \ln\frac{1}{\zeta} , \tag{5.24}$$

of which the second term is purely NNLL. Therefore, when integrating over the emissions' phase space, we can set all rapidity bounds to the NLL limit $\ln(1/\sqrt{y_{\rm cut}})$. This contribution then amounts to an additional factor in the phase space integral of an NLL-accurate ensemble as is the case in Eq. (5.22), prompting us to collect the two corrections together to define the running-coupling part of $\delta\mathcal{F}_{\rm sc}$ as follows:

$$\begin{aligned}\delta\mathcal{F}^{\rm rc}_{\rm sc}(\lambda) = \frac{\pi}{\alpha_s(\mu_R)} \int_0^\infty \frac{d\zeta}{\zeta} \int_0^{2\pi} \frac{d\phi}{2\pi} \sum_{\ell=1,2} \int_0^1 d\xi^{(\ell)} \left(\delta R'_{{\rm NNLL},\ell} + \lambda R''_\ell \ln\frac{1}{\zeta}\right) \times \\ \times \int d\mathcal{Z}[\{R'_{{\rm NLL},\ell_i}, k_i\}] \times \\ \times \left[\Theta\left(1 - \lim_{y_{\rm cut}\to 0} \frac{\overline{y}_3^{\rm sc}(\{\tilde{p}\}, k, \{k_i\})}{y_{\rm cut}}\right) - \Theta(1-\zeta)\Theta\left(1 - \lim_{y_{\rm cut}\to 0} \frac{\overline{y}_3^{\rm sc}(\{\tilde{p}\}, \{k_i\})}{y_{\rm cut}}\right)\right] ,\end{aligned} \tag{5.25}$$

where

$$\lambda R''_\ell = \frac{C_F}{2\pi} \beta_0 \alpha_s^2(\sqrt{y_{\rm cut}}Q) \ln\frac{1}{y_{\rm cut}} . \tag{5.26}$$

Now we turn our attention to the NNLL-rapidity-bound piece of the soft-collinear correction. Given that the observable in this case depends on the rapidity fractions of the emissions, this correction is more complex and cannot be accounted for by Eq. (5.21). To study how the form of this correction is modified, let us consider a given ensemble of n emissions $k_1, \ldots, k_n$, strongly ordered in rapidity and collinear to the same hard leg, say $\ell = 1$. All of the emissions have the NLL rapidity bound $\ln 1/\sqrt{y_{\rm cut}}$ except for the emission k_j which has the exact rapidity bound $\ln(Q/k_{tj}) > \ln(1/\sqrt{y_{\rm cut}})$. This relation can be proved by considering the following. If pseudo-particles k_I and k_J are recombined, the tranvserse momentum of the resulting jet $|\vec{k}_{tI} + \vec{k}_{tJ}|$ will be larger than k_{tI} and k_{tJ}. This is because a clustering occurs only if $\vec{k}_{tI} \cdot \vec{k}_{tJ} > 0$ in the NLL algorithm. By induction, in all configurations which result in two jets ($\overline{y}_3^{\rm sc}(\{\tilde{p}\}, \{k_i\}) < y_{\rm cut}$), one has that $k_{ti} \leq \sqrt{y_{\rm cut}}Q$ for all particles k_i.

Now let us consider a given ordering of transverse momenta $\{k_{ti}\}$ of the n emissions. For such a configuration of transverse momenta, $n!$ rapidity orderings are available. Each ra-

pidity ordering corresponds to a potentially-different value for the observable in its NLL version, $\overline{y}_3^{\rm sc}(\{\tilde{p}\},\{k_i\})$. We assume that all emissions but k_j have the NLL rapidity bound $\ln(1/\sqrt{y_{\rm cut}})$, whereas $\eta_j < \ln(Q/k_{tj})$. Without loss of generality, we start by considering the generic ordering $\eta_1 > \eta_2 > \cdots > \eta_j > \cdots > \eta_n$. We can identify two possible scenarios: 1) when the most forward emission has the NLL rapidity bound, $\eta_1 < \ln(1/\sqrt{y_{\rm cut}})$, and 2) when it is the 'special' NNLL emission, $\ln(1/\sqrt{y_{\rm cut}}) < \eta_1 < \ln(Q/k_{t1})$.

1) In the first case, after including running couplings and colour factors, the corresponding rapidity integral is

$$\begin{aligned} I_1^{(n)} &= \left(\frac{C_F}{\pi}\right)^n \prod_{i=1}^n \alpha_s(k_{ti}) \int^{\ln(1/\sqrt{y_{\rm cut}})} d\eta_1 \int^{\eta_1} d\eta_2 \cdots \int^{\eta_{j-1}} d\eta_j \cdots \int d\eta_n \\ &= \left(\frac{C_F}{\pi}\right)^n \prod_{i=1}^n \alpha_s(k_{ti}) \frac{1}{n!} \ln^n \frac{1}{\sqrt{y_{\rm cut}}}\,. \end{aligned} \tag{5.27}$$

We stress that this result is the same regardless of the rapidity bound of emissions $k_2,\cdots,k_n$. To neglect subleading effects, we can expand the strong coupling in Eq. (5.27), as in Eq. (5.24). This leads to

$$\begin{aligned} I_1^{(n)} &= \left(\frac{C_F}{\pi}\right)^n \alpha_s^n(\sqrt{y_{\rm cut}}Q) \frac{1}{n!} \ln^n \frac{1}{\sqrt{y_{\rm cut}}} + \beta_0 \alpha_s^{n+1}(\sqrt{y_{\rm cut}}Q) \left(\frac{C_F}{\pi}\right)^n \frac{1}{n!} \ln^n \frac{1}{\sqrt{y_{\rm cut}}} \sum_{i=1}^n \ln\frac{1}{\zeta_i} + \\ &\quad + \mathcal{O}(\mathrm{N^3LL}) \\ &\simeq \frac{(R'_\ell(y_{\rm cut}))^n}{n!} + \lambda R''_\ell(y_{\rm cut}) \frac{(R'_\ell(y_{\rm cut}))^{n-1}}{n!} \sum_{i=1}^n \ln\frac{1}{\zeta_i}\,, \end{aligned} \tag{5.28}$$

where we used

$$\ln\frac{Q}{k_{ti}} = \ln\frac{1}{\sqrt{y_{\rm cut}}} + \ln\frac{1}{\sqrt{\zeta_i}}\,, \tag{5.29}$$

and $\zeta_i = (k_{ti}/Q)^2/y_{\rm cut}$.
In Eq. (5.28) we recognise the NLL contribution (the first term) that gives rise to the function $\mathcal{F}_{\rm NLL}$. The other term of Eq. (5.28) is a NNLL correction proportional to β_0 in Eq. (5.25), i.e. it is a contribution already accounted for in $\delta\mathcal{F}_{\rm sc}^{\rm rc}$, that starts at $\mathcal{O}(\alpha_s^3)$.

2) The configurations in which $\ln(1/\sqrt{y_{\rm cut}}) < \eta_1 < \ln(Q/k_{t1})$ leads to

$$I_2^{(n)} = \left(\frac{C_F}{\pi}\right)^n \prod_{i=1}^n \alpha_s(k_{ti}) \int_{\ln(1/\sqrt{y_{\rm cut}})}^{\ln(Q/k_{t1})} d\eta_1 \int^{\eta_1} d\eta_2 \cdots \int^{\eta_{j-1}} d\eta_j \cdots \int d\eta_n\,. \tag{5.30}$$

The bound in η_2 can be replaced with $\ln(1/\sqrt{y_{\rm cut}})$ since the region where $\eta_2 > \ln(1/\sqrt{y_{\rm cut}})$ gives rise to a subleading correction. Moreover, the argument of the running coupling can

be replaced with $\sqrt{y_{\rm cut}}Q$ for all emissions at NNLL. With these replacements we have

$$I_2^{(n)} = \left(\frac{C_F}{\pi}\right)^n \alpha_s^n(Q\sqrt{y_{\rm cut}})\frac{1}{(n-1)!}\ln^{n-1}\frac{1}{\sqrt{y_{\rm cut}}}\ln\frac{1}{\sqrt{\zeta_1}}$$
$$= (1-\lambda)R''_\ell(y_{\rm cut})\frac{(R'_\ell(y_{\rm cut}))^{n-1}}{(n-1)!}\ln\frac{1}{\zeta_1}\,. \tag{5.31}$$

Eq. (5.31) gives a pure NNLL contribution from applying the exact rapidity bound for one emission, and it is obtained in the limit of strong rapidity ordering. We denote this correction by $\delta\mathcal{F}_{\rm sc}^{\rm rap}$. The configuration in which two emissions are close in rapidity here gives a subleading correction; there is no overlap with the configurations contributing to the clustering correction. The exact rapidity bound matters only for the most forward/backward emission. Accordingly, in order to compute $\delta\mathcal{F}_{\rm sc}^{\rm rap}$ to all orders, we set emission k with the correct bound to be the most forward/backward, and we randomly generate the rapidity fractions of the remaining emissions. This gives

$$\delta\mathcal{F}_{\rm sc}^{\rm rap}(\lambda) = \frac{\pi}{\alpha_s(\mu_R)}\int_0^\infty\frac{d\zeta}{\zeta}\int_0^{2\pi}\frac{d\phi}{2\pi}\sum_{\ell=1,2}(1-\lambda)R'_\ell\ln\frac{1}{\zeta}\int d\mathcal{Z}[\{R'_{{\rm NLL},\ell_i},k_i\}]\times$$
$$\times\left[\Theta\left(1-\lim_{y_{\rm cut}\to0}\frac{\overline{y}_3^{\rm sc}(\{\tilde{p}\},k,\{k_i\})}{y_{\rm cut}}\right)-\Theta(1-\zeta)\Theta\left(1-\lim_{y_{\rm cut}\to0}\frac{\overline{y}_3^{\rm sc}(\{\tilde{p}\},\{k_i\})}{y_{\rm cut}}\right)\right]_{\xi^{(\ell)}=1}, \tag{5.32}$$

where now $\zeta,\xi^{(\ell)},\phi$ refer to the emission k with exact rapidity bound, and $(1-\lambda)R''_\ell = C_F/(2\pi)\alpha_s(\sqrt{y_{\rm cut}}Q)$. The condition $\xi^{(\ell)}=1$ indicates the rapidity fraction of k has been fixed to 1 reflecting the fact that the emission with the correct rapidity bound must be the most forward/backward in rapidity. In the case of the event shapes, the integrals over the rapidity fractions can be evaluated inclusively, and the sum

$$\delta\mathcal{F}_{\rm sc}^{\rm rc}(\lambda)+\delta\mathcal{F}_{\rm sc}^{\rm rap}(\lambda) \tag{5.33}$$

reproduces the soft-collinear correction formulated in Sec. 4.2.

5.5 Hard-collinear Corrections

The hard-collinear and recoil corrections describe configurations in which a parton of the ensemble is emitted collinearly to one of the Born legs and carries a significant fraction z of the emitter's momentum. This leads to an altered observable parametrisation due to the non-negligible recoil that a hard emission induces on the diquark system. It also gives rise to a matrix element correction, taking into account the full expression for a gluon with any kinematically allowed fraction z of its parent quark.

5.5.1 Matrix Element Correction

The hard-collinear correction takes into account the exact matrix element for a single hard-collinear emission, k. As it does not alter the observable definition, $\delta\mathcal{F}_{\rm hc}$ takes the

same form as for event shapes (with explicit rapidity integration, taken into account by the measure $d\mathcal{Z}[\{R'_{\mathrm{NLL},\ell_i}, k_i\}]$). For a full derivation of this correction see Sec. 4.3.2.

$$\delta\mathcal{F}_{\mathrm{hc}}(\lambda) = \sum_{\ell=1,2} \frac{\alpha_s(\sqrt{y_{\mathrm{cut}}}Q)}{2\alpha_s(\mu_R)} \int_0^\infty \frac{d\zeta}{\zeta} \int_0^{2\pi} \frac{d\phi}{2\pi} \int d\mathcal{Z}[\{R'_{\mathrm{NLL},\ell_i}, k_i\}] \int_0^1 \frac{dz}{z} \left(z p_{qg}(z) - 2C_F\right) \times$$
$$\times \left[\Theta\left(1 - \lim_{y_{\mathrm{cut}}\to 0} \frac{\overline{y}_3^{\mathrm{sc}}(\{\tilde{p}\}, k, \{k_i\})}{y_{\mathrm{cut}}}\right) - \Theta\left(1 - \lim_{y_{\mathrm{cut}}\to 0} \frac{\overline{y}_3^{\mathrm{sc}}(\{\tilde{p}\}, \{k_i\})}{y_{\mathrm{cut}}}\right)\Theta(1-\zeta)\right], \tag{5.34}$$

where $z p_{qg} = C_F(1 + (1-z)^2)$.

5.5.2 Observable-Definition Correction: Recoil

The recoil correction implements the effect of the hard-collinear emission on the observable parametrisation by taking into account the exact kinematics of recoil. For a hard-collinear parton k, the approximation $\overline{y}_3^{\mathrm{sc}}(\{\tilde{p}\}, k) = (k_t/Q)^2$ is no longer valid because this transverse momentum is defined with respect to a fixed emitter axis which, for soft particles, coincides with their actual emitters. The recoil instigated by a hard emission breaks the coincidence between these two axes. As such we must explicitly derive the expression for the transverse momentum between a special hard emission, k and its now-displaced emitter. Additionally, the recoil splits the system irrevocably and non-trivially: soft-collinear emissions up to this point will have been emitted with respect to the original axis (which we freely set to be the thrust axis), whereas all subsequent emissions will be emitted from the new, recoiled axis. The y_3 algorithms operate on final state particles, i.e. the y_{ij} pairings correspond to emissions and hard quarks *after* all emissions have occurred. If no clustering partner is found, soft-collinear radiation emitted with respect to the thrust axis will be recombined with the recoiled quark axis, i.e. *not* their emitter. Our entire treatment of the event kinematics must change. To help elucidate this abstract point we include a diagram of a single hard-collinear emission event in Fig. 5.3 and refer the reader to Sec. 4.3 for a full derivation of recoil kinematics.

The relationship between k_t and k'_t is

$$\vec{k}_t \simeq \vec{k}'_t + z\vec{p}'_{\ell,t}\,, \qquad \vec{p}'_{\ell,t} \equiv -\sum_{i\,\in\,\mathcal{H}^{(\ell)}} \vec{k}_{ti}\,, \tag{5.35}$$

where $\vec{p}'_{\ell,t}$ is the transverse momentum of the emitting parton, and the sum runs over all of the remaining soft-collinear emissions emitted off $\tilde{p}_\ell$, for which $z_i \to 0$ (for these emissions the transverse momentum with respect to the thrust axis coincides with the one computed with respect to the emitter). Using the full recoiled expressions for k and $\tilde{p_1}$ the value of y_3 in this system is

$$y_3^{\mathrm{hc}}(\{\tilde{p}\}, k) = \frac{\min\{z, 1-z\}^2}{Q^2} \left|\frac{\vec{k}_t}{z} - \frac{\vec{p}_{\ell,t}}{1-z}\right|^2 = \min\left\{\frac{1}{1-z}, \frac{1}{z}\right\}^2 \left(\frac{k'_t}{Q}\right)^2, \tag{5.36}$$

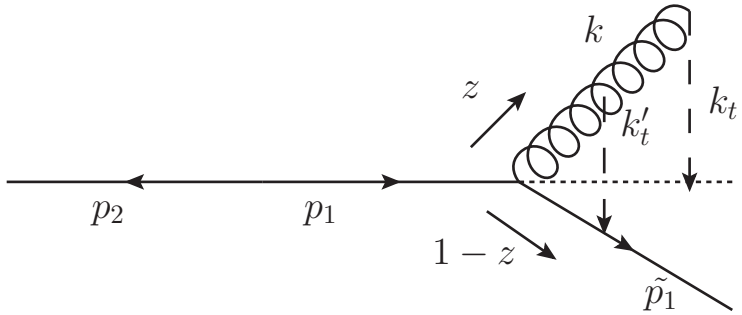

Figure 5.3: The kinematics of recoil: one of the Born partons, p_1 emits a hard emission, k and subsequently recoils to become $\tilde{p_1}$. The dotted line shows the continuation of the original parton axis, coinciding with the thrust axis. k carries a fraction z of the original parton energy, where z is now allowed to take any value between zero and one. k_t is the transverse momentum of k with respect to the thrust axis, whereas k'_t is the transverse momentum of k with respect to its emitter $\tilde{p_1}$. For $z \to 0$ the recoil effect is negligible and k_t and k'_t coincide.

where $\vec{p}_{\ell,t} = \vec{p}'_{\ell,t} - \vec{k}_t$ is the transverse momentum of the Born emitter $\tilde{p}_\ell$ with respect to the thrust axis. Note that, since k is the most energetic parton of the ensemble, its rapidity fraction is by construction the largest of all. We construct an algorithm that can properly deal with the presence of a hard-collinear emission, called $y_3^{\rm hc}$, which is defined:

1. Find the index I of the parton with the smallest $y_3(\{\tilde{p}\}, k_i) (= \overline{y}_3^{\rm sc}(\{\tilde{p}\}, k_i)$ for the soft-collinear partons and $y_3^{\rm hc}(\{\tilde{p}\}, k)$ for the hard-collinear one).

2. Find k_J as in step 2 of the NLL algorithm.

3. If k_J is found, recombine partons I and J into a new pseudo-particle k_P with $\vec{k}_{tP} = \vec{k}_{tI} + \vec{k}_{tJ}$ and $\xi_P^{(\ell)} = \xi_J^{(\ell)}$. Otherwise, k_I is clustered with the Born leg $\tilde{p}_\ell$ it was emitted off as $\vec{p}_{\ell,t} = \vec{k}_{tI} + \vec{p}_{\ell,t}$, and removed from the list of pseudo-particles. If k_P contains the hard-collinear parton (say parton $k_I = k$ is the hard-collinear one) the corresponding $y_3(\{\tilde{p}\}, k_P)$ will be

$$y_3^{\rm hc}(\{\tilde{p}\}, k_P) = \frac{\min\{z, 1-z\}^2}{Q^2} \left| \frac{\vec{k}_{tP}}{z} - \frac{\vec{p}_{\ell,t}}{1-z} \right|^2 .$$

   This quantity will be used in step 1 of the next iteration.

4. Repeat until only one pseudo-particle k_P remains, and set $y_3(\{\tilde{p}\}, k_1, \ldots, k_n) = y_3(\{\tilde{p}\}, k_P)$.

The recoil correction then takes the form

$$\delta\mathcal{F}_{\rm rec}(\lambda) = \sum_{\ell=1,2} \frac{\alpha_s(\sqrt{y_{\rm cut}}Q)}{2\alpha_s(\mu_R)} \int_0^\infty \frac{d\zeta}{\zeta} \int_0^{2\pi} \frac{d\phi}{2\pi} \int d\mathcal{Z}[\{R'_{{\rm NLL},\ell_i}, k_i\}] \int_0^1 dz\, p_{qg}(z) \times$$
$$\times \left[\Theta\left(1 - \lim_{y_{\rm cut}\to 0} \frac{y_3^{\rm hc}(\{\tilde{p}\}, k', \{k_i\})}{y_{\rm cut}}\right) - \Theta\left(1 - \lim_{y_{\rm cut}\to 0} \frac{\overline{y}_3^{\rm sc}(\{\tilde{p}\}, k, \{k_i\})}{y_{\rm cut}}\right)\right] , \tag{5.37}$$

where $\zeta y_{\rm cut} Q^2 = (k_t')^2$, and the momentum of the hard-collinear gluon k' is a function of ζ, $\vec{\tilde{p}}'_{\ell,t}$, and z. The momentum k in the second theta-function is obtained from k' by taking the limit $z \to 0$.

5.6 Soft-wide angle Correction

This correction describes the contribution from configurations where an ensemble of soft-collinear partons is accompanied by an emission k at wide angles with respect to its emitter. This violates the small-angle assumption made on the NLL-observable and necessitates a modified algorithm which is correctly parametrised in the presence of the soft-wide angle emission. We introduce the algorithm $y_3^{\rm wa}$, which reduces to $\overline{y}_3^{\rm sc}$ for any emissions that do not include the special k. $y_3^{\rm wa}(\{\tilde{p}\}, k)$, however, is equal to the full expression for the distance measure given in Eq. (5.2). Since, by definition, the wide-angle emission has the smallest rapidity fraction amongst all emissions, if it recombines with any of the other collinear partons, it will be pulled at larger rapidity fractions (recall the NLL algorithm item 3 from Sec. 5.2.1). Therefore, the result of the recombination will be the same as if k were soft and collinear. It follows that the soft-wide angle contribution is non-zero only if k does not cluster with any of the soft-collinear emissions.
Therefore the expression of y_3 is equal to the distance measure between k and its emitter,

$$y_3(\{\tilde{p}\}, k) = 2\frac{E^2}{Q^2}\left(1 - |\cos\theta|\right) , \tag{5.38}$$

where θ is the angle with respect to the direction identified by the Born momenta, which remain back-to-back in the presence of soft emissions, and practically coincides with the thrust axis. The corresponding observable $y_3^{\rm wa}(\{\tilde{p}\}, k, \{k_i\})$ can be computed by means of the NLL algorithm for strongly-ordered emissions, but where one uses Eq. (5.38) to express $y_3(\{\tilde{p}\}, k)$ for the soft-wide-angle emission k. As soon as the latter is clustered with any of the remaining soft-collinear emissions, the algorithm simply reduces to the NLL one in its original form. The soft-wide angle contribution takes the form

$$\begin{aligned}\delta\mathcal{F}_{\rm wa}(\lambda) = C_F \frac{\alpha_s(\sqrt{y_{\rm cut}}Q)}{\alpha_s(\mu_R)} \int_0^\infty \frac{d\zeta}{\zeta} \int_{-\infty}^{\infty} d\eta \int_0^{2\pi} \frac{d\phi}{2\pi} \int d\mathcal{Z}[\{R'_{{\rm NLL},\ell_i}, k_i\}] \\ \times \left[\Theta\left(1 - \lim_{y_{\rm cut}\to 0} \frac{y_3^{\rm wa}(\{\tilde{p}\}, k, \{k_i\})}{y_{\rm cut}}\right) - \Theta\left(1 - \lim_{y_{\rm cut}\to 0} \frac{\overline{y}_3^{\rm sc}(\{\tilde{p}\}, k, \{k_i\})}{y_{\rm cut}}\right)\right] ,\end{aligned} \tag{5.39}$$

with $\zeta y_{\rm cut} Q^2 = k_t^2$, and η the emission's rapidity with respect to the thrust axis. In the second Θ-function all emissions are treated as soft-collinear, even the special emission. To be clear, the special emission maintains its k_t, ϕ and hemisphere, but is now treated as if it were collinear.

5.7 Clustering Correction

This correction describes an ensemble of soft-collinear partons emitted off the Born legs of which at most two are close in rapidity, the remaining ones being strongly separated in angle. For this kinematic configuration we need to amend the algorithm $\overline{y}_3^{\rm sc}$ outlined in Sec. 5.2.1 to include the potential clustering of two emissions that are close in rapidity. The resulting algorithm, which we call $y_3^{\rm sc}$, is identical to the strongly-ordered one, except in its dealing with y_{ab} where k_a, k_b are the emissions close in rapidity. We consider an arbitrary point in the clustering sequence. These particles may have already been involved in clusterings and live within pseudo-particles which we will call k_{J_a}, k_{J_b}. An additional step is needed after step 1:

1b. If pseudo-particles k_{J_a} and k_{J_b} are close in rapidity (i.e. if neither k_a nor k_b have been recombined with a pseudo-particle with larger $\xi^{(\ell)}$), check whether k_{J_a} and k_{J_b} cluster, i.e. if

$$\min\{E_{J_a}, E_{J_b}\}^2 |\vec{\theta}_{J_a} - \vec{\theta}_{J_b}|^2 < \min\{k_{tJ_a}, k_{tJ_b}\}^2 \tag{5.40}$$

is satisfied, where $\vec{\theta}_i = \vec{k}_{ti}/E_i$. If so, recombine k_{J_a} and k_{J_b} by adding transverse momenta vectorially, and set the rapidity fraction of the resulting pseudo-particle k_J to $\xi_J^{(\ell)} \simeq \xi_{J_a}^{(\ell)} \simeq \xi_{J_b}^{(\ell)}$.

The clustering correction takes into account only the scenario in which two emissions close in angle cluster thanks to the full algorithm expression.

$$\begin{aligned}\delta\mathcal{F}_{\rm clust}(\lambda) = \frac{1}{2!}\int_0^\infty \frac{d\zeta_a}{\zeta_a}\int_0^{2\pi}\frac{d\phi_a}{2\pi}\sum_{\ell_a=1,2}\int_0^1 d\xi_a^{(\ell_a)}\left(\frac{2C_F\lambda}{\beta_0}\frac{R''_{\ell_a}(y_{\rm cut})}{\alpha_s(\mu_R)}\right)\times \\ \times\int_0^\infty\frac{d\kappa}{\kappa}\int_{-\infty}^\infty d\eta\int_0^{2\pi}\frac{d\phi}{2\pi}\int d\mathcal{Z}[\{R'_{{\rm NLL},\ell_i}, k_i\}]\times \\ \times\left[\Theta\left(1-\lim_{y_{\rm cut}\to 0}\frac{y_3^{\rm sc}(\{\tilde{p}\}, k_a, k_b, \{k_i\})}{y_{\rm cut}}\right) - \Theta\left(1-\lim_{y_{\rm cut}\to 0}\frac{\overline{y}_3^{\rm sc}(\{\tilde{p}\}, k_a, k_b, \{k_i\})}{y_{\rm cut}}\right)\right],\end{aligned} \tag{5.41}$$

where the $\{k_i\}$ are the soft-collinear emissions from before. We have parametrised the phase space of the emission k_b as we did for the correlated emissions in Sec. 4.5, namely in terms of the variables

$$\kappa = k_{t,b}/k_{t,a} \qquad \eta = \eta_b - \eta_a\,, \qquad \phi = \phi_b - \phi_a\,. \tag{5.42}$$

In terms of these variables k_b can be written as

$$k_b = \kappa\, Q\,\sqrt{\zeta_a y_{\rm cut}}(\cosh(\eta_a+\eta), \cos(\phi_a+\phi), \sin(\phi_a+\phi), \sinh(\eta_a+\eta))\,. \tag{5.43}$$

In order to eliminate subleading effects, in the calculation of the observable we impose that k_b belongs to the same hemisphere as k_a. In practice, this is accomplished by setting $\ell_b = \ell_a$ and $\xi_b^{(\ell_a)} = \xi_a^{(\ell_a)} + {\rm sign}(\eta)\delta\xi$, with $\delta\xi$ an arbitrarily small quantity.
The effect of two emissions close in rapidity that end up in different jets is captured by

the correlated correction, described in the next section.

5.8 Correlated Correction

The correlated correction describes the same ensemble of independently-emitted soft-collinear partons of the previous section. The property of rIRC safety ensures that the splitting can be treated inclusively at NLL. This was done in $R_{\rm NLL}(v)$. At NNLL the splitting must be resolved explicity, and so we allow the full algorithm to run on the real correlated emissions living in the multiple emissions function. This gives

$$\begin{aligned}\delta\mathcal{F}_{\rm correl}(\lambda) = &\int_0^\infty \frac{d\zeta_a}{\zeta_a}\int_0^{2\pi}\frac{d\phi_a}{2\pi}\sum_{\ell_a=1,2}\int_0^1 d\xi_a^{(\ell_a)}\left(\frac{2C_F\lambda}{\beta_0}\frac{R''_{\ell_a}(y_{\rm cut})}{\alpha_s(\mu_R)}\right)\times\\ &\times\int_0^\infty\frac{d\kappa}{\kappa}\int_{-\infty}^{\infty}d\eta\int_0^{2\pi}\frac{d\phi}{2\pi}\frac{1}{2!}C_{ab}(\kappa,\eta,\phi)\int d\mathcal{Z}[\{R'_{{\rm NLL},\ell_i},k_i\}]\times\\ &\times\left[\Theta\left(1-\lim_{y_{\rm cut}\to 0}\frac{y_3^{\rm sc}(\{\tilde p\},k_a,k_b,\{k_i\})}{y_{\rm cut}}\right)-\Theta\left(1-\lim_{y_{\rm cut}\to 0}\frac{\overline{y}_3^{\rm sc}(\{\tilde p\},k_a+k_b,\{k_i\})}{y_{\rm cut}}\right)\right],\end{aligned} \tag{5.44}$$

where

$$C_{ab}(\kappa,\eta,\phi)=\frac{\tilde M^2(k_a,k_b)}{M^2_{sc}(k_a)M^2_{sc}(k_b)}\,, \tag{5.45}$$

is the ratio of the correlated matrix element $\tilde M^2(k_a,k_b)=M^2(k_a,k_b)-M^2(k_a)M^2(k_b)$ (i.e. the difference of the full two-parton matrix element and the independent emission contribution) to the product of the two soft-collinear matrix elements for the emissions of k_a and k_b. Notice that C_{ab} depends only on the correlation variables κ,η,ϕ defined in Eq. (5.42). The observable $y_3^{\rm sc}(\{\tilde p\},k_a,k_b,\{k_i\})$ is computed with the same algorithm used for the clustering correction. In the inclusive approximation $y_3^{\rm sc}(\{\tilde p\},k_a+k_b,\{k_i\})$ reduces to the NLL value $\overline{y}_3^{\rm sc}(\{\tilde p\},k_a+k_b,\{k_i\})$ in which case the result is zero. As is done for the clustering correction, we impose that k_b belongs to the same hemisphere as k_a in order to neglect undesired subleading effects. While for the Durham the observable $y_3^{\rm sc}(\{\tilde p\},k_a,k_b,\{k_i\})$ is computed using the algorithm given above for the clustering corrections, in the case of the Cambridge the final expression simplifies considerably. The Cambridge result is discussed in Sec. 5.9.5.

5.9 Analytic Results for the Cambridge Algorithm

Until this point we have been working with the Durham algorithm. In the next sections we will see that results for the NNLL multiple emissions functions $\{\delta\mathcal{F}\}$ for the two-jet rate in the Cambridge algorithm can be produced by making simplifications on those derived for the Durham algorithm. Recall from Sec. 5.2.2 that due to the Cambridge algorithm's energy-independent ordering variable there can be no clustering when emissions are widely separated in rapidity, i.e. there can be no clustering between any two emissions at NLL accuracy. This fact allows us to factorise the effect of each special emission since the NNLL

kinematics cannot be 'mixed up' into the soft-collinear ensemble via clustering as was the case for the Durham multiple emissions functions. Even for the clustering and correlated corrections we can consider that there are two special emissions which cannot talk to the rest of the ensemble. Hence we will be left with a contribution from the ensemble as a whole, and a contribution from just one special emission or a pair of correlated emissions, which can be determined analytically.

5.9.1 Soft-collinear Correction

The form of the soft-collinear corrections $\delta\mathcal{F}_{\rm sc}$ given in Eqs. (5.25) and (5.32) can be simplified using the normalisation of the soft-collinear ensemble in the Cambridge algorithm (Eq. 5.17) giving

$$\begin{aligned}
&\Theta\left(1-\lim_{y_{\rm cut}\to 0}\frac{\overline{y}_3^{\rm sc}(\{\tilde{p}\},k,\{k_i\})}{y_{\rm cut}}\right)-\Theta(1-\zeta)\Theta\left(1-\lim_{y_{\rm cut}\to 0}\frac{\overline{y}_3^{\rm sc}(\{\tilde{p}\},\{k_i\})}{y_{\rm cut}}\right)\\
&=\left[\Theta\left(1-\lim_{y_{\rm cut}\to 0}\frac{\overline{y}_3^{\rm sc}(\{\tilde{p}\},k)}{y_{\rm cut}}\right)-\Theta(1-\zeta)\right]\prod_{i=1}^{n}\Theta\left(1-\lim_{y_{\rm cut}\to 0}\frac{y_3^{\rm sc}(\{\tilde{p}\},k_i)}{y_{\rm cut}}\right)=0\,, \quad (5.46)
\end{aligned}$$

where we made use of the definition of $\zeta = y_3^{\rm sc}(\{\tilde{p}\},\{k\})/y_{\rm cut}$. This result trivially leads to $\delta\mathcal{F}_{\rm sc}^{C}(\lambda) = 0$. Intuitively this makes sense: even though we are taking into account running coupling and correct rapidity limits, we are still left with a soft-collinear ensemble of emissions widely separated in angle, and so by the Cambridge algorithm these cannot cluster.

5.9.2 Hard-collinear Corrections

Matrix Element Correction

We start from the hard-collinear matrix element contribution to $\delta\mathcal{F}$ for the Durham algorithm in Eq. (5.34). We use the fact that the measure $d\mathcal{Z}[\{R'_{{\rm NLL},\ell_i},k_i\}]$ integrates to one to cancel the effect of the soft-collinear ensemble. The remaining piece is the effect of the hard-collinear emission,

$$\begin{aligned}
\delta\mathcal{F}_{\rm hc}^{C}(\lambda) &= \sum_{\ell=1,2}\frac{\alpha_s(\sqrt{y_{\rm cut}}Q)}{2\alpha_s(\mu_R)}\int_0^\infty\frac{d\zeta}{\zeta}\int_0^{2\pi}\frac{d\phi}{2\pi}\times\\
&\times\int_0^1\frac{dz}{z}\left(zp_{qg}(z)-2C_F\right)\left[\Theta\left(1-\lim_{y_{\rm cut}\to 0}\frac{\overline{y}_3^{\rm sc}(\{\tilde{p}\},k)}{y_{\rm cut}}\right)-\Theta(1-\zeta)\right]=0\,,
\end{aligned} \quad (5.47)$$

where we used the fact that $\zeta = y_3^{\rm sc}(\{\tilde{p}\},\{k\})/y_{\rm cut}$. Again, this vanishing result should not be surprising. A change in the matrix element of one emission has no effect on the system's ability to cluster particles with the Cambridge algorithm. The observable maintains its NLL value, allowing for the cancellation of Θ-functions.

Observable-Definition Correction: Recoil

For the recoil correction, we use the same rephrasing of emission kinematics as was developed in Sec. 4.3 and further discussed in Sec. 5.5.2 for the two-jet rate. The normalisation

condition of Eq. (5.17) leads to a simplified formula for $\delta\mathcal{F}_{\rm rec}$ (Eq. (5.37)) in which the contribution from the hard-collinear emission factorises with respect to the soft-collinear ones. Since the hard-collinear emission k propagates at very high rapidity, it lives in a region apart from the soft-collinear ensemble. We have,

$$\Theta\left(1-\lim_{y_{\rm cut}\to 0}\frac{y_3^{\rm hc}(\{\tilde{p}\},k',\{k_1,\dots,k_n\})}{y_{\rm cut}}\right)=\Theta\left(1-\lim_{y_{\rm cut}\to 0}\frac{y_3^{\rm hc}(\{\tilde{p}\},k')}{y_{\rm cut}}\right)\times \\ \times\prod_{i=1}^{n}\Theta\left(1-\lim_{y_{\rm cut}\to 0}\frac{y_3^{\rm sc}(\{\tilde{p}\},k_i)}{y_{\rm cut}}\right). \tag{5.48}$$

The integration of the soft-collinear ensemble's contribution over the measure $d\mathcal{Z}[\{R'_{{\rm NLL},\ell_i},k_i\}]$ gives one, leaving just the contribution from the hard-collinear emission,

$$\delta\mathcal{F}^C_{\rm rec}(\lambda)=\sum_{\ell=1,2}\frac{\alpha_s(\sqrt{y_{\rm cut}}Q)}{2\alpha_s(\mu_R)}\int_0^\infty\frac{d\zeta}{\zeta}\int_0^{2\pi}\frac{d\phi}{2\pi}\times \\ \times\int_0^1 dz\,p_{qg}(z)\left[\Theta\left(1-\lim_{y_{\rm cut}\to 0}\frac{y_3^{\rm hc}(\{\tilde{p}\},k')}{y_{\rm cut}}\right)-\Theta\left(1-\lim_{y_{\rm cut}\to 0}\frac{\overline{y}_3^{\rm sc}(\{\tilde{p}\},k)}{y_{\rm cut}}\right)\right]. \tag{5.49}$$

Using the expression for the observable in the presence of a hard-collinear emission taken from Eq. (5.36),

$$\frac{y_3^{\rm hc}(\{\tilde{p}\},k')}{y_{\rm cut}}=\min\left\{\frac{1}{1-z},\frac{1}{z}\right\}^2\zeta=\frac{1}{\max(z^2,(1-z)^2)}\zeta\,, \tag{5.50}$$

which can be plugged in Eq. (5.49) to obtain

$$\delta\mathcal{F}^C_{\rm rec}(\lambda)=\frac{\alpha_s(\sqrt{y_{\rm cut}}Q)}{\alpha_s(\mu_R)}\int_0^1 dz\,p_{qg}(z)\ln\left[\max(z^2,(1-z)^2)\right]=C_F\frac{\alpha_s(\sqrt{y_{\rm cut}}Q)}{\alpha_s(\mu_R)}\left(3-\frac{\pi^2}{3}-3\ln 2\right). \tag{5.51}$$

5.9.3 Soft-wide angle Correction

For the Cambridge algorithm the wide-angle correction to the multiple emissions function takes the simplified form

$$\delta\mathcal{F}^C_{\rm wa}(\lambda)=C_F\frac{\alpha_s(\sqrt{y_{\rm cut}}Q)}{\alpha_s(\mu_R)}\int_0^\infty\frac{d\zeta}{\zeta}\int_{-\infty}^{\infty}d\eta\int_0^{2\pi}\frac{d\phi}{2\pi}\int d\mathcal{Z}[\{R'_{{\rm NLL},\ell_i},k_i\}] \\ \times\left[\Theta\left(1-\lim_{y_{\rm cut}\to 0}\frac{y_3^{\rm wa}(\{\tilde{p}\},k)}{y_{\rm cut}}\right)\Theta\left(1-\lim_{y_{\rm cut}\to 0}\frac{\overline{y}_3^{\rm sc}(\{\tilde{p}\},\{k_i\})}{y_3^{\rm wa}(\{\tilde{p}\},k)}\right)\right. \\ \left.-\Theta\left(1-\lim_{y_{\rm cut}\to 0}\frac{y_3^{\rm sc}(\{\tilde{p}\},k)}{y_{\rm cut}}\right)\Theta\left(1-\lim_{y_{\rm cut}\to 0}\frac{\overline{y}_3^{\rm sc}(\{\tilde{p}\},\{k_i\})}{y_3^{\rm sc}(\{\tilde{p}\},k)}\right)\right], \tag{5.52}$$

thanks to the factorisation of the soft-collinear ensemble from the special emission living in the large angle region. Since the Cambridge algorithm does not cluster objects widely separated in rapidity, the only non-trivial contribution comes when the soft wide-angle emission is the last particle to be recombined, namely if $y_3^{\rm wa}(\{\tilde{p}\},k)>\overline{y}_3^{\rm sc}(\{\tilde{p}\},\{k_i\})$. We

then obtain

$$\delta\mathcal{F}^C_{\rm wa}(\lambda) = C_F \frac{\alpha_s(\sqrt{y_{\rm cut}}Q)}{\alpha_s(\mu_R)} \int_0^\infty \frac{d\zeta}{\zeta} \int_{-\infty}^\infty d\eta \int_0^{2\pi} \frac{d\phi}{2\pi} \int d\mathcal{Z}[\{R'_{{\rm NLL},\ell_i}, k_i\}] \times \left[\Theta\left(1 - \lim_{y_{\rm cut}\to 0} \frac{y_3^{\rm wa}(\{\tilde{p}\}, k)}{y_{\rm cut}}\right) - \Theta\left(1 - \lim_{y_{\rm cut}\to 0} \frac{y_3^{\rm sc}(\{\tilde{p}\}, k)}{y_{\rm cut}}\right)\right] . \tag{5.53}$$

Writing the full expression for the Cambridge distance measure Eq. (5.1) in terms of ζ and η, the three-jet resolution parameter for the Born quarks plus emission k is given by

$$\frac{y_3^{\rm wa}(\{\tilde{p}\}, k)}{y_{\rm cut}} = \zeta\left(1 + e^{-2|\eta|}\right) , \tag{5.54}$$

from which it follows that

$$\delta\mathcal{F}^C_{\rm wa}(\lambda) = -C_F \frac{\alpha_s(\sqrt{y_{\rm cut}}Q)}{\alpha_s(\mu_R)} \int_{-\infty}^\infty d\eta \, \ln\left(1 + e^{-2|\eta|}\right) = -C_F \frac{\pi^2}{12} \frac{\alpha_s(\sqrt{y_{\rm cut}}Q)}{\alpha_s(\mu_R)} . \tag{5.55}$$

5.9.4 Clustering Correction

The clustering correction to the multiple emissions function in the Cambridge algorithm simply reduces to a clustering of two correlated soft-collinear partons. Emissions from the rest of the ensemble are widely separated in rapidity from each other and so all other clustering is forbidden. This fact allows us to make the replacement

$$\Theta\left(1 - \lim_{y_{\rm cut}\to 0} \frac{y_3^{\rm sc}(\{\tilde{p}\}, k_a, k_b, k_1, \ldots, k_n)}{y_{\rm cut}}\right) = \Theta\left(1 - \lim_{y_{\rm cut}\to 0} \frac{y_3^{\rm sc}(\{\tilde{p}\}, k_a, k_b)}{y_{\rm cut}}\right) \times \times \prod_{i=1}^n \Theta\left(1 - \lim_{y_{\rm cut}\to 0} \frac{y_3^{\rm sc}(\{\tilde{p}\}, k_i)}{y_{\rm cut}}\right) . \tag{5.56}$$

The contribution of any number of widely separated emissions gives one, due to the normalisation property of the measure $d\mathcal{Z}[\{R'_{{\rm NLL},\ell_i}, k_i\}]$ shown in Eq. (5.17). We implement these simplifications in the clustering contribution result for the Durham algorithm in Eq. (5.41), giving

$$\delta\mathcal{F}^C_{\rm clust}(\lambda) = \frac{1}{2!} \int_0^\infty \frac{d\zeta_a}{\zeta_a} \int_0^{2\pi} \frac{d\phi_a}{2\pi} \sum_{\ell_a=1,2} \int_0^1 d\xi_a^{(\ell_a)} \left(\frac{2C_F\lambda}{\beta_0} \frac{R''_{\ell_a}(y_{\rm cut})}{\alpha_s(\mu_R)}\right) \int_0^\infty \frac{d\kappa}{\kappa} \int_{-\infty}^\infty d\eta \int_0^{2\pi} \frac{d\phi}{2\pi} \times \times \left[\Theta\left(1 - \lim_{y_{\rm cut}\to 0} \frac{y_3^{\rm sc}(\{\tilde{p}\}, k_a, k_b)}{y_{\rm cut}}\right) - \Theta\left(1 - \lim_{y_{\rm cut}\to 0} \frac{\overline{y}_3^{\rm sc}(\{\tilde{p}\}, k_a, k_b)}{y_{\rm cut}}\right)\right] . \tag{5.57}$$

The clustering correction takes into account the effect from correlated emissions which cluster under the full clustering conditions. Since no clustering is allowed at NLL in the Cambridge algorithm, $\overline{y}_3^{\rm sc}(\{\tilde{p}\}, k_a, k_b) = \max(\overline{y}_3^{\rm sc}(\{\tilde{p}\}, k_a), \overline{y}_3^{\rm sc}(\{\tilde{p}\}, k_b))$. By definition the emissions must cluster in the modified algorithm, i.e. $y_3^{\rm sc}(\{\tilde{p}\}, k_a, k_b) = y_3^{\rm sc}(\{\tilde{p}\}, k_a + k_b)$, for a non-zero result. Substituting these expressions for the NLL and modified soft-collinear

algorithms gives,

$$\begin{aligned}\delta\mathcal{F}^{C}_{\text{clust}}(\lambda) = \frac{1}{2!}\int_0^\infty \frac{d\zeta_a}{\zeta_a}\int_0^{2\pi}\frac{d\phi_a}{2\pi}\sum_{\ell_a=1,2}\int_0^1 d\xi_a^{(\ell_a)}\left(\frac{2C_F\lambda}{\beta_0}\frac{R''_{\ell_a}(y_{\text{cut}})}{\alpha_s(\mu_R)}\right)\int_0^\infty\frac{d\kappa}{\kappa}\int_{-\infty}^{\infty}d\eta\int_0^{2\pi}\frac{d\phi}{2\pi}\times \\ \times\left[\Theta\left(1-\lim_{y_{\text{cut}}\to 0}\frac{y_3^{\text{sc}}(\{\tilde{p}\},k_a+k_b)}{y_{\text{cut}}}\right)-\Theta\left(1-\lim_{y_{\text{cut}}\to 0}\frac{\max(y_3^{\text{sc}}(\{\tilde{p}\},k_a),y_3^{\text{sc}}(\{\tilde{p}\},k_b))}{y_{\text{cut}}}\right)\right]\times \\ \times\,\Theta_{\text{clust}}\,,\end{aligned} \tag{5.58}$$

where Θ_{clust} restricts the allowed phase space to the region where the two emissions k_a and k_b cluster. Using the ordering variable for the Cambridge algorithm (Eq. (5.1)) in the small-angle approximation, emissions a and b will cluster if

$$|\vec{\theta_a}-\vec{\theta_b}|^2<\min\{\theta_a,\theta_b\}^2 \qquad\Leftrightarrow\qquad \Theta_{\text{clust}}=\Theta\left(\ln(2\cos\phi)-|\eta|\right)\Theta\left(\frac{\pi}{3}-|\phi|\right). \tag{5.59}$$

Applying these constraints gives

$$\begin{aligned}\delta\mathcal{F}^{C}_{\text{clust}}(\lambda) &= \sum_{\ell_a=1,2}\left(\frac{2C_F\lambda}{\beta_0}\frac{R''_{\ell_a}(y_{\text{cut}})}{\alpha_s(\mu_R)}\right)\int_0^\infty\frac{d\kappa}{\kappa}\int_{-\frac{\pi}{3}}^{\frac{\pi}{3}}\frac{d\phi}{2\pi}\ln(2\cos\phi)\ln\left(\frac{\max\{1,\kappa^2\}}{1+\kappa^2+2\kappa\cos\phi}\right) \\ &\approx \sum_{\ell_a=1,2}\left(\frac{2C_F\lambda}{\beta_0}\frac{R''_{\ell_a}(y_{\text{cut}})}{\alpha_s(\mu_R)}\right)(-0.49394)\,.\end{aligned} \tag{5.60}$$

5.9.5 Correlated Correction

We again take the result for the Durham algorithm, this time from Eq. (5.44), separating out the disparate-rapidity soft-collinear ensemble which are incapable of clustering, and write

$$\begin{aligned}\delta\mathcal{F}^{C}_{\text{correl}}(\lambda) = \int_0^\infty \frac{d\zeta_a}{\zeta_a}\int_0^{2\pi}\frac{d\phi_a}{2\pi}\sum_{\ell_a=1,2}\int_0^1 d\xi_a^{(\ell_a)}\left(\frac{2C_F\lambda}{\beta_0}\frac{R''_{\ell_a}(y_{\text{cut}})}{\alpha_s(\mu_R)}\right)\int_0^\infty\frac{d\kappa}{\kappa}\int_{-\infty}^{\infty}d\eta\times \\ \times\int_0^{2\pi}\frac{d\phi}{2\pi}\frac{1}{2!}C_{ab}(\kappa,\eta,\phi)\times \\ \times\left[\Theta\left(1-\lim_{y_{\text{cut}}\to 0}\frac{\max\{y_3^{\text{sc}}(\{\tilde{p}\},k_a),y_3^{\text{sc}}(\{\tilde{p}\},k_b)\}}{y_{\text{cut}}}\right)-\Theta\left(1-\lim_{y_{\text{cut}}\to 0}\frac{y_3^{\text{sc}}(\{\tilde{p}\},k_a+k_b)}{y_{\text{cut}}}\right)\right]\times \\ \times\,(1-\Theta_{\text{clust}})\,,\end{aligned} \tag{5.61}$$

where Θ_{clust} is defined in Eq. (5.59). It is clear that $\delta\mathcal{F}_{\text{correl}}$ is non-zero only when k_a and k_b are *not* clustered in the first Θ function. This leads to

$$\begin{aligned}\delta\mathcal{F}^{C}_{\text{correl}}(\lambda) = \sum_{\ell_a=1,2}\left(\frac{2C_F\lambda}{\beta_0}\frac{R''_{\ell_a}(y_{\text{cut}})}{\alpha_s(\mu_R)}\right)\int_0^\infty\frac{d\kappa}{\kappa}\int_0^{2\pi}\frac{d\phi}{2\pi}\frac{1}{2!}\int_{-\infty}^{\infty}d\eta\,C_{ab}(\kappa,\eta,\phi)\times \\ \times\ln\left(\frac{1+\kappa^2+2\kappa\cos\phi}{\max\{1,\kappa^2\}}\right)(1-\Theta_{\text{clust}})\,.\end{aligned} \tag{5.62}$$

This integral can be evaluated numerically giving

$$\delta\mathcal{F}^{C}_{\rm correl}(\lambda) \approx \sum_{\ell_a=1,2} \left(\frac{\lambda}{\beta_0} \frac{R''_{\ell_a}(y_{\rm cut})}{\alpha_s(\mu_R)} \right) (2.1011 C_A + 1.496 \times 10^{-2} n_f)\,. \tag{5.63}$$

Chapter 6

Validation of Results

in which I show how the ARES *resummation compares to data and previous theory calculations.*

We have completed a full and exact NNLL resummation of seven event shape observables and the two-jet rate in $e^+e^- \to 2$ jets. We now turn to contextualising our calculations with other event shape and jet rate determinations. Firstly this is a validation of our results and secondly it allows us to combine resummed and fixed-order solutions which are valid across the entire range of observable values.

6.1 Matching the Resummation to Fixed-Order Results

Resummed calculations are necessary to restore the reliability of the perturbative series in α_s at small observable values. In order to obtain a calculation of observable cross-sections accurate across the entire range of observable values $(0, 1)$ we must match our resummed results with standard fixed-order calculations.
We use the $\log(R)$-matching scheme [15], expanding the expression of the master formula given in Eq. (4.9) to a given order i in α_s,

$$\Sigma(v) = \sum_{i=1,\ j\geq i-1} \Sigma_{ij} \alpha_s^i L^j \,, \qquad L = \ln 1/v \,, \tag{6.1}$$

where the maximum i is determined by the fixed-order accuracy to which we are matching, while the maximum $j = 2i$. The initial j value in Eq. (6.1) corresponds to NNLL terms. The expansion coefficients $\{\Sigma_{ij}\}$ are determined analytically by expanding the exponential Sudakov factor and collecting the terms appearing at each order. We expand our NNLL resummation to third order in α_s which requires $i \in (1, 3)$ and $j \in (i-1, 2i)$. Note that a leading logarithmic term is now any term of the form $\alpha_s^n\{L^{2n}, L^{2n-1}, \ldots, L^{n+1}\}$ since we have expanded the exponent and revealed the original logarithmic structure initially discussed in Sec. 2.2.4. The expansion of Eq. (6.1) neglects higher order terms in α_s that are not captured by fixed-order calculations. Re-shuffling the perturbative series to its original form allows us to match the logarithmically enhanced pieces of the calculation to fixed-order pieces, order by order in α_s.

At orders higher than α_s^2 the analytic expansion coefficients become extensive and are excluded here for brevity. Full expressions for all Σ_{ij} in the above i, j ranges and for the eight observables considered are given in Appendix A. Below we give a flavour of the coefficients by stating those relevant for two-jet rate matching, up to NLO and NNLL.

$$\begin{aligned}
\Sigma_{12} &= -\frac{A_1}{2} \\
\Sigma_{11} &= -B_1 \\
\Sigma_{10} &= \pi^2 C_F - 7C_F + \mathcal{F}_{10} \\
\Sigma_{24} &= \frac{A_1^2}{8} \\
\Sigma_{23} &= \frac{A_1 B_1}{2} - \frac{2}{3}\pi A_1 \beta_0 \\
\Sigma_{22} &= \frac{A_1}{2}\left(-\pi^2 C_F + 7C_F - \mathcal{F}_{10}\right) - \frac{A_2}{2} + \frac{B_1^2}{2} - \pi\beta_0 B_1 + \mathcal{F}_{22} \\
\Sigma_{21} &= B_1\left(-\pi^2 C_F + 7C_F - \mathcal{F}_{10}\right) + \frac{1}{3}\left(-3B_2 + C_F\left(-\pi^3\beta_0 + 6\pi\beta_0\right) + 3\mathcal{F}_{21}\right) .
\end{aligned} \tag{6.2}$$

The $A_i(B_i)$ are constants parametrising leading-logarithmic (NLL) contributions from i emissions. Their observable-specific values are given in Appendix A.

Looking at Eq. (6.2) it is clear that we will need to know the value of the multiple emissions functions for a given number of emissions and at a given logarithmic order. We employ `ARES` to produce the numerical expansion of the multiple emissions functions, formulated similarly to the full-result expansion of Eq. (6.1),

$$\mathcal{F}_{\mathrm{NLL}}(\lambda) + \frac{\alpha_s(Q)}{\pi}\delta\mathcal{F}_{\mathrm{NNLL}}(\lambda) = \sum_{i=1, j\geq i-1} \mathcal{F}_{ij}\left(\frac{\alpha_s}{2\pi}\right)^i L^j . \tag{6.3}$$

The expanded multiple emissions functions (including every kinematic contribution) are given in Table 6.1 for the event shapes we considered, and in Table 6.2 for the two-jet rate in the Durham and Cambridge algorithms.

	T	C	ρ_H	B_T	B_W	T_M	O
$\mathcal{F}_{22}$	-23.394(6)	-23.394(6)	-11.697(4)	-74.121(6)	-27.332(7)	-53.287(7)	42.975(9)
$\mathcal{F}_{33}$	-208.252(3)	-208.252(3)	-119.324(2)	-724.49(2)	-371.76(2)	-563.24(7)	513.96(8)
$\mathcal{F}_{10}$	-5.4396	-1.0532	-5.4396	0	0	0	0
$\mathcal{F}_{21}$	-19.951(7)	-70.157(1)	-20.401(9)	61.45(2)	59.65(2)	-10.080(9)	80.79(5)
$\mathcal{F}_{32}$	-463.51(6)	-1427.72(5)	-247.79(4)	-717.1(1)	335.8(9)	-1287.0(8)	-79.(5)

Table 6.1: Expansion coefficients for the multiple emissions function up to $\mathcal{O}(\alpha_s^3)$ at NLL ($\mathcal{F}_{22}$, $\mathcal{F}_{33}$), and NNLL ($\mathcal{F}_{10}$, $\mathcal{F}_{21}$, and $\mathcal{F}_{32}$). The digit in brackets signifies the error.

Plugging in the order-specific values from Eq. (6.2) and Tables 6.1 and 6.2 to Eq. (6.1), we match to distributions from the event generators `EVENT2` [48] and `EERAD3` [49]. Fixed-order event generators determine the coefficients of α_s for a given observable. Hence we

	Durham	Cambridge
$\mathcal{F}_{22}$	-2.1932(2)	0
$\mathcal{F}_{33}$	-15.831(7)	0
$\mathcal{F}_{10}$	-8.5114(0)	-8.5114(0)
$\mathcal{F}_{21}$	-14.631(3)	-5.635(3)
$\mathcal{F}_{32}$	10.8(4)	81.86(3)

Table 6.2: Numerical expansion coefficients to $\mathcal{O}(\alpha_s^3)$ for the multiple emissions functions $\mathcal{F}_{\rm NLL}$ ($\mathcal{F}_{22}$, $\mathcal{F}_{33}$) and its NNLL correction $\mathcal{F}_{\rm NNLL}$ ($\mathcal{F}_{10}$, $\mathcal{F}_{21}$, $\mathcal{F}_{32}$).

are matching according to:

$$\begin{aligned} C_1 &\approx \Sigma_{12}L^2 + \Sigma_{11}L + \Sigma_{10} \\ C_2 &\approx \Sigma_{24}L^4 + \Sigma_{23}L^3 + \Sigma_{22}L^2 + \Sigma_{21}L \\ &\text{etc,} \end{aligned} \tag{6.4}$$

where equality will hold in the limit that the fixed-order is entirely replaced by the resummation. In order to obtain stable numerical results we in fact consider the *differences* of two observables v_1, v_2 with similar soft-collinear scaling,

$$\Delta(v_1, v_2) = \left(\frac{1}{\sigma_0} \frac{d\sigma^{\rm NLO}}{d \ln \frac{1}{v_1}} - \frac{1}{\sigma_0} \frac{d\sigma^{\rm NNLL}|_{\rm expanded}}{d \ln \frac{1}{v_1}} \right) - \{v_1 \to v_2\} \ , \tag{6.5}$$

where σ_0 is the Born cross-section, the first term in the bracket is the NLO differential distribution in $\ln 1/v_1$, given by the fixed-order Monte Carlo and the second term is our resummed differential distribution, expanded to NLO.
The resummation should correctly model the distribution in the small-v region, so when we subtract the expansion of the resummation from the fixed order distribution as above, we expect to get zero. Fig. 6.1 shows the difference $\Delta(v_1, v_2)$ for the seven event shapes we consider. One can observe that, indeed, for small values of the observables[1] the difference between the expanded resummation and the fixed order generator does tend to zero. Similarly, Fig. 6.2 shows the vanishing difference between the NLO fixed-order approximation and the expanded resummed result according to Eq. 6.1 for the two-jet rate in the Durham and Cambridge algorithms.

Confident that our resummation is behaving correctly in the relevant small-v region, at least for small orders in the coupling, we investigate its effect when combined with fixed-order results. This combination will generate a distribution that is valid and accurate across the entirety of a given observable's allowed values.
We take the hard scale to be equal to the Z-boson mass ($Q = M_Z$), therefore using the coupling $\alpha_s(M_Z) = 0.118$. In order to probe theory uncertainties we add an extra

[1] $\ln 1/v$ on the x-axis of Fig. 6.1 refers to the limit taken for the value of the *generic* observable V in `ARES`.

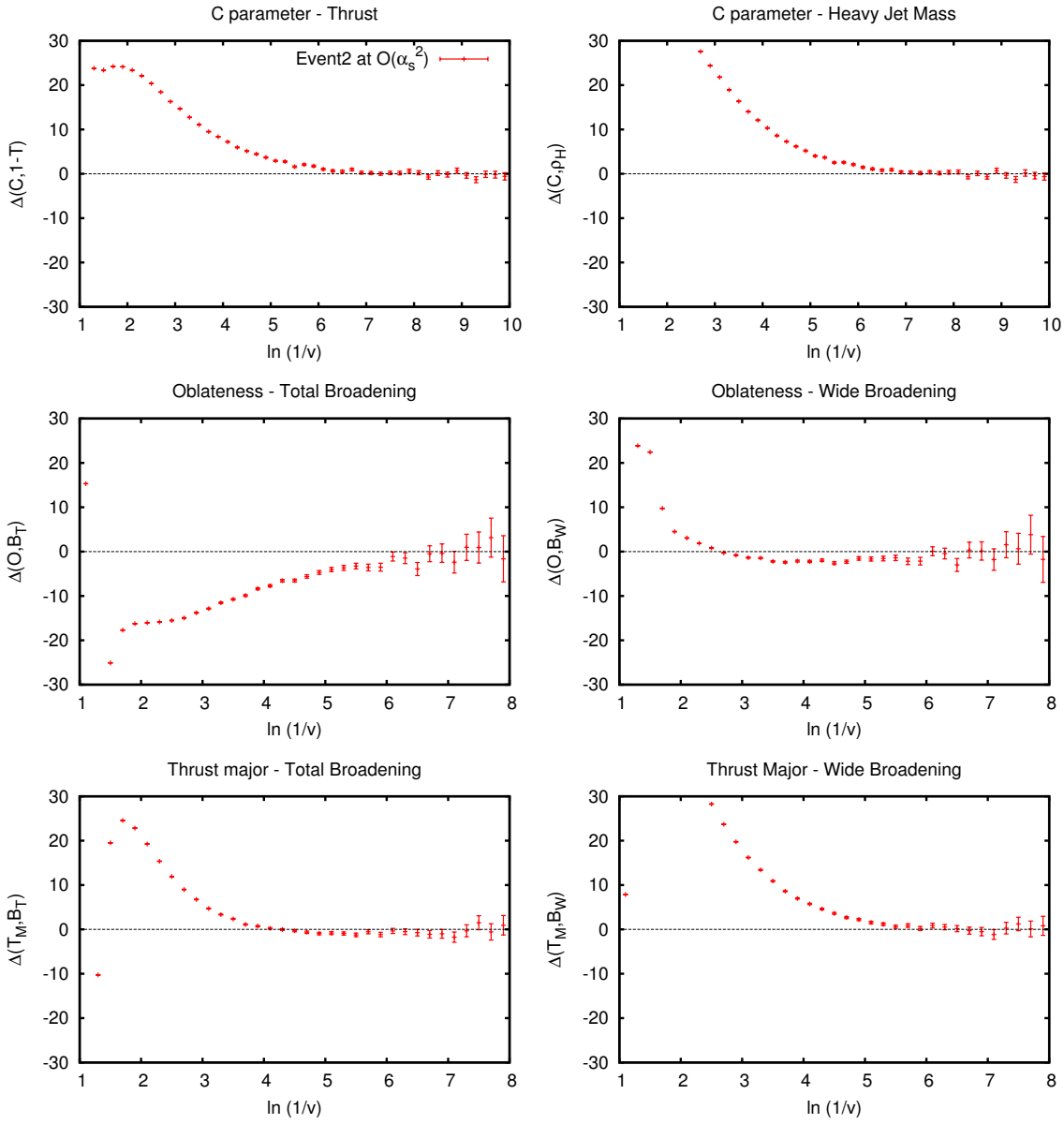

Figure 6.1: Difference between the NLO differential distributions of pairs of observables after subtracting the expansion of the NNLL resummation formula up to (and including) $\mathcal{O}(\alpha_s^2 L^0)$ (see Eq. (6.5)). To obtain these distributions we used about 10^{11} events.

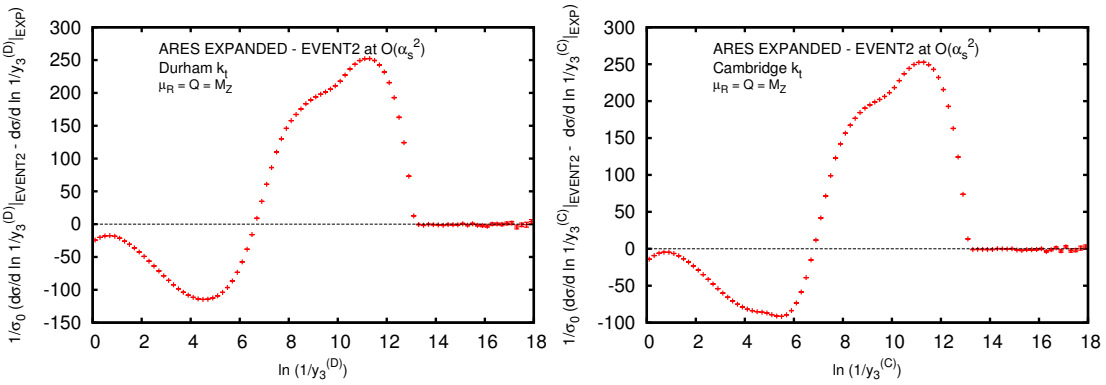

(a) Durham (b) Cambridge

Figure 6.2: Differences between the fixed order event generator `EVENT2` and the expansion of the NNLL resummed result to $\mathcal{O}(\alpha_s^2)$, for the two-jet rate in a) the Durham and b) the Cambridge algorithms. To obtain these distributions we used about 10^{11} events.

argument x and modify the logarithms,

$$\ln \frac{x}{v} \to \ln \left(1 + \left(\frac{x}{v}\right) - \left(\frac{x}{v_{\max}}\right)\right) . \tag{6.6}$$

This ensures that that the distribution vanishes at the kinematic endpoint $v_{\max}$ where further hard emissions are prohibited by phase space (taken from the NNLO result). Our theoretical uncertainties are obtained by varying, one at a time, x and the renormalisation scale μ_R by a factor of two in either direction around the central values $x = 1$ and $\mu_R = Q$. We now match to NNLO distributions using the fixed order generator `EERAD3`. Fig. 6.3 shows that the matched resummation+fixed-order and pure fixed-order results agree down to very small values of v, with the exact value depending on the observable. Below this value the fixed-order result is not reliable due to the soft and collinear logarithms becoming large. The resummed result cures this behaviour, taming the peak to smaller values and a smoother turnover. We now turn our attention to the impact our work has had on existing resummed results. Fig. 6.4 displays the impact of the move from NLL resummation of event shapes to NNLL resummation. Generally the NNLL resummation has the effect of reducing the theory uncertainties, as well as broadening the peak to slightly higher values of the observable. A facsimile of Fig. 6.4, now showing the two-jet rate, is shown in Fig. 6.5. The effect of the NNLL resummation on the previous state-of-the-art NLL resummation is, in the case of the Durham algorithm, primarily to theory error. For the Cambridge algorithm, NNLL corrections are quite large, and the NNLL uncertainty is larger than the NLL one, which seems to be underestimated. This effect can be understood by observing that the NLL prediction for the Cambridge algorithm is trivial and does not contain any information about multiple emissions effects. These effects appear first at NNLL, explaining the sizeable numerical corrections. Hence the NLL theory uncertainty as estimated in Fig. 6.5 is unable to capture large subleading effects.

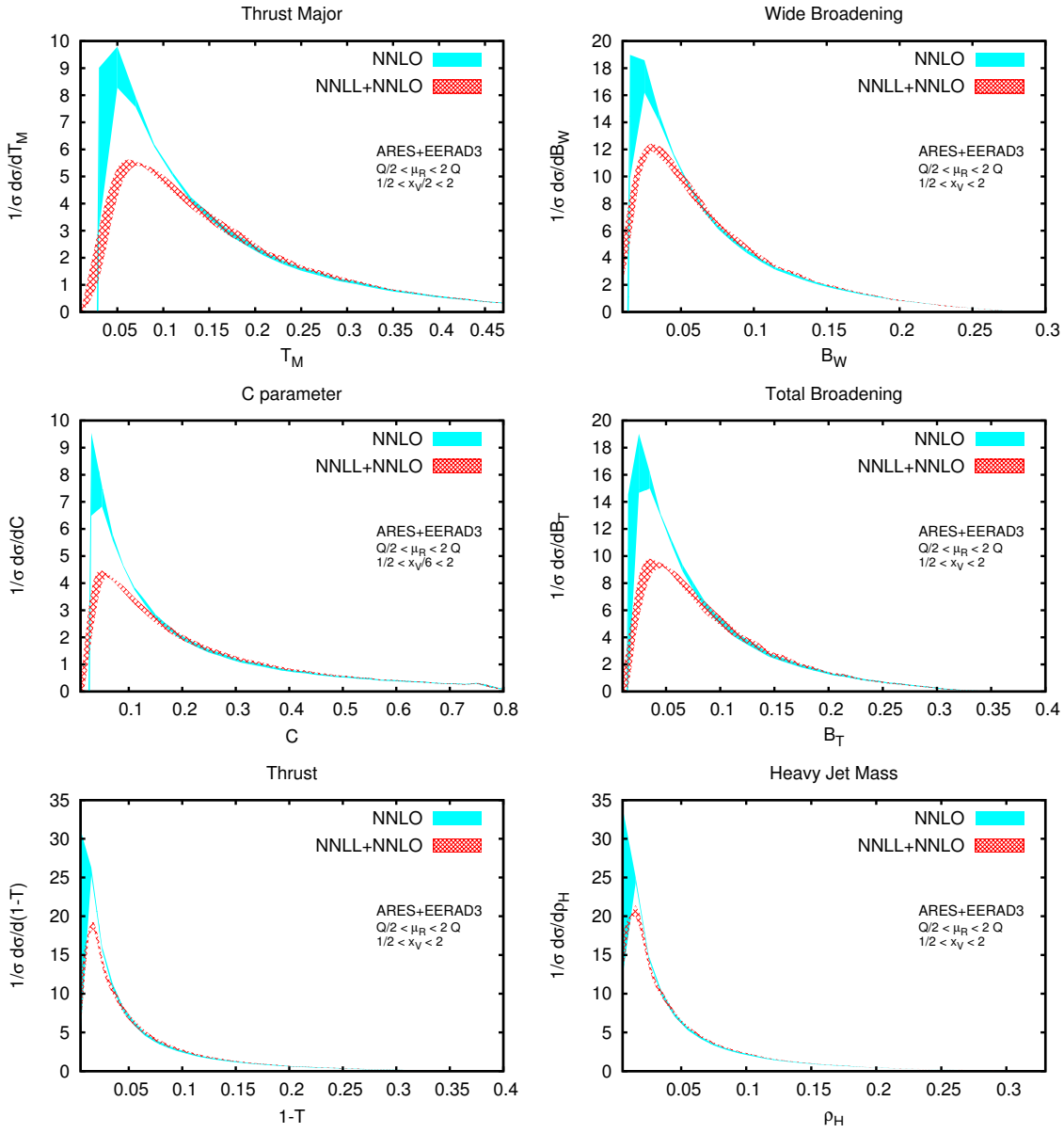

Figure 6.3: Differential distributions for six of the event-shape observables considered at NNLL+NNLO (red band) and NNLO (blue band).

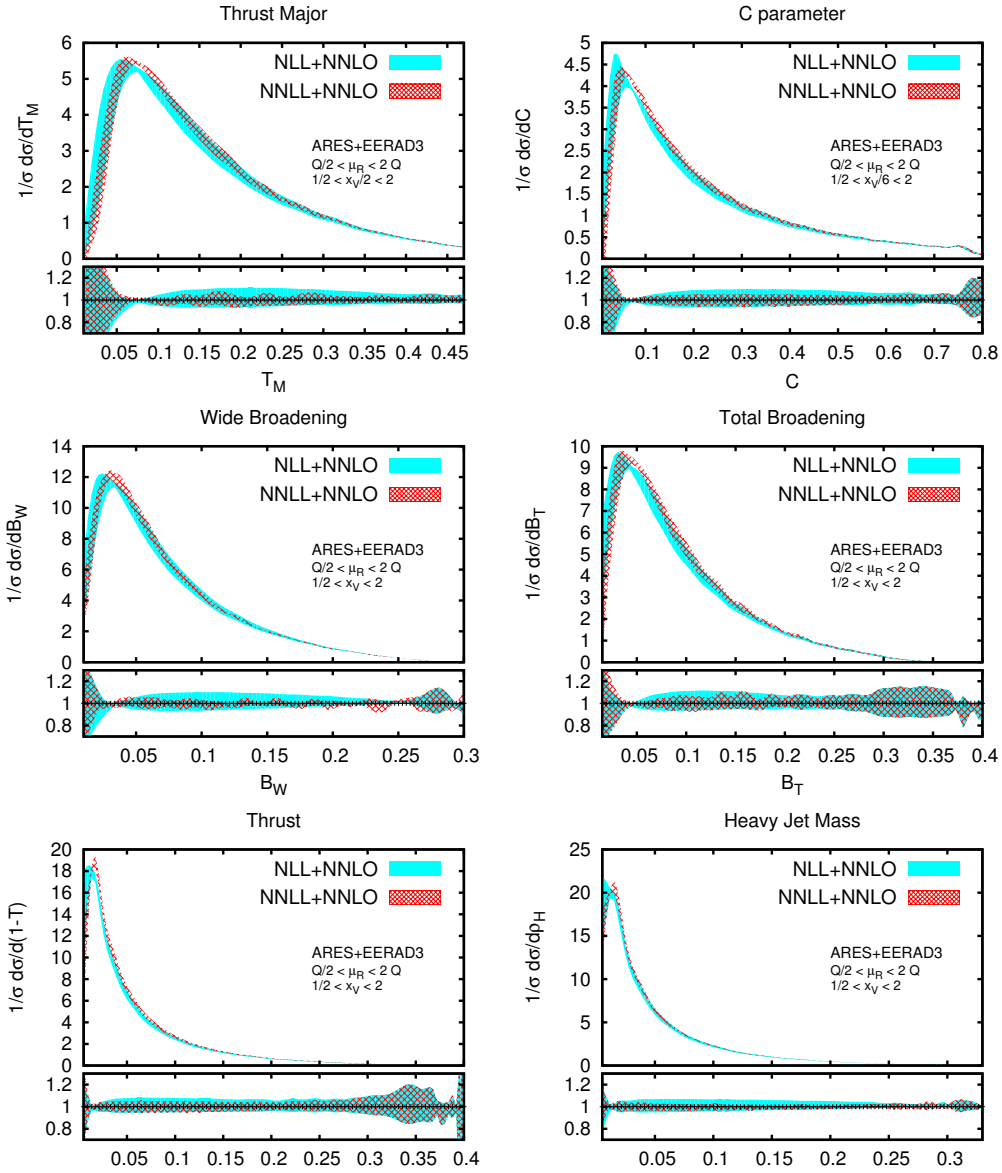

Figure 6.4: Matched distributions for six of the event-shape observables considered at NNLL+NNLO (red band) and NLL+NNLO (blue band). The lower panel of each plot shows the ratio of the NNLL+NNLO and NLL+NNLO bands to the corresponding central values.

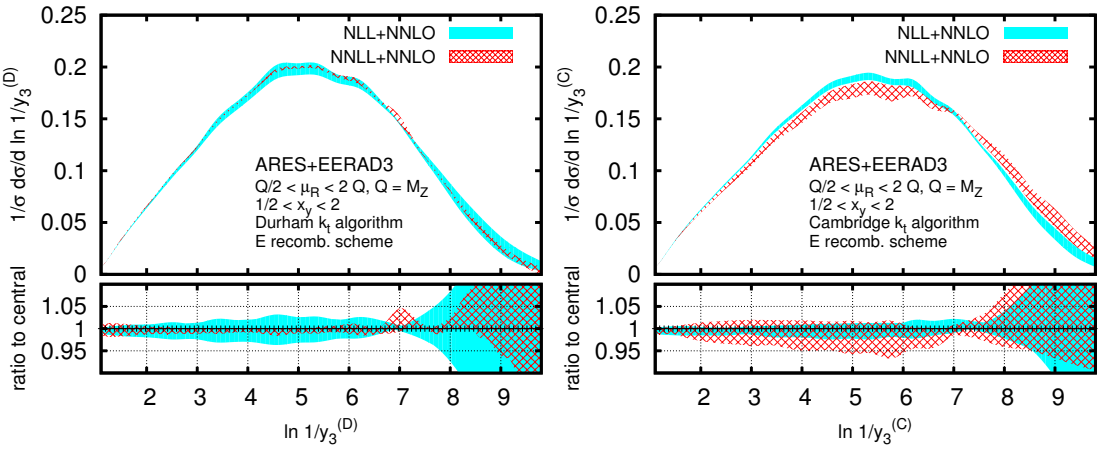

(a) Durham (b) Cambridge

Figure 6.5: Differential distributions for the three-jet resolution in the Durham (left) and Cambridge (right) algorithms. The plots show both the NLL+NNLO (blue/solid) and the NNLL+NNLO (red/hatched) results.

6.2 Comparison of the Resummation to Data

Finally, we exhibit the comparison of our resummation of the two-jet rate at NNLL to data. The Large Electron Positron (LEP) collider at CERN was operational between and 1989 and 2000 and took measurements from collider energies of 91 to 209 GeV. The hard-scattering Born process that we have considered, $e^+e^- \to 2$ jets, is one that was extensively probed by LEP, so our resummations provide predictions for LEP data measurements.

We combine our expanded resummed predictions with NNLO results from `EERAD3` and plot the resulting matched distribution to data from the L3 collaboration at LEP2 [50] at collider energy 206 GeV. See the resulting plot in Fig. 6.6. The matched resummed+fixed order distribution shows very good agreement with the data. In particular the agreement of values down to small y_{cut} ($\ln y_{\text{cut}} = -7$ corresponds to $y_{\text{cut}} \sim 9 \times 10^{-4}$) demonstrate the success of our work in accurately describing the dynamics of QCD jets in the region dominated by soft-gluon emissions. The error bands are produced by varying the modified logarithm parameter x (defined in Eq. (6.6)) and the renormalization scale μ_R by a factor of two in each direction. The error bands are small, down to even the lowest values of y_{cut}. As discussed in the previous section the y_3 in the Cambridge algorithm experiences larger theory uncertainties than in the Durham algorithm. Since the NLL contribution to the Cambridge is trivial, NNLL is the first order at which the result contains any meaningful kinematics. Hence the NNLL prediction can be thought of as 'first order in $\mathcal{F}$', with correspondingly large uncertainties. The NLL uncertainties on the other hand are relatively small, being unable to capture effects to which the calculation is ignorant. In the lower plot one can see that the ratio of the resummed+fixed-order results to data remains within 5% of the data value. Notice also that only at very small values of the observable (beyond $\ln y_{\text{cut}} = -6$) do the theory uncertainties go outwith the experimental

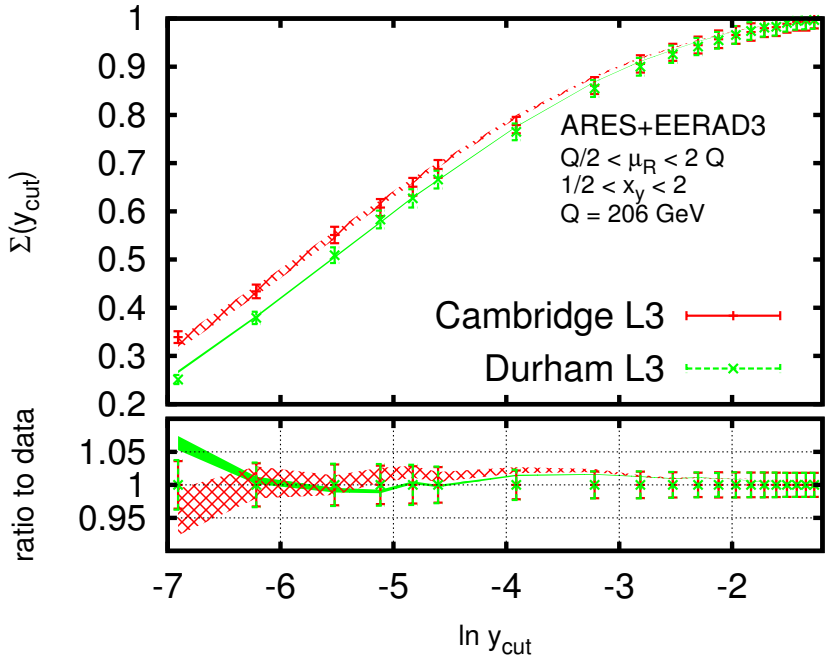

Figure 6.6: Comparison of NNLL+NNLO predictions for the two-jet rate to data from the L3 collaboration [50].

error bars. Fig. 6.6 shows that our resummed predictions have reached maximum non-redundant precision; we are taking full advantage of the data afforded to us by collider experiments.

Chapter 7

Conclusions and Perspectives

in which I recap the impact of our work and look at its further-reaching effects.

This work establishes a framework for generic final-state resummation of global and rIRC-safe observables in $e^+e^- \to 2$ jets with state-of-the-art precision. Resummed calculations are vital to render standard perturbative results applicable across the full phase space available to QCD radiation. To best employ the myriad of measurements taken by detectors these calculations must push the boundaries of accuracy as far as possible.

As validation of our method and proof of its wide applicability we have explicitly determined the resummation of seven event shapes and the two-jet rate in both the Cambridge and Durham jet clustering algorithms.

Designing the resummation formula such that it is applicable to the two-jet rate is a significant step forward in QCD phenomenology. No factorisation formula is known for y_3 in the Durham algorithm and so no previous attempts to resum this observable to NNLL accuracy had been made, despite its useful insensitivity to hadronisation.

The resummation of the two-jet rate to NNLL accuracy has enabled an alternative and precise extraction of the strong coupling. Previous fits to α_s were carried out using next-to-leading logarithmic approximations for y_3 (NNLO+NLLA) [51,52]. We have completed the region in which y_3 is known to third order[1], complementing the currently available N^{3}LO results [53]. We note that the NNLL effects are of comparable size to those at NLL and so it is expected that the reduction in uncertainty will be significant.

Our method is systematic, starting from the NLL-complete formalism of `CAESAR` and, one by one, relaxing the assumptions made therein to produce kinematic scenarios accurate to NNLL. The `CAESAR` methodology hinges on the known scaling of an observable in the presence of an ensemble of soft-collinear, widely separated emissions. We therefore let one of these emissions deviate from its collinearity, softness, or remoteness from the rest of the ensemble. For every allowed deviation either the matrix element for that emission or the observable definition will deviate from its soft-collinear approximation. This causes the real emissions function to pick up a contribution from the new kinematics. Of course every emission carries a single factor of α_s and so only one emission in each ensemble can

[1] NNLL+N^{3}LO is exact in its terms proportional to α_s, α_s^2 and α_s^3. Of course the resummation includes higher order terms in α_s too.

be allowed the freedom of the full phase space. This simple fact ensures the presence of all the contributions necessary for NNLL accuracy, and no more.
Our method allows us to deal with every global rIRC-safe observable in $e^+e^- \to q\bar{q}$ in the same way - an unusual credential in the field of soft-gluon resummation. In so doing we have enabled NNLL resummation to become the state-of-the-art.
In addition to deriving an analytical master formula we have written a framework of numerical implementation that allows one to resum an observable of interest given four parameters characterising that observable's soft-collinear scaling. `ARES` provides the user with the relevant subroutines to run Monte Carlo integrations for each contribution to the real emissions function. Included in `ARES`' functionality is the expansion of the resummation up to three orders in α_s, allowing for quick comparison to fixed order or other resummed results. The technical features of `ARES` are discussed in Appendix B.
We have validated the method by matching to fixed order and as such have produced cross-sections of the eight collider observables which are valid across the full reach of phase-space. Resummations of the C-parameter, thrust major and oblateness are additional new results determined by the `ARES` method. The remaining event shapes were confirmed to agree with previously calculated results.
It is increasingly expected that phenomenological tools be automated and flexible. This work provides both theorists and experimentalists with the most precise theoretical computation of a chosen collider observable in its small-value limit. The extension of this framework to include e^+e^- annihilation to n-jet processes and hadron-hadron collisions is within reach. Further work on obtaining the generic NNLL Sudakov radiator will allow us access to an even wider range of observables. The aforementioned steps would deem `ARES` a complete recasting of `CAESAR` to NNLL accuracy. Furthermore, this method and its accompanying code are systematically extendible even beyond NNLL accuracy.

We have introduced a novel technique, and its automated implementation, for resummation of a wide class of observables to next-to-next-to-leading-logarithmic accuracy in e^+e^- annihilation. We have presented explicit results for eight observables, including the first NNLL resummation of the two-jet rate in the Durham and Cambridge algorithms, an observable crucial for determination of the strong coupling of Quantum Chromodynamics (QCD). This work presents an important step forward in precision calculations for phenomenology.

Chapter 8

Acknowledgements

Thank you.

Firstly to my supervisor, Andrea Banfi, for his enthusiasm and commitment to this project and to physics in general. He was always there to have long discussions with and to share his knowledge. I also thank my collaborators Pier Monni and Giulia Zanderighi for their support and patience.
To my fellow PhD students in TPP, in particular Djuna, Christopher, Chris, Tugba and Andy, for their friendship and for their part in making Sussex a fantastic place to study. I wish them the best of luck in their futures!
To my first physics collaborator, Kirsty Hunter, for continued rationale and whimsy in perfect doses.

To everyone at the West Hill and the Chimney House for sharing good tunes and beer. Especially to Jason Pegg, Robin Doody, Justine Smith and Phil Masters, for their excellent company and dancing.
Ruth Condon, Adam Mould, Paul Quinn, Anna Schwarz, William Shaw and Louise Wells all gave invaluable help with the hard sums.
Jess and Kate, my adopted family, thank you for gracefully tolerating the unintelligible squiggles I left about the place and for having astonishingly unending confidence in me.

Finally, I am hugely grateful to my family for their constant support and encouragement throughout my studies: Kyle has always been there to lend an ear; Mum always encouraged me to find the happy quark; and to Dad, for taking me to Kelvingrove and showing me what can happen when you ask difficult questions.

Bibliography

[1] A. Banfi, H. McAslan, P. F. Monni and G. Zanderighi, JHEP **1505** (2015) 102 doi:10.1007/JHEP05(2015)102 [arXiv:1412.2126 [hep-ph]].

[2] A. Banfi, H. McAslan, P. F. Monni and G. Zanderighi, Phys. Rev. Lett. **117** (2016) no.17, 172001 doi:10.1103/PhysRevLett.117.172001 [arXiv:1607.03111 [hep-ph]].

[3] A. Banfi, G. P. Salam and G. Zanderighi, JHEP **0503** (2005) 073 doi:10.1088/1126-6708/2005/03/073 [hep-ph/0407286].

[4] R. K. Ellis, W. J. Stirling and B. R. Webber, "QCD and collider physics," Camb. Monogr. Part. Phys. Nucl. Phys. Cosmol. **8** (1996) 1.

[5] T. Muta, "Foundations of Quantum Chromodynamics: An Introduction to Perturbative Methods in Gauge Theories, (3rd ed.)," World Scientific Lecture Notes in Physics **78** (2010)

[6] M. E. Peskin and D. V. Schroeder, "An Introduction to quantum field theory," Reading, USA: Addison-Wesley (1995) 842 p

[7] C. Patrignani *et al.* [Particle Data Group Collaboration], Chin. Phys. C **40** (2016) no.10, 100001. doi:10.1088/1674-1137/40/10/100001

[8] T. Gleisberg, S. Hoeche, F. Krauss, M. Schonherr, S. Schumann, F. Siegert and J. Winter, JHEP **0902** (2009) 007 doi:10.1088/1126-6708/2009/02/007 [arXiv:0811.4622 [hep-ph]].

[9] B. R. Webber, Nucl. Phys. B **238** (1984) 492. doi:10.1016/0550-3213(84)90333-X

[10] B. Andersson, G. Gustafson, G. Ingelman and T. Sjostrand, Phys. Rept. **97** (1983) 31. doi:10.1016/0370-1573(83)90080-7

[11] T. Sjostrand, Comput. Phys. Commun. **39** (1986) 347. doi:10.1016/0010-4655(86)90096-2

[12] Y. L. Dokshitzer, G. Marchesini and B. R. Webber, Nucl. Phys. B **469** (1996) 93 doi:10.1016/0550-3213(96)00155-1 [hep-ph/9512336].

[13] Y. I. Azimov, Y. L. Dokshitzer, V. A. Khoze and S. I. Troyan, Z. Phys. C **27** (1985) 65. doi:10.1007/BF01642482

[14] T. Becher and M. D. Schwartz, JHEP **0807**, 034 (2008) doi:10.1088/1126-6708/2008/07/034 [arXiv:0803.0342 [hep-ph]].

[15] S. Catani, L. Trentadue, G. Turnock and B. R. Webber, Nucl. Phys. B **407** (1993) 3. doi:10.1016/0550-3213(93)90271-P

[16] E. Farhi, Phys. Rev. Lett. **39** (1977) 1587. doi:10.1103/PhysRevLett.39.1587

[17] S. Brandt, C. Peyrou, R. Sosnowski and A. Wroblewski, Phys. Lett. **12** (1964) 57. doi:10.1016/0031-9163(64)91176-X

[18] G. C. Fox and S. Wolfram, Nucl. Phys. B **149** (1979) 413 Erratum: [Nucl. Phys. B **157** (1979) 543]. doi:10.1016/0550-3213(79)90120-2, 10.1016/0550-3213(79)90003-8

[19] P. E. L. Rakow and B. R. Webber, Nucl. Phys. B **191** (1981) 63. doi:10.1016/0550-3213(81)90286-8

[20] R. Barate *et al.* [ALEPH Collaboration], Phys. Rept. **294** (1998) 1. doi:10.1016/S0370-1573(97)00045-8

[21] J. C. Collins, D. E. Soper and G. Sterman, Nucl. Phys. B **250** (1985) 199.

[22] S. Catani, G. Turnock, B. R. Webber and L. Trentadue, Phys. Lett. B **263**, 491 (1991).

[23] S. Catani and B. R. Webber, Phys. Lett. B **427**, 377 (1998) [hep-ph/9801350].

[24] S. Catani, G. Turnock and B. R. Webber, Phys. Lett. B **295** (1992) 269.

[25] S. Catani, Yu. L. Dokshitzer, M. Olsson, G. Turnock and B. R. Webber, Phys. Lett. B **269** (1991) 432.

[26] S. Catani, Y. L. Dokshitzer and B. R. Webber, Phys. Lett. B **322**, 263 (1994).

[27] G. Dissertori and M. Schmelling, Phys. Lett. B **361** (1995) 167.

[28] A. J. Larkoski, D. Neill and J. Thaler, JHEP **1404** (2014) 017 [arXiv:1401.2158 [hep-ph]].

[29] A. Banfi, G. P. Salam and G. Zanderighi, Phys. Lett. B **584** (2004) 298 doi:10.1016/j.physletb.2004.01.048 [hep-ph/0304148].

[30] P. F. Monni, T. Gehrmann and G. Luisoni, JHEP **1108** (2011) 010 doi:10.1007/JHEP08(2011)010 [arXiv:1105.4560 [hep-ph]].

[31] Y. T. Chien and M. D. Schwartz, JHEP **1008** (2010) 058 [arXiv:1005.1644 [hep-ph]].

[32] T. Becher and G. Bell, JHEP **1211** (2012) 126 [arXiv:1210.0580 [hep-ph]].

[33] S. Alioli, C. W. Bauer, C. J. Berggren, A. Hornig, F. J. Tackmann, C. K. Vermilion, J. R. Walsh and S. Zuberi, JHEP **1309** (2013) 120 [arXiv:1211.7049 [hep-ph]].

[34] A. Banfi, P. F. Monni, G. P. Salam and G. Zanderighi, Phys. Rev. Lett. **109** (2012) 202001 [arXiv:1206.4998 [hep-ph]].

[35] I. W. Stewart, F. J. Tackmann, J. R. Walsh and S. Zuberi, arXiv:1307.1808 [hep-ph].

[36] S. Catani, M. Grazzini and A. Torre, arXiv:1408.4564 [hep-ph].

[37] A. Banfi, G. P. Salam and G. Zanderighi, JHEP **0201** (2002) 018 doi:10.1088/1126-6708/2002/01/018 [hep-ph/0112156].

[38] R. W. L. Jones, M. Ford, G. P. Salam, H. Stenzel and D. Wicke, JHEP **0312** (2003) 007 doi:10.1088/1126-6708/2003/12/007 [hep-ph/0312016].

[39] G. Altarelli and G. Parisi, Nucl. Phys. B **126** (1977) 298. doi:10.1016/0550-3213(77)90384-4

[40] S. Catani, B. R. Webber and G. Marchesini, Nucl. Phys. B **349** (1991) 635. doi:10.1016/0550-3213(91)90390-J

[41] Y. L. Dokshitzer, A. Lucenti, G. Marchesini and G. P. Salam, Nucl. Phys. B **511** (1998) 396 [Erratum-ibid. B **593** (2001) 729] [hep-ph/9707532].

[42] J. E. Huth *et al.*, In *Snowmass 1990, Proceedings, Research directions for the decade* 134-136 and Fermilab Batavia - FERMILAB-Conf-90-249 (90/12,rec.Mar.91) 6 p. (105313)

[43] S. D. Ellis, Z. Kunszt and D. E. Soper, Phys. Rev. Lett. **62** (1989) 726. doi:10.1103/PhysRevLett.62.726

[44] G. P. Salam, Eur. Phys. J. C **67** (2010) 637 doi:10.1140/epjc/s10052-010-1314-6 [arXiv:0906.1833 [hep-ph]].

[45] S. Catani, Y. L. Dokshitzer, M. Olsson, G. Turnock and B. R. Webber, Phys. Lett. B **269** (1991) 432.

[46] Y. L. Dokshitzer, G. D. Leder, S. Moretti and B. R. Webber, JHEP **9708** (1997) 001 [hep-ph/9707323].

[47] S. Bentvelsen and I. Meyer, Eur. Phys. J. C **4** (1998) 623 doi:10.1007/s100520050232 [hep-ph/9803322].

[48] S. Catani and M. H. Seymour, Nucl. Phys. B **485** (1997) 291 [Erratum-ibid. B **510** (1998) 503] [hep-ph/9605323].

[49] A. Gehrmann-De Ridder, T. Gehrmann, E. W. N. Glover and G. Heinrich, Comput. Phys. Commun. **185** (2014) 3331 [arXiv:1402.4140 [hep-ph]].

[50] P. Achard *et al.* [L3 Collaboration], Phys. Rept. **399** (2004) 71 [hep-ex/0406049].

[51] G. Abbiendi *et al.* [OPAL Collaboration], Eur. Phys. J. C **45** (2006) 547 doi:10.1140/epjc/s2005-02417-4 [hep-ex/0507047].

[52] S. Kluth, Rept. Prog. Phys. **69** (2006) 1771 doi:10.1088/0034-4885/69/6/R04 [hep-ex/0603011].

[53] A. Gehrmann-De Ridder, T. Gehrmann, E. W. N. Glover and G. Heinrich, Phys. Rev. Lett. **100** (2008) 172001 doi:10.1103/PhysRevLett.100.172001 [arXiv:0802.0813 [hep-ph]].

[54] D. Binosi and L. Theussl, Comput. Phys. Commun. **161** (2004) 76 doi:10.1016/j.cpc.2004.05.001 [hep-ph/0309015].

Appendix A

Ingredients for the NNLL Master Formula

in which I include the full definitions of the ingredients needed for the ARES *method of resummation.*

A.1 Sudakov Radiator

The functions g_1, g_2 and g_3 of the radiator defined in Eq. (4.8) can be parametrised as

$$g_i(\lambda) = \sum_{\ell=1,2} g_i^{(\ell)}(\lambda)\,, \tag{A.1}$$

where ℓ denotes one of the two hard legs and $\lambda = \alpha_s\beta_0 \ln 1/v$. The $g_i^{(\ell)}$ can be expressed in terms of the scaling parameters a and b_ℓ used in the generic observable definition (given in Eq. (3.18)) as follows

$$g_1^{(\ell)}(\lambda) = \frac{A_1\left((a+b_\ell-2\lambda)\ln\left(1-\frac{2\lambda}{a+b_\ell}\right)-(a-2\lambda)\ln\left(1-\frac{2\lambda}{a}\right)\right)}{4\pi b_\ell\beta_0\lambda}\,, \tag{A.2}$$

$$\begin{aligned} g_2^{(\ell)}(\lambda) = {} & \frac{A_2\left(a\ln\left(1-\frac{2\lambda}{a}\right)-(a+b_\ell)\ln\left(1-\frac{2\lambda}{a+b_\ell}\right)\right)}{8\pi^2 b_\ell {\beta_0}^2} + \frac{B_1\ln\left(1-\frac{2\lambda}{a+b_\ell}\right)}{4\pi\beta_0} \\ & + \frac{A_1\left(\beta_1(a+b_\ell)\ln^2\left(1-\frac{2\lambda}{a+b_\ell}\right)+2\beta_1(a+b_\ell)\ln\left(1-\frac{2\lambda}{a+b_\ell}\right)\right)}{8\pi b_\ell {\beta_0}^3} \\ & - A_1\frac{\ln\left(1-\frac{2\lambda}{a}\right)\left(a\beta_1\ln\left(1-\frac{2\lambda}{a}\right)+2a\beta_1\right)}{8\pi b_\ell {\beta_0}^3} \\ & + \frac{A_1\left(\ln\left(1-\frac{2\lambda}{a+b_\ell}\right)-\ln\left(1-\frac{2\lambda}{a}\right)\right)}{4\pi b_\ell\beta_0}\ln x^2 \\ & - \frac{A_1\left(\ln\left(1-\frac{2\lambda}{a+b_\ell}\right)-\ln\left(1-\frac{2\lambda}{a}\right)\right)}{2\pi b_\ell\beta_0}\ln\bar{d}_\ell\,, \end{aligned} \tag{A.3}$$

$$
\begin{aligned}
g_3^{(\ell)}(\lambda) = & \frac{\beta_1 B_1 \left((a+b_\ell)\ln\left(1-\frac{2\lambda}{a+b_\ell}\right)+2\lambda\right)}{2{\beta_0}^2(a+b_\ell-2\lambda)} \\
& + \frac{A_2\beta_1\left(a^2(a+b_\ell-2\lambda)\ln\left(1-\frac{2\lambda}{a}\right)-(a+b_\ell)^2(a-2\lambda)\ln\left(1-\frac{2\lambda}{a+b_\ell}\right)+6b_\ell\lambda^2\right)}{8\pi b_\ell{\beta_0}^3(a-2\lambda)(a+b_\ell-2\lambda)} \\
& + \frac{A_1\left({\beta_1}^2(a+b_\ell)^2(a-2\lambda)\ln^2\left(1-\frac{2\lambda}{a+b_\ell}\right)-4b_\ell\lambda^2\left(\beta_0\beta_2+{\beta_1}^2\right)\right)}{8b_\ell{\beta_0}^4(a-2\lambda)(a+b_\ell-2\lambda)} \\
& - \frac{aA_1\ln\left(1-\frac{2\lambda}{a}\right)\left(2\beta_0\beta_2(a-2\lambda)+a{\beta_1}^2\ln\left(1-\frac{2\lambda}{a}\right)+4{\beta_1}^2\lambda\right)}{8b_\ell{\beta_0}^4(a-2\lambda)} \\
& + \frac{A_1(a+b_\ell)\ln\left(1-\frac{2\lambda}{a+b_\ell}\right)\left(\beta_0\beta_2(a+b_\ell-2\lambda)+2{\beta_1}^2\lambda\right)}{4b_\ell{\beta_0}^4(a+b_\ell-2\lambda)} \\
& - \frac{A_1}{8(a-2\lambda)(a+b_\ell-2\lambda)}\ln^2 x^2 + \Bigg[\frac{\pi a{\beta_0}^2B_1+\lambda\left(A_2\beta_0-2\pi\left(A_1\beta_1+{\beta_0}^2B_1\right)\right)}{4\pi{\beta_0}^2(a-2\lambda)(a+b_\ell-2\lambda)} \\
& + \frac{A_1\beta_1\left((a+b_\ell)(a-2\lambda)\ln\left(1-\frac{2\lambda}{a+b_\ell}\right)-a(a+b_\ell-2\lambda)\ln\left(1-\frac{2\lambda}{a}\right)\right)}{4b_\ell{\beta_0}^2(a-2\lambda)(a+b_\ell-2\lambda)}\Bigg]\ln x^2 \\
& - \frac{A_1}{2(a-2\lambda)(a+b_\ell-2\lambda)}\ln^2\bar{d}_\ell + \frac{A_1}{2(a-2\lambda)(a+b_\ell-2\lambda)}\ln\bar{d}_\ell\ln x^2 \\
& - \frac{\pi a{\beta_0}^2B_1+\lambda\left(A_2\beta_0-2\pi\left(A_1\beta_1+{\beta_0}^2B_1\right)\right)}{2\pi{\beta_0}^2(a-2\lambda)(a+b_\ell-2\lambda)}\ln\bar{d}_\ell \\
& + \frac{A_1\beta_1\left(a(a+b_\ell-2\lambda)\ln\left(1-\frac{2\lambda}{a}\right)-(a+b_\ell)(a-2\lambda)\ln\left(1-\frac{2\lambda}{a+b_\ell}\right)\right)}{2b_\ell{\beta_0}^2(a-2\lambda)(a+b_\ell-2\lambda)}\ln\bar{d}_\ell \\
& + \frac{7}{8b_\ell}C_F\frac{1}{1-\frac{2}{a+b_\ell}\lambda}\Theta(b_\ell)+h(\lambda)\,,
\end{aligned}
\tag{A.4}
$$

where $\ln\bar{d}_\ell = \int_0^{2\pi}\frac{d\phi}{2\pi}\ln(d_\ell g_\ell(\phi))$ and $\Theta(b_\ell)=1(0)$ for $b_\ell>0$ ($b_\ell=0$). The terms involving x arise from our modification of the logarithms in Eq. (6.6) and serve to probe the theory uncertainties. In the above definitions we have set the renormalisation scale $\mu_R=Q$, but in order to further probe theory uncertainties one may make the substitutions given in Eq. (A.5) and vary $\mu_R'\in(\mu_R/2,2\mu_R)$.

$$
\begin{aligned}
& g_1(\lambda)\to g_1(\lambda)\,, \\
& g_2(\lambda)\to g_2(\lambda)+\lambda^2 g_1'(\lambda)\ln\frac{{\mu_R'}^2}{Q^2}\,, \\
& g_3(\lambda)\to g_3(\lambda)+\pi\left(\beta_0\lambda g_2'(\lambda)+\frac{\beta_1}{\beta_0}\lambda^2 g_1'(\lambda)\right)\ln\frac{{\mu_R'}^2}{Q^2}+ \\
& \qquad\qquad +\pi\left(\beta_0\lambda^2 g_1'(\lambda)+\frac{\beta_0}{2}\lambda^3 g_1''(\lambda)\right)\ln^2\frac{{\mu_R'}^2}{Q^2}\,,
\end{aligned}
\tag{A.5}
$$

where the prime on the g_i functions denotes differentiation by λ.

The $b_\ell \to 0$ limit of Eqs. A.2 to A.4 is well-defined and finite and is relevant for the g_i functions of broadening-type event shapes and the two-jet rate.
As discussed in Secs. 4.1.3 and 5.3.1 the general form of the NNLL Sudakov factor is not known. Here we parametrise this ignorance with the function $h(\lambda)$. We extract $h(\lambda)$ from previously known resummations via observables with the same soft-collinear scaling as those that we consider. Thrust and thrust-type observables take the remaining piece of their radiator from [14, 30],

$$\begin{aligned} h^{(\tau)}(\lambda) = &-A_3^{(\tau)} \frac{\lambda^2}{8\pi^2 {\beta_0}^2 (1-2\lambda)(2-2\lambda)} - B_2^{(\tau)} \frac{\lambda}{8\pi\beta_0(1-\lambda)} \\ &+ C_F \frac{\pi^2}{24} \frac{1}{1-2\lambda} + C_F \left(\frac{1}{4} - \frac{\pi^2}{12}\right) \frac{1}{1-\lambda} + C_F \left(-\frac{19}{8} + \frac{7}{24}\pi^2\right) , \end{aligned} \tag{A.6}$$

whilst the radiator for broadening-type event shapes is extracted from [34],

$$\begin{aligned} h^{(k_t)}(\lambda) = &-A_3^{(k_t)} \frac{\lambda^2}{8\pi^2 {\beta_0}^2 (1-2\lambda)^2} - B_2^{(k_t)} \frac{\lambda}{4\pi\beta_0(1-2\lambda)} \\ &+ C_F \left(\frac{1}{4} - \frac{\pi^2}{24}\right) \frac{1}{1-2\lambda} + C_F \left(-\frac{19}{8} + \frac{7}{24}\pi^2\right) . \end{aligned} \tag{A.7}$$

The $h(\lambda)$ function for the two-jet rate in both algorithms is also taken from [34], with $a = 2$ this time,

$$\begin{aligned} h^{(y_3)}(\lambda) = &-A_3^{(y_3)} \frac{\lambda^2}{32\pi^2 \beta_0^2 (1-\lambda)^2} - B_2^{(y_3)} \frac{\lambda}{8\pi\beta_0(1-\lambda)} + \\ &+ C_F \left(\frac{1}{4} - \frac{\pi^2}{24}\right) \frac{1}{1-\lambda} + C_F \left(-\frac{19}{8} + \frac{7\pi^2}{24}\right) . \end{aligned} \tag{A.8}$$

The first terms of the QCD β-function are

$$\begin{aligned} \beta_0 &= \frac{11C_A - 2n_f}{12\pi} , \\ \beta_1 &= \frac{17C_A^2 - 5C_A n_f - 3C_F n_f}{24\pi^2} , \\ \beta_2 &= \frac{2857C_A^3 + (54C_F^2 - 615C_F C_A - 1415C_A^2)n_f + (66C_F + 79C_A)n_f^2}{3456\pi^3} . \end{aligned} \tag{A.9}$$

The A_i and B_i are the coefficients of the leading-logarithmic and next-to-leading-logarithmic contributions, respectively, from i soft-collinear emissions and are given by

$$\begin{aligned} A_1 &= 2C_F , \\ B_1 &= -3C_F , \\ A_2 &= C_F \left(C_A \left(\frac{67}{9} - \frac{\pi^2}{3}\right) - \frac{10}{9} n_f\right) . \end{aligned} \tag{A.10}$$

Beyond second order in A and first order in B the coefficients are observable-dependent.

For thrust-type event shapes,

$$B_2^{(\tau)} = -2\left(C_F^2\left(-\frac{\pi^2}{2}+\frac{3}{8}+6\zeta_3\right)+C_FC_A\left(\frac{11\pi^2}{18}+\frac{17}{24}-3\zeta_3\right)+C_FT_Fn_f\left(-\frac{1}{6}-\frac{2}{9}\pi^2\right)\right),$$
$$\begin{aligned}A_3^{(\tau)} = {}& C_FC_A^2\left(\frac{245}{12}-\frac{67}{27}\pi^2+\frac{11}{3}\zeta_3+\frac{22}{5}\zeta_2^2\right)+C_F^2T_Fn_f\left(-\frac{55}{6}+8\zeta_3\right)-\frac{8}{27}C_FT_F^2n_f^2\\ &+C_FC_AT_Fn_f\left(-\frac{209}{27}+\frac{20}{27}\pi^2-\frac{28}{3}\zeta_3\right)+\pi\beta_0C_F\left(C_A\left(\frac{808}{27}-28\zeta_3\right)-\frac{224}{27}T_Fn_f\right),\end{aligned} \tag{A.11}$$

whilst for broadening-type event shapes and the two-jet rate,

$$\begin{aligned}B_2^{(k_t)} = B_2^{(y_3)} &= B_2^{(\tau)}+2\pi\beta_0\zeta_2C_F\,,\\ A_3^{(k_t)} = A_3^{(y_3)} &= A_3^{(\tau)}-8\pi^2\beta_0^2\zeta_2C_F\,.\end{aligned} \tag{A.12}$$

A.2 Auxiliary Functions

The fundamental logarithmic structure of the exponentiated pieces of the resummation are contained in the $g_i(\lambda)$ functions given in the previous section, but we do not directly work with these functions in the derivation of the ARES master formula of Chapters 4 and 5. Rather, we use functions arising from expansions of the original radiator Eq. (4.8),

$$R'_{\mathrm{NLL},\ell}(v) = \frac{A_1\left(\ln\left(1-\frac{2\lambda}{a+b_\ell}\right)-\ln\left(1-\frac{2\lambda}{a}\right)\right)}{2\pi b_\ell\beta_0}\,, \tag{A.13}$$

$$\begin{aligned}\delta R'_{\mathrm{NNLL},\ell}(v) = \frac{\alpha_s(Q)}{\pi}\Bigg[&-\frac{A_1\beta_1\left(a(a+b_\ell-2\lambda)\ln\left(1-\frac{2\lambda}{a}\right)\right)}{2b_\ell{\beta_0}^2(a-2\lambda)(a+b_\ell-2\lambda)}-\\ &-\frac{A_1\beta_1\left((a+b_\ell)(a-2\lambda)\ln\left(1-\frac{2\lambda}{a+b_\ell}\right)+2b_\ell\lambda\right)}{2b_\ell{\beta_0}^2(a-2\lambda)(a+b_\ell-2\lambda)}\\ &+\frac{A_1\lambda}{(a-2\lambda)(a+b_\ell-2\lambda)}\ln\frac{\mu_R^2}{Q^2}-\frac{A_1}{2(a-2\lambda)(a+b_\ell-2\lambda)}\ln x^2\\ &+\frac{A_2\lambda}{2\pi\beta_0(a-2\lambda)(a+b_\ell-2\lambda)}\Bigg]\,,\end{aligned} \tag{A.14}$$

$$R''_\ell(v) = \frac{\alpha_s(Q)}{\pi}\frac{A_1}{(a-2\lambda)(a+b_\ell-2\lambda)}\,. \tag{A.15}$$

A.3 Expansion Coefficients

The expansion coefficients according to Eq. (6.1), allowing for matching to fixed-order distributions, are shown below for generic observables.

$$
\begin{aligned}
\Sigma_{12} &= -\frac{2A_1}{a(a+b)} \\
\Sigma_{11} &= -\frac{2B_1}{a+b} \\
\Sigma_{10} &= C_F(\pi^2-7)+\mathcal{F}_{10} \\
\Sigma_{24} &= \frac{2A_1^2}{a^2(a+b)^2} \\
\Sigma_{23} &= -\frac{8\pi^2 A_1\beta_0}{3\pi a^2(a+b)^2}\,(b+2a)+\frac{4A_1B_1}{a(a+b)^2} \\
\Sigma_{22} &= \frac{2A_1}{a(a+b)}\left(C_F(7-\pi^2)-\mathcal{F}_{10}\right)-\frac{2A_2}{a(a+b)^2}\,(b+a)+\frac{2B_1^2}{(a+b)^2}-\frac{4\pi\beta_0 B_1}{(a+b)^2}+\mathcal{F}_{22} \\
\Sigma_{36} &= -\frac{4A_1^3}{3a^3(a+b)^3} \\
\Sigma_{35} &= \frac{16\pi\beta_0 A_1^2(2a+b)}{3a^3(a+b)^3}-\frac{4A_1^2B_1}{a^2(a+b)^3} \\
\Sigma_{34} &= \frac{2A_1^2}{a^3(a+b)^3}\left((a^2+ab)\left(\left(\pi^2-7\right)C_F+\mathcal{F}_{10}\right)\right)+\frac{8\pi\beta_0 A_1B_1(7a+2b)}{3a^2(a+b)^3}- \\
&-\frac{2A_1\mathcal{F}_{22}}{a(a+b)^3}(a^2+2ab+a^2b^2)+\frac{4A_1A_2}{a^2(a+b)^3}(a+b)-\frac{16\pi^2\beta_0^2A_1}{3a^3(a+b)^3}\left(3a^2+3ab+b^2\right)- \\
&-\frac{4A_1B_1^2}{a(a+b)^3}\,.
\end{aligned}
\tag{A.16}
$$

Once the observable-specific A_3, B_2 coefficients living in $h(\lambda)$ come into play the matching coefficients cannot be given generically. Therefore the set of coefficients given in Eq. (A.16) are completed by

$$
\begin{aligned}
\Sigma_{21}^{(\tau)} &= B_1\left(-\frac{1}{2}\pi^2C_F+\frac{11}{4}C_F-\mathcal{F}_{10}\right)-\frac{B_2^{(\tau)}}{2}+\pi\beta_0C_F+\mathcal{F}_{21} \\
\Sigma_{21}^{(b_t)} &= 2B_1\left(C_F(7-\pi^2)-\mathcal{F}_{10}\right)-2B_2^{(b_t)}+2\pi\beta_0C_F\left(2-\frac{1}{3}\pi^3\beta_0C_F\right)+\mathcal{F}_{21} \\
\Sigma_{21}^{(y_3)} &= B_1\left(C_F(7-\pi^2)-\mathcal{F}_{10}\right)-2B_2^{(y_3)}+2\pi\beta_0C_F\left(2-\frac{1}{3}\pi^3\beta_0C_F\right)+\mathcal{F}_{21}
\end{aligned}
$$

$$
\begin{aligned}
\Sigma_{33}^{(\tau)} &= A_1 B_1 \left(\frac{C_F\pi^2}{2} - \frac{11C_F}{4} + \mathcal{F}_{10}\right) + \\
&+A_1\left(-4\pi^2\beta_1 + \frac{B_2^{(\tau)}}{2} - \beta_0 C_F\pi^3 + \frac{9\pi\beta_0 C_F}{2} - 2\pi\beta_0\mathcal{F}_{10} - \mathcal{F}_{21}\right) + \\
&+A_2(B_1 - 4\pi\beta_0) - \frac{B_1^3}{6} + \pi\beta_0 B_1^2 + B_1\left(-\frac{4}{3}\pi^2\beta_0^2 - \mathcal{F}_{22}\right) + \mathcal{F}_{33} \\
\Sigma_{33}^{(b_t)} &= 4A_1 B_1\left(C_F(\pi^2-7) + \mathcal{F}_{10}\right) + \\
&+2A_1\left(-\frac{16\pi^2\beta_1}{3} + 2B_2^{(b_t)} - 2\pi^3\beta_0 C_F + \frac{44\pi\beta_0 C_F}{3} - \frac{8\pi\beta_0\mathcal{F}_{10}}{3} - \mathcal{F}_{21}\right) + \\
&+A_2\left(4B_1 - \frac{32\pi\beta_0}{3}\right) - \frac{4B_1^3}{3} + 8\pi\beta_0 B_1^2 + 2B_1\left(-\frac{16\pi^2\beta_0^2}{3} - \mathcal{F}_{22}\right) + \mathcal{F}_{33} \\
\Sigma_{33}^{(y_3)} &= \frac{1}{2}A_1 B_1\left(C_F(\pi^2-7) + \mathcal{F}_{10}\right) + \\
&+\frac{1}{2}A_1\left(-\frac{8\pi^2\beta_1}{3} + 2B_2^{(y_3)} - \frac{2\pi^3\beta_0 C_F}{3} + \frac{16\pi\beta_0 C_F}{3} - \frac{4\pi\beta_0\mathcal{F}_{10}}{3} - \mathcal{F}_{21}\right) + \\
&+A_2\left(\frac{B_1}{2} - \frac{4\pi\beta_0}{3}\right) - \frac{B_1^3}{6} + \pi\beta_0 B_1^2 + B_1\left(-\frac{4\pi^2\beta_0^2}{3} - \mathcal{F}_{22}\right) + \mathcal{F}_{33}
\end{aligned}
$$

$$
\begin{aligned}
\Sigma_{32}^{(\tau)} &= C_F^2 A_1\left(-\frac{1}{8}\pi^4 + \frac{11\pi^2}{8} - \frac{85}{32}\right) + C_F A_1\left(\frac{11}{4} - \frac{\pi^2}{2}\right)\mathcal{F}_{10} + \\
&+A_2\left(-\frac{C_F\pi^2}{2} + \frac{11C_F}{4} - \mathcal{F}_{10}\right) - \frac{A_3}{2} + \frac{1}{2}B_1^2\left(\frac{C_F\pi^2}{2} - \frac{11C_F}{4} + \mathcal{F}_{10}\right) + \\
&+\frac{B_1 B_2}{2} + B_1\left(-2\pi^2\beta_1 - \frac{\pi^3\beta_0 C_F}{2} + \frac{7\pi\beta_0 C_F}{4} - \pi\beta_0\mathcal{F}_{10} - \mathcal{F}_{21}\right) - \\
&-\pi\beta_0 B_2 + 4\pi^2\beta_0^2 C_F\left(\frac{1}{2} + \frac{\pi^2}{3}\right) + \left(\frac{C_F\pi^2}{2} - \frac{11C_F}{4}\right)\mathcal{F}_{22} + \mathcal{F}_{32} \\
\Sigma_{32}^{(b_t)} &= C_F^2 A_1\left(-\pi^4 + 14\pi^2 - \frac{187}{4}\right) + 2C_F A_1\left(7-\pi^2\right)\mathcal{F}_{10} + \\
&+2A_2\left(C_F(7-\pi^2) - \mathcal{F}_{10}\right) - 2A_3 + 2B_1^2\left(C_F(\pi^2-7) + \mathcal{F}_{10}\right) + \\
&+4B_1 B_2 + 2B_1\left(-8\pi^2\beta_1 - \frac{4\pi^3\beta_0 C_F}{3} + 10\pi\beta_0 C_F - 2\pi\beta_0\mathcal{F}_{10} - \mathcal{F}_{21}\right) - 8\pi\beta_0 B_2 + \\
&+4\pi^2\beta_0^2 C_F\left(4 - \frac{2\pi^2}{3}\right) + \left(C_F(\pi^2-7)\right)\mathcal{F}_{22} + \mathcal{F}_{32} \\
\Sigma_{32}^{(y_3)} &= C_F^2 A_1\left(-\frac{1}{4}\pi^4 + \frac{7\pi^2}{2} - \frac{187}{16}\right) + C_F\frac{A_1}{2}\left(7-\pi^2\right)\mathcal{F}_{10} + \\
&+\frac{A_2}{2}\left(C_F(-\pi^2+7) - \mathcal{F}_{10}\right) - 2A_3 + \frac{B_1^2}{2}\left(C_F(\pi^2-7) + \mathcal{F}_{10}\right) + \\
&+2B_1 B_2 + B_1\left(-4\pi^2\beta_1 - \frac{\pi^3\beta_0 C_F}{3} + 3\pi\beta_0 C_F - \pi\beta_0\mathcal{F}_{10} - \mathcal{F}_{21}\right) - \\
&-8\pi\beta_0 B_2 + 4\pi^2\beta_0^2 C_F\left(4 - \frac{2\pi^2}{3}\right) + \left(C_F(\pi^2-7)\right)\mathcal{F}_{22} + \mathcal{F}_{32}\,.
\end{aligned}
\tag{A.17}
$$

We reproduce Tables 6.1 and 6.2, showing the expanded multiple emissions functions necessary for NNLO+NNLL matching for the seven event shapes and two jet rates that

we consider.

	T	C	ρ_H	B_T	B_W	T_M	O
$\mathcal{F}_{22}$	-23.394(6)	-23.394(6)	-11.697(4)	-74.121(6)	-27.332(7)	-53.287(7)	42.975(9)
$\mathcal{F}_{33}$	-208.252(3)	-208.252(3)	-119.324(2)	-724.49(2)	-371.76(2)	-563.24(7)	513.96(8)
$\mathcal{F}_{10}$	-5.4396	-1.0532	-5.4396	0	0	0	0
$\mathcal{F}_{21}$	-19.951(7)	-70.157(1)	-20.401(9)	61.45(2)	59.65(2)	-10.080(9)	80.79(5)
$\mathcal{F}_{32}$	-463.51(6)	-1427.72(5)	-247.79(4)	-717.1(1)	335.8(9)	-1287.0(8)	-79.(5)

Table A.1: Numerical expansion coefficients to $\mathcal{O}(\alpha_s^3)$ for the multiple emissions functions $\mathcal{F}_{\mathrm{NLL}}$ and its NNLL correction $\mathcal{F}_{\mathrm{NNLL}}$ for event shape observables.

	Durham	Cambridge
$\mathcal{F}_{22}$	-2.1932(2)	0
$\mathcal{F}_{33}$	-15.831(7)	0
$\mathcal{F}_{10}$	-8.5114(0)	-8.5114(0)
$\mathcal{F}_{21}$	-14.631(3)	-5.635(3)
$\mathcal{F}_{32}$	10.8(4)	81.86(3)

Table A.2: Numerical expansion coefficients to $\mathcal{O}(\alpha_s^3)$ for the multiple emissions functions $\mathcal{F}_{\mathrm{NLL}}$ and its NNLL correction $\mathcal{F}_{\mathrm{NNLL}}$ for the two-jet rate in the Durham and Cambridge algorithms.

Appendix B

ARES: Numerical Implementation of NNLL Resummation

in which I discuss the technicalities of building Monte Carlos to compute resummed cross-sections.

We have implemented the calculation of the real resolved emission contributions of Chapters 4 and 5, the $\delta\mathcal{F}$s, in a computer code entitled Automated Resummer of Event Shapes (ARES). ARES is a modular framework capable of calculating the various $\delta\mathcal{F}$ functions using a soft-collinear ensemble, an optional special emission and the kinematically-appropriate algorithm. The kinematic routines hold for any relevant observable (see Sec. 3.1 for details). ARES includes modules to determine the expansion of any $\delta\mathcal{F}$-function to first, second or third order in α_s. This allows us to validate our resummed results against analytic calculations, and to match to fixed-order results. Thanks to its modular structure ARES does not require modification to incorporate extra processes and observables, rather it just requires the inclusion of additional modules. It is also systematically extendable to any desired logarithmic order.

B.1 Emissions' Phase Space

The formalism we use for our resummation is inspired by the CAESAR philosphy [3]. However ARES differs from CAESAR in its implementation of emissions. The emissions in CAESAR can be viewed as physically viable emissions: they are truly generated from the quark-antiquark dipole and the system properly obeys energy-momentum conservation. Conversely the ARES emissions are not physical: they could not be interfaced with a general-purpose event generator as is common for parton shower implementations. ARES emissions do not conserve energy-momentum; instead the emissions can be thought of as probes into the relevant regions of phase space. This is successful because of the moveable nature of the boundaries between hard-collinear, soft-wide angle and soft-collinear phase space. In the frame of an ensemble of soft-collinear particles the phase space available to a hard-collinear or soft-wide-angle emission is tiny, so the exact position of the special emission does not matter. We do not need to test whether our generated emissions are safely within

predetermined phase-space boundaries, rather that they have appropriate *separation*.

Event shapes are insensitive to the rapidity fractions of emissions and jet rates only depend on the ordering of emissions in rapidity and k_t. Therefore it is only important that the *ordering* of rapidity fractions is physical:

$$\xi_{\text{swa}} < \xi_{\text{sc}} < \xi_{\text{hc}} \tag{B.1}$$

We use this freedom to decide that a soft-collinear emission has $\xi \in (-1, 1)$, that a soft-wide-angle emission has $\xi = 0$ and that a hard-collinear emission has $\xi = \pm 2$ (the actual values of fractional rapidity need not be physical!). This ensures that the different types of radiation are suitably separated and that their ordering in η is physical.

B.1.1 Rescaling

As discussed above it is only the relative positions of emissions that are important. As such, and to maximally simplify our numerical integrations, we work with rescaled variables.
The phase space available to different emissions is shown in Fig. B.1. We can rescale the

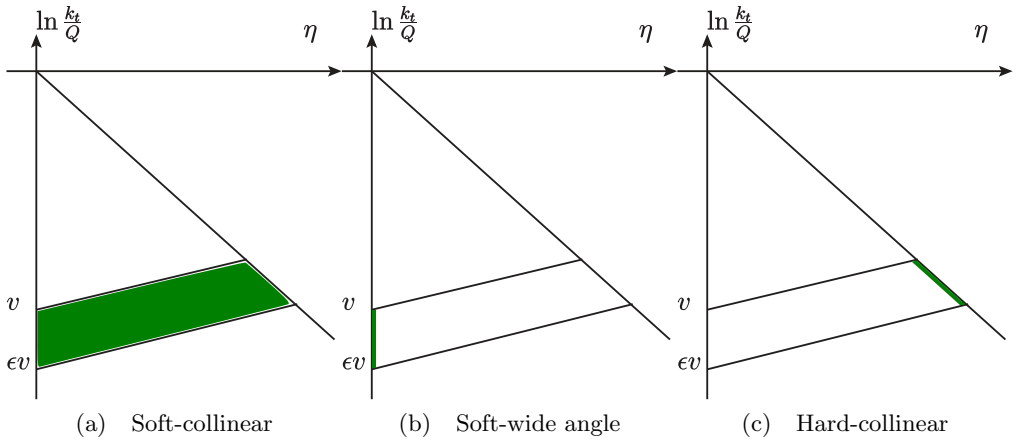

Figure B.1: Phase spaces available to various emissions (shown for emissions emitted from p_1).

emissions in this space, extending or shrinking the rapidity and transverse momentum ranges. rIRC safety stipulates that the multiple emission function is conformally invariant under such a rescaling, as long as ϵ is kept constant (i.e. the boundaries may move but their distance must remain $= \ln 1/\epsilon$). We take advantage of this fact and re-express the emissions to obtain order-one kinematic variables. Thus we can safely use standard double precision, without the risk of incurring cancellation errors.
This is another way in which `ARES` differs from `CAESAR`. All of the routines in `ARES` operate in the $v \to 0$ limit. Therefore the $\mathcal{F}$-functions are independent of v, as well as ϵ, so no limits have to be taken numerically. `CAESAR`, on the other hand, makes no such assumptions. The limit $v \to 0$ *is* taken numerically and so arbitrary precision must be used to ensure this limit is sufficiently close to zero.

The natural kinematic variables describing gluon emission are transverse momentum k_t, rapidity η and azimuthal angle ϕ. We rescale the rapidity of each emission by the maximum allowed value (using Eq. (3.40)). We then rephrase each emission's transverse momentum into a quantity describing an emission's effect on the observable (this is of course proportional to its transverse momentum), $\zeta = V(\{\tilde{p}\}, k)/v$. Each emission is now expressed in terms of three order-one kinematic variables, (ξ, ζ, ϕ).
In the next section we carry out further manipulations of the $\delta\mathcal{F}$ expressions in order that they can be easily implemented in a Monte Carlo program.

B.2 Monte Carlo Determination of Real Emission Corrections

In Sec. 3.1.5 we manipulated the NLL multiple emissions function into a form that can be evaluated using a Monte Carlo integration. In this section we will show how the Monte Carlo procedures of `ARES` efficiently determine the values of its NNLL corrections, $\{\delta\mathcal{F}\}$. We use the hard-collinear correction to the multiple emissions function as our example. We stress that the steps shown here for $\delta\mathcal{F}_{\rm hc}$ can be applied to all of the remaining NNLL corrections as well as the NLL $\mathcal{F}$-function. Both event shapes and the two-jet rate in the Cambridge algorithm allow for simplications to be made on the $\delta\mathcal{F}$ functions. In order to produce the most generic expressions we will use the Durham two-jet rate as our test observable in the following.

We begin with the expression for the hard-collinear matrix element contribution given in Eq. (5.34), comprising of the contribution from the special hard-collinear emission and the contribution from a soft-collinear ensemble. We choose to pick out the emission with the largest of all $V_{\rm sc}(\{p\}, k_i)$, calling it k_1, and neglect all emissions k_i with $v_i < \epsilon v_1$, with corrections suppressed by powers of $v_1 \sim v$. In order to work with order-one values of the observable, rather than the natural but numerically-limiting $v_i \ll 1$, we will rescale all emission-contributions by $V_{\rm sc}(\{p\}, k_1) \equiv \zeta_1$. The rescaled expression can take two forms. 1) The form arising when k_1 belongs to the soft-collinear ensemble, and 2) that in which k_1 is identified with the special emission.

1) Considering the first case, $\zeta < \zeta_1$,

$$\begin{aligned}\delta\mathcal{F}^{<}_{\rm hc} = &\sum_{\ell_1=1,2} R'_{{\rm NLL},\ell_1} \int_0^\infty \frac{d\zeta_1}{\zeta_1}\zeta_1^{R'_{\rm NLL}} \int_0^{2\pi}\frac{d\phi_1}{2\pi}\int_0^{\zeta_1}\frac{d\zeta}{\zeta}\int_0^{2\pi}\frac{d\phi}{2\pi}\sum_{\ell=1,2}\frac{\alpha_s(v^{\frac{1}{a+b_\ell}}Q)}{\alpha_s(Q)(a+b_\ell)}\times \\ &\times\int_0^1\frac{dz}{z}(zp_\ell(z)-2C_\ell)\left[\epsilon^{R'_{\rm NLL}}\sum_{n=0}^{\infty}\frac{1}{n!}\prod_{i=2}^{n+1}\sum_{\ell_i=1,2}R'_{{\rm NLL},\ell_i}\int_{\epsilon\zeta_1}^{\zeta_1}\frac{d\zeta_i}{\zeta_i}\int_0^{2\pi}\frac{d\phi_i}{2\pi}\right]\times \\ &\times\left[\Theta\left(1-\lim_{v\to0}\frac{V_{\rm sc}(\{\tilde{p}\},k,k_1,\ldots,k_{n+1})}{v}\right)-\Theta(1-\zeta)\Theta\left(1-\lim_{v\to0}\frac{V_{\rm sc}(\{\tilde{p}\},k_1,\ldots,k_{n+1})}{v}\right)\right].\end{aligned} \tag{B.2}$$

We now perform a change of variables, rescaling all emissions in the event by ζ_1, defining $\tilde{\zeta} = \zeta/\zeta_1$ and $\tilde{\zeta}_i = \zeta_i/\zeta_1$. Each emission's momenta $\tilde{k}_i$ is rescaled such that

$$V_{\rm sc}(\{\tilde{p}\}, \tilde{k}_i) = v_i/\zeta_1 \,. \tag{B.3}$$

Since V is rIRC safe we have

$$V_{\rm sc}(\{\tilde{p}\}, k_1, \ldots, k_{n+1}) = \zeta_1 V_{\rm sc}(\{\tilde{p}\}, \tilde{k}_1, \ldots, \tilde{k}_{n+1}) \,. \tag{B.4}$$

Substituting this rescaling into Eq. (B.2) gives,

$$\begin{aligned}
\delta\mathcal{F}^{<}_{\rm hc} = \sum_{\ell_1=1,2} R'_{{\rm NLL},\ell_1} \int_0^\infty \frac{d\zeta_1}{\zeta_1} \zeta_1^{R'_{\rm NLL}} \int_0^{2\pi} \frac{d\phi_1}{2\pi} \int_0^1 \frac{d\tilde{\zeta}}{\tilde{\zeta}} \int_0^{2\pi} \frac{d\phi}{2\pi} \sum_{\ell=1,2} \frac{\alpha_s(v^{\frac{1}{a+b_\ell}}Q)}{\alpha_s(Q)(a+b_\ell)} \times \\
\times \int_0^1 \frac{dz}{z} (z p_\ell(z) - 2C_\ell) \left[\epsilon^{R'_{\rm NLL}} \sum_{n=0}^{\infty} \frac{1}{n!} \prod_{i=2}^{n+1} \sum_{\ell_i=1,2} R'_{{\rm NLL},\ell_{\rm i}} \int_\epsilon^1 \frac{d\tilde{\zeta}_i}{\tilde{\zeta}_i} \int_0^{2\pi} \frac{d\phi_i}{2\pi} \right] \times \\
\times \left[\Theta\left(1 - \zeta_1 \lim_{v\to 0} \frac{V_{\rm sc}(\{\tilde{p}\}, \tilde{k}, \tilde{k}_1, \ldots, \tilde{k}_{n+1})}{v}\right) - \right. \\
\left. - \Theta(1-\zeta_1\tilde{\zeta}) \Theta\left(1 - \zeta_1 \lim_{v\to 0} \frac{V_{\rm sc}(\{\tilde{p}\}, \tilde{k}_1, \ldots, \tilde{k}_{n+1})}{v}\right) \right] .
\end{aligned} \tag{B.5}$$

This allows us to perform the integration with respect to ζ_1 and obtain

$$\begin{aligned}
\delta\mathcal{F}^{<}_{\rm hc} = \sum_{\ell_1=1,2} \frac{R'_{{\rm NLL},\ell_1}}{R'_{\rm NLL}} \int_0^{2\pi} \frac{d\phi_1}{2\pi} \int_0^1 \frac{d\tilde{\zeta}}{\tilde{\zeta}} \int_0^{2\pi} \frac{d\phi}{2\pi} \sum_{\ell=1,2} \frac{\alpha_s(v^{\frac{1}{a+b_\ell}}Q)}{\alpha_s(Q)(a+b_\ell)} \int_0^1 \frac{dz}{z} (z p_\ell(z) - 2C_\ell) \times \\
\times \left[\epsilon^{R'_{\rm NLL}} \sum_{n=0}^{\infty} \frac{1}{n!} \prod_{i=2}^{n+1} \sum_{\ell_i=1,2} R'_{{\rm NLL},\ell_{\rm i}} \int_\epsilon^1 \frac{d\tilde{\zeta}_i}{\tilde{\zeta}_i} \int_0^{2\pi} \frac{d\phi_i}{2\pi} \right] \times \\
\times \left[\exp\left(-R_{\rm NLL} \ln \lim_{v\to 0} \frac{V_{\rm sc}(\{\tilde{p}\}, \tilde{k}, \tilde{k}_1, \ldots, \tilde{k}_{n+1})}{v} \right) \right. \\
\left. - \exp\left(-R'_{\rm NLL} \ln \max\left[\tilde{\zeta}, \lim_{v\to 0} \frac{V_{\rm sc}(\{\tilde{p}\}, \tilde{k}_1, \ldots, \tilde{k}_{n+1})}{v} \right] \right) \right] .
\end{aligned} \tag{B.6}$$

2) In the case that the special emission is the one with the largest $V_{\rm sc}(\{p\}, k_i)$,

$$\begin{aligned}\delta\mathcal{F}^{>}_{\rm hc} = &\int_0^\infty \frac{d\zeta}{\zeta}\zeta^{R'_{\rm NLL}} \int_0^{2\pi}\frac{d\phi}{2\pi}\sum_{\ell=1,2}\frac{\alpha_s(v^{\frac{1}{a+b_\ell}}Q)}{\alpha_s(Q)(a+b_\ell)}\int_0^1\frac{dz}{z}(zp_\ell(z)-2C_\ell)\times\\
&\times\left[\epsilon^{R'_{\rm NLL}}\sum_{n=0}^\infty\frac{1}{n!}\prod_{i=1}^n\sum_{\ell_i=1,2}R'_{{\rm NLL},\ell_{\rm i}}\int_{\epsilon\zeta}^{\zeta}\frac{d\zeta_i}{\zeta_i}\int_0^{2\pi}\frac{d\phi_i}{2\pi}\right]\times\\
&\times\left[\Theta\left(1-\lim_{v\to0}\frac{V_{\rm sc}(\{\tilde p\},k,k_1,\dots,k_n)}{v}\right)-\Theta(1-\zeta)\Theta\left(1-\lim_{v\to0}\frac{V_{\rm sc}(\{\tilde p\},k_1,\dots,k_n)}{v}\right)\right],\end{aligned} \tag{B.7}$$

where for clarity of notation we have kept the special emission variables devoid of subscript, and now $\zeta > \zeta_1$. We rescale the soft-collinear ensemble by the special emission's contribution, defining $\tilde\zeta_i = \zeta_i/\zeta$. Again exploiting the rIRC safety properties of the observable from Eq. (B.4), we find

$$\begin{aligned}\delta\mathcal{F}^{>}_{\rm hc} = &\int_0^\infty \frac{d\zeta}{\zeta}\zeta^{R'_{\rm NLL}} \int_0^{2\pi}\frac{d\phi}{2\pi}\sum_{\ell=1,2}\frac{\alpha_s(v^{\frac{1}{a+b_\ell}}Q)}{\alpha_s(Q)(a+b_\ell)}\int_0^1\frac{dz}{z}(zp_\ell(z)-2C_\ell)\times\\
&\times\left[\epsilon^{R'_{\rm NLL}}\sum_{n=0}^\infty\frac{1}{n!}\prod_{i=1}^n\sum_{\ell_i=1,2}R'_{{\rm NLL},\ell_{\rm i}}\int_{\epsilon}^{1}\frac{d\tilde\zeta_i}{\tilde\zeta_i}\int_0^{2\pi}\frac{d\phi_i}{2\pi}\right]\times\\
&\times\left[\Theta\left(1-\zeta\lim_{v\to0}\frac{V_{\rm sc}(\{\tilde p\},\tilde k,\tilde k_1,\dots,\tilde k_n)}{v}\right)-\Theta(1-\zeta)\Theta\left(1-\zeta\lim_{v\to0}\frac{V_{\rm sc}(\{\tilde p\},\tilde k_1,\dots,\tilde k_n)}{v}\right)\right].\end{aligned} \tag{B.8}$$

This allows us to perform the integration with respect to ζ, to obtain

$$\begin{aligned}\delta\mathcal{F}^{>}_{\rm hc} = &\frac{1}{R'_{\rm NLL}}\int_0^{2\pi}\frac{d\phi}{2\pi}\sum_{\ell=1,2}\frac{\alpha_s(v^{\frac{1}{a+b_\ell}}Q)}{\alpha_s(Q)(a+b_\ell)}\int_0^1\frac{dz}{z}(zp_\ell(z)-2C_\ell)\times\\
&\times\left[\epsilon^{R'_{\rm NLL}}\sum_{n=0}^\infty\frac{1}{n!}\prod_{i=1}^n\sum_{\ell_i=1,2}R'_{{\rm NLL},\ell_{\rm i}}\int_{\epsilon}^{1}\frac{d\tilde\zeta_i}{\tilde\zeta_i}\int_0^{2\pi}\frac{d\phi_i}{2\pi}\right]\times\\
&\times\left[\exp\left(-R'_{\rm NLL}\ln\lim_{v\to0}\frac{V_{\rm sc}(\{\tilde p\},\tilde k,\tilde k_1,\dots,\tilde k_n)}{v}\right)\right.\\
&\left.-\exp\left(-R'_{\rm NLL}\ln\max\left[1,\lim_{v\to0}\frac{V_{\rm sc}(\{\tilde p\},\tilde k_1,\dots,\tilde k_n)}{v}\right]\right)\right].\end{aligned} \tag{B.9}$$

Of course the full contribution is the sum of the two possible cases, $\delta\mathcal{F}_{\rm hc} = \delta\mathcal{F}^{>}_{\rm hc} + \delta\mathcal{F}^{<}_{\rm hc}$.

Eqs. (B.6) and (B.9) are multi-dimensional integrations involving order-one ζ_i variables. Notice that it is a simple step to perform the expansion of $\delta\mathcal{F}_{\rm hc}$ from this expression: choosing the number of emissions to be two or three (via n) will give the α_s^2 or α_s^3 piece, respectively. The observable determination is sometimes even accessible with an analytic calculation for small n.